UNIVERSITY OF TWENTE.

Feasibility analysis of a double leg perturbator robotic setup for the purposes of joint impedance estimation

Master Thesis

BME

ET - BE

August 13, 2024

Prof. dr. ir. H. van der Kooij,
dr. S.U. Yavuz,
dr. M.E. Eveld
Kees Wuister Bsc, s1949942

Abstract

Joint impedance is an important metric used for robotic gait trainers and rehabilitative therapies used to improve the walking ability of neurologically impaired people. Joint impedance is an important metric which describes the relation between resultant joint torques and changes in position, velocity and acceleration, thus influencing the movement and posture of the joint. Though the joint impedance of either the ankle, the hip, or the knee in the leg have been assessed during walking in isolation, thus far the joint impedance values of all three joints of the leg have not been succesfully identified simultaneously. Van der Kooij et al. identified the hip and knee joint impedance values accurately during the swing phase using the Lower Limb Perturbator (LOPER) [1]. However, this setup did not accurately estimate the ankle joint impedance. In this research the LOPER was expanded with an extra perturbator attached to the shank to assess the feasibility of using a double pusher setup to identify the joint impedance values of all joints in the leg during the swing phase of walking. Participants walked on a treadmill with the LOPER attached and were given 4 different types of perturbations using the double this expanded double pusher setup of the LOPER. The feasibility of this setup was tested by assessing two requirements of the setup: the transparency, and the joint angle response. The transparency was assessed using three criteria set in previous research. These were: the root mean square interaction force during unperturbed walking should not exceed 10 N, the peak interaction force during unperturbed walking should not exceed 20 N, and the joint angle deviations created by walking with the LOPER should remain smaller than the difference found between different participants when both walk without the LOPER. The joint angle responses were tested using a newly set criterion in this research based on the results of previous research. This criterion stated that the peak joint angle response of the perturbations should at least be 0.07 rad. All three conditions concerning the transparency were not met in testing due to problems with the stability of the LOPER setup during testing. The fourth criterion concerning the joint angle response was met for one perturbation condition. No joint impedance estimations have been done due to the transparency being insufficient. However, if a new controller would be implemented in the expanded LOPER setup, then the combined perturbations on the thigh and shank do show promise in sufficiently perturbing the leg for the purposes of joint impedance estimation.

Keywords: *Joint Impedance, Joint impedance estimation, human gait analysis, Gait training, knee stiffness, hip stiffness, ankle stiffness, transparency*

Acknowledgements

First and foremost I would like to thank my daily supervisor Maura Eveld, who has always been able to lend me help whenever I needed it and was always open to answer my questions and offer guidance whenever I needed it, as well as looking out for me and making sure that I wouldn't be overworking myself. Also many thanks to Irfan Refai for helping in the first half year of this assignment, as you have always been willing to give helpful feedback and guidance during our meetings. Michiel Ligtenberg has been of great help throughout this research. We have spent many hours in the lab together making sure that the physical experimental setup was set properly, and he has made sure that the several modifications needed for this assignment were done to the experimental setup. I would of course also like to thank my entire master committee for taking the time to read taking the time to read and grade my master assignment. Next to my committee, I am also very grateful for my sister Willemijn Wuister, who has also taken her time to review and improve my thesis.

My friends here at the utwente have been a great well of support as I could always count to discuss problems with them, but also as they gave me some much needed distractions in the shape of a good conversation or a game of cards. In particular I would like to thank Edmée with whom I have spent countless afternoons studying and giving me some motivation to keep on working. Finally, my girlfriend Carlijn has been a rock of moral support throughout this entire research, both on a personal and academic level.
Kees Wuister,
August 13, 2024

Contents

1 Introduction

1.1 Gait training

As of 2016, there have been roughly 67 million recorded cases of people suffering from a stroke worldwide, and as of 2019 there were 20 million known cases of people suffering from Spinal Cord injuries. Due to the improvements in healthcare and lifestyle, these numbers are expected to rise in the future. This increases the pressure to deliver proper care to these patients [2, 3].

What these, and other neurological disabilities have in common, is that patients lose proper control over their lower limbs, decreasing their mobility during daily life. This loss of mobility can have far-reaching consequences on both their quality of life, as well as their physical health [4, 5]. It is therefore of interest to improve both the quality of life and the health of recovering stroke patients by finding a way to improve their mobility. One method to increase this mobility is to allow them to regain control of their lower extremities. In previous studies, it was found that the optimal rehabilitative techniques to increase the motor control of these patients made use of early adapted, task specific training, preferably mixing different rehabilitative techniques [6, 7, 8]. Some examples of such different rehabilitative techniques may for example be physiotherapy or the use of orthotic devices [9]. In recent years, the use of robotic assistive devices has become more and more prevalent. Exoskeletons such as G-EO, Lokomat, Rewalk, and others have already become commercially available for this exact purpose [10, 11]. Exoskeletons such as the Rewalk assist the human body in walking, standing, sitting down, and standing up by delivering assistive torques to the legs at the joints, improving their mobility in daily life. These systems are often controlled by either a joystick or using controllers based on centre of mass position, pelvis orientation, or EMG signals [10].

In order to increase the mobility of stroke patients, it is important to understand the control of the lower extremities in the human body, both for stroke patients, as well as for healthy people [12]. One way to identify the control mechanisms used is to identify and estimate the mechanical behaviour of specific joints during tasks. One mechanical factor which influences the position, balance and movement of the joints is the joint impedance [13]. By knowing what the joint impedance values of both healthy and impaired humans are, better controllers and algorithms can be created for exoskeletons. These controllers will then be able to mimic regular human walking better, and create gait training systems that create more targeted training. In general a better understanding of joint impedance, and therefore of human movement control, allows for more targeted care for patients [14].

1.2 Joint Impedance

In biomechanics, the joint impedance describes the time-variant torques delivered by a joint as a direct consequence of the joint positions, velocities and accelerations [15]. The joint impedance is therefore often described using a second order differential equation describing the relation between the joint torque (τ) and the stiffness (K), damping (D), and inertia (I) as a function of the time variant joint angle (θ) (Eq. 1) [14, 16]. The joint impedance has been found to be dependent on many different parameters such as: joint position, muscle activation, perturbation amplitude, perturbation speed, and perturbation direction [12, 17, 18]. Moreover, the joint impedance is known to be dynamic during a gait cycle [19]. The total joint impedance is often divided into two distinct categories, the passive impedance; describing properties such as the stiffness and damping of the tendons and tissues surrounding the joint, and active; which is the joint impedance produced through (voluntary) contractions of the muscles surrounding the joint.

$$\tau(t) = I\ddot{\theta}(t) + D\dot{\theta}(t) + K\theta(t) \tag{1}$$

In order to correctly estimate the joint impedance of the legs, a number of different methods have already been considered. All joint impedance research is done by delivering a mechanical perturbation to the joint during a specific task given to the participant, to which the mechanical response of the human body to the perturbation is measured. System identification techniques are then applied to these perturbation responses

to estimate the impedance values of the participant [20].

In order for a robotic device to effectively allow for joint impedance estimation, it is necessary for the interaction forces between the participant and the robotic device to be minimised when the leg isn't perturbed. Such that the robotic does not influence the walking gait during unperturbed walking. In fact, in an ideal situation, the robotic device would be perfectly "transparent", meaning that the participant would not notice the actual device attached to them but only the environment, though this is not possible. The ability of the device to model the desired virtual dynamics is called the transparency of the robotic device [21]. Within this joint impedance study this means that a more transparent a robotic setup creates less noticeable interactions between the robot and the participant when the leg isn't perturbed.

There are two distinct types of mechanical perturbations which can be applied by a robotic pusher for the purposes of joint impedance estimation. Either a force perturbation and the position or kinematic response is measured of the subject, or a position perturbation is used, and the subsequent dynamic response of the subject is measured. Both approaches have their own advantages and disadvantages. Using position perturbations, leads to faster perturbations, and is therefore better at identifying the high frequency response of the joint. Because the active joint impedance always has a slight delay, these perturbations are better at identifying the passive joint impedance [20, 22]. Moreover, due to the increased velocity of the perturbations, the damping, of the leg, which is velocity dependent, is generally more accurately identified using position perturbations [23]. One of the major disadvantages of position perturbations however lies in the fact that, in order to correctly apply position perturbations, it is required for the participant to deliver some constant torque or force during testing, which is used to compare the mechanical response of the leg. Since the human body does not use force tracking innately, this creates the need for external force tracking feedback, and a physical setup which allows for less natural movement and natural movement of the participant [24, 23]. Conversely, force perturbations allow the participant to use position feedback, which allows the participant and the perturbations to simulate daily life perturbations, and consequently perturbations responses, more accurately. This is because the participant is capable of using their own propioceptive and visual position feedback as they would in their daily life [24].

1.3 State of the art

Historically, most joint impedance estimation of the leg joints has been done during static conditions, such as in a standing or sitting position in which the leg does not move unless perturbed [24, 23, 25, 26]. However, it has been shown that the joint impedance does change for the knee in dynamic conditions. Therefore research of the joint impedance during dynamic tasks such as walking is important. This does bring new challenges to correctly estimate the joint impedance, as new physical experimental setups are needed which allow for unimpeded walking while still creating accurate perturbations [27].

In the sections below, there will be an overview of the joint impedance estimation research done up to now for each specific joint. Describing the methods used, their findings, and their current shortcomings.

1.3.1 Ankle joint impedance estimation

Of all the joints in the lower limb, the most complete overview of the joint impedance during walking gait has been created for the ankle [15, 19, 28]. E.J. Rouse et al. investigated the joint impedance of the ankle, specifically during the stance phase [15]. In this research, participants walked along a path, at which in the centre there was a small plate which could rotate along the medial axis. When the participant's foot was placed on this plate during walking, the plate would randomly give a small rotational position perturbation. Using the ground reaction forces (F_x, F_z) and the distance between the centre of pressure and the centre of the rotating plate (δ_x, δ_z) during the perturbation, the torques (τ) as a result of the perturbation could be calculated using eq. 2 [15]. The torques of the unperturbed steps were collected and were subtracted from the perturbed steps such that only the torques as a direct result of the perturbation were assessed. Using these torques the impedance values could be estimated using a second order parametric model based on eq. 1. This research was the first to look at actual time-dependent ankle stiffness during walking gait. Using this method it was possible to accurately estimate the ankle joint impedance during the stance phase, showing

a Variance Accounted For (VAF) of around 98% for the reconstructed joint angles using the estimated joint impedance values. It was found that the impedance values change significantly during the stance phase, increasing as the stance phase progresses.

$$\tau = F_z \delta_x + F_x \delta_z \tag{2}$$

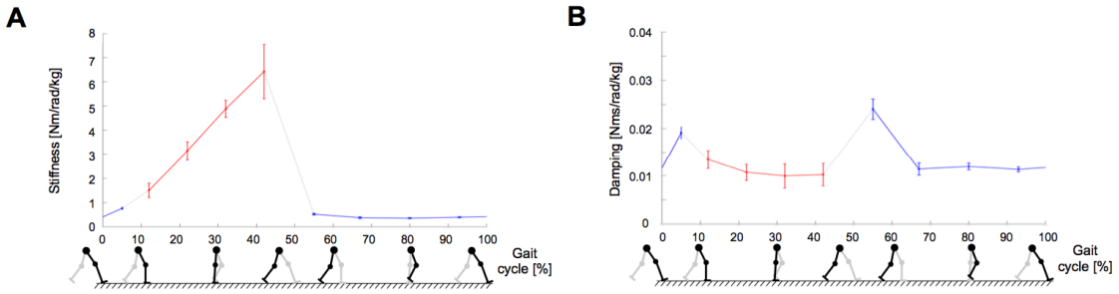

Figure 1: Ankle impedance during a walking gait cycle. Figure A is the stiffness and figure B is the damping, the red line are the results generated by [4, 15], the blue line are the results generated by [19]. Source: [28]

In order to also estimate the ankle stiffness during the swing phase of the gait cycle, H. Lee et al. have worked on a different setup [19, 28]. In this research they used the perturberator robot. This is an exoskeleton directly attached to the lower leg at the shank and the back of the foot. At the ankle a motor could deliver torques to the ankle joint. This robot allowed for quick force perturbations at all times during the gait cycle on the ankle. In this research, continuous random torque perturbations were given throughout the gait cycle. The robot was capable of estimating also the joint angle using a nonlinear transformation. Using the measured torques and the estiamted joint angles, the joint impedance of the ankle could be estimated used system identification techniques. Combining both this research and the previous research of E.J. Rouse, it has been possible to map the time variant ankle impedance during the entire gait cycle during typical human walking gait, as is visible in Fig. 1 [28].

The ankle joint impedance has also been estimated for people with neuromechanical lower limb impairments using a similar setup as the setup used by Rouse et al. [12, 15, 29]. During stance phase, the ankle stiffness increases for stroke patients compared to healthy patients. Moreover, the stiffness and damping stay more constant throughout the stance phase of walking for the impaired participants compared to unimpaired people. This suggests that people with neuromechanical impairments lose their ability to modulate their joint impedance quickly.

The results of the previous research has led to advancements in the understanding of the joint impedance of the leg. However, these works still have a number of shortcomings. For example, all of the previously mentioned research was done using pure ankle perturbations. This means that inter-joint impedance has not been identified in this research. The influence of bi-articular muscles cannot therefore be identified using these perturbations. These muscles increase the joint impedance during perturbations which are applied at the shank or even at or above the knee [24]. Moreover, the perturberator robot used to estimate the ankle joint impedance during the swing phase added a substantial weight to the leg when walking. This weight influences the dynamics of the leg and therefore also the subject's gait pattern at the knee and hip [19]. Finally, Rouse et al. used position perturbations for their research, while Lee et al. have used torque perturbations [15, 19]. This means that the joint impedance estimations may not be completely comparable due to the different perturbation types, which also influences the perturbation speed and magnitude, which do influence the joint impedance [12, 22].

1.3.2 Knee joint impedance estimation

In the last decade, an effort has been made to create a better understanding of the knee joint impedance as well during walking gait. Using the ETH exoskeleton, M. Tucker estimated the knee impedance values during the swing phase of walking gait [30]. This system worked similarly to the perturberator robot. It delivers a torque perturbation directly to the knee, and measures the knee angle using an internal sensor built into the knee brace. Using a second order parametric model based on the internal dynamics of the system, the stiffness and the damping can then be calculated for the knee joint [31].

Recently, Y. Nazon has generated an accurate estimation of the knee joint during the (almost) complete gait cycle as well using the M-BLUE exoskeleton; An exoskeleton which is attached to the leg with an actuator at the knee, capable of delivering torques directly to the knee [20]. The system delivered torque perturbations during six different timings of the gait cycle during both the stance and swing phase of the system. The human response to the torque perturbations was measured using motion capture. Using the kinematic motion capture data and the torques data from the ETH setup during the unperturbed steps, the dynamics of unperturbed walking were subtracted from the perturbed data. This left only the dynamics and kinematics as a direct result of the perturbation. This data was then used as input for a least squares regressive model to estimate the stiffness, damping and Inertia [20]. All impedance values are normalised for the mass of the participant.

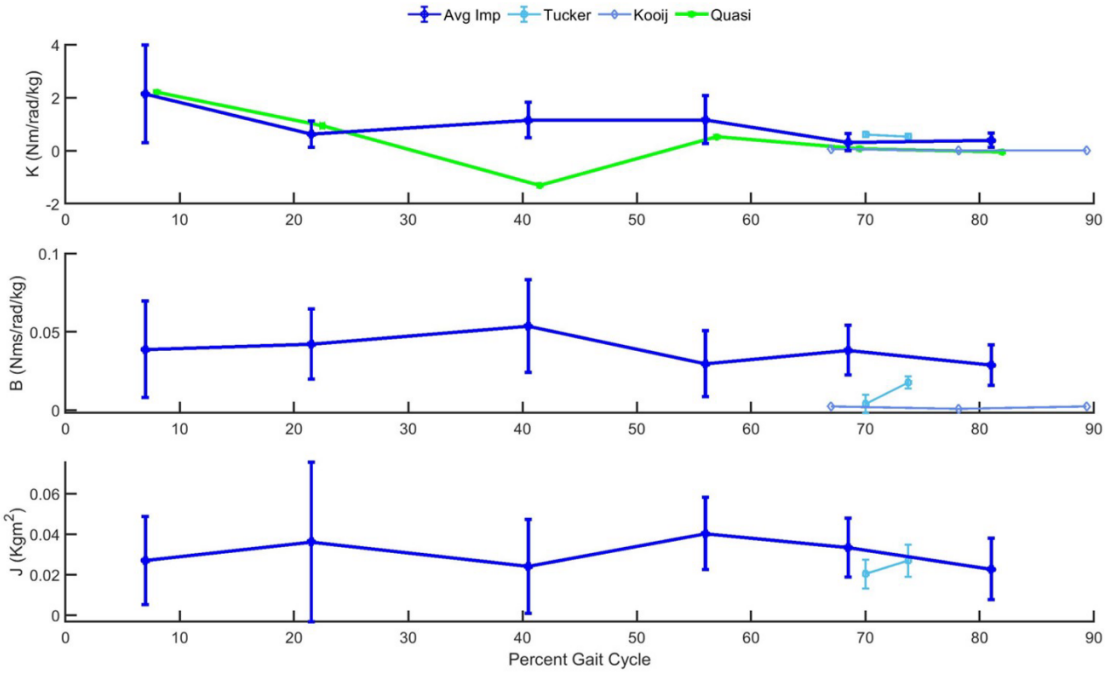

Figure 2: The normalised Knee stiffness (and Quasi-stiffness (green)), damping and Inertia as estimated by Y. Nazon (dark blue) compared to the impedance values estimated by Tucker et al. [31] (cyan) and van der Kooij et al [1] (light blue) during the entire gait cycle. The joint stiffness of the knee is consistent for all the different reseach, however, the damping values are higher than those found in other research. Image source: [20]

Though the results of Nazon are most insightful, there is still much research to be done on the knee impedance. The impedance estimations of Nazon are accurate, showing a VAF of 91 %, but they do show large discrepancies for the damping of the knee joint compared to the research done by Tucker et al. and van der Kooij et al [20]. The discrepancies are mainly ascribed to the shorter response window which assessed in this research (100 ms) compared to those of van der Kooij et al (250 ms). This means that the impedance values found by Y. Nazon are mainly the impedance values created by the passive joint response, while van der Kooij et al

describe the joint impedance values created by muscle activation [20]. This is explained by the fact that any active muscle responses will only be possible after a delay of 50 ms [25]. When comparing to Tucker, Nazon ascribes the difference in the damping values found either to the lower estimation accuracy of Tucker's research, or some unaccounted dynamics in Tucker's experiments [20, 31]. Next to this, the exoskeletal system used by both Nazon and Tucker still add some mass and inertia to the leg of the participant, influencing the dynamics of the leg of the participant. For the ETH exoskeleton the mass of the system is 3.5 kg [30]. Although no exact mass has been given for modified the M-BLUE exoskeleton by Nazon, the mechanical parts of the M-BLUE exoskeleton still weigh 1.4 kg [32]. For both the systems, this would still be enough to influence the leg dynamics during walking gait [33].

1.3.3 Hip joint impedance estimation

The hip joint impedance gait has not yet been extensively studied compared to the knee and the ankle, particularly during dynamic conditions. Huang et al. have looked intensively at the hip joint impedance during static conditions. The subject would have a free-hanging leg in which the knee was locked such that the leg remained straight at all times. the participant's weight was supported by a frame and two bars to which the participant had to push themselves up. Underneath the support structure a cable system was used which could perturb the leg when necessary. The participant would have a screen in front of them, in which they got visual feedback of the current force they were exerting upon the exoskeleton, as well as the target force they had to apply to the exoskeleton (relaxed, 10 N or 20 N). Using this setup, leg was perturbed using a position perturbation of 20 mm lasting 150 ms in either the forward or backwards directiion at random times. These tests were repeated for a number of different conditions, and in each condition, the hip was put in a different angle, varying from 0° to 55°. Using this setup, the stiffness was estimated using the difference in torque between the unperturbed situation and during the last 100 ms of the perturbation. Using the Laplace transform of the hip joint angle and the torques measurement signals, the damping was estimated. In this research, any correlations between the stiffness and damping, and the perturbation direction, joint angle, and current force output of the leg were compared. The stiffness is influenced by the perturbation direction, joint angle and force output, but no correlation could be shown for these parameters and the damping, presumably due to the small deviations of the damping of the hip joint compared to its stiffness [23]. Though others suggest this may also be a result of the unmodelled cable dynamics [20].

The research done by Huang et al. is useful for posture control, and shows several important relations between joint stiffness and direction, perturbation amplitude, joint angle, and muscle activation [23]. The results do still differ from other research done however on the hip joint impedance, most notably research done by van der Kooij et al. using the Lower Extremity Powered ExoSkeleton (LOPES) system. Though this is most likely attributed to the difference in age of the test subjects [23]. One thing the research done by Huang et al does not examine however, is the dynamic joint impedance. The only in depth research done on the hip impedance during walking gait, has up till now however only been done by van Asseldonk et al. and van der Kooij et al. Both of the researchers have made use of a different system called the Lower limb Perturbator (LOPER). Joint impedance estimation during dynamic tasks is still important to identify, as the joint impedance is time varying during dynamic tasks, and the joint impedance is different during dynamic tasks compared to static tasks [19, 27]. In the section below, the research with the LOPER and LOPES setup will be explained more in depth, as well as the conclusions from this research.

1.3.4 LOPER and LOPES research

Van Asseldonk et al. and van der Kooij et al. have tried to estimate the joint impedance of all three joints simultaneously during the swing phase using the LOPER and LOPES systems (Fig. 3). These systems work using a robotic device behind the participant which is attached to the participant using carbon rods. These robotic devices follow the leg movements while not giving any perturbations, leading to minimal interaction between the human and the robot. When a perturbation is applied the system delivers a linear force to the leg segment [1, 24, 33]. Using the LOPER system, linear forces were applied to the thigh in the anterior-posterior direction. These perturbations were applied at different timings during the swing phase. As this does not perturb a single joint in isolation, but a segment, both the hip and knee were perturbed using this method, allowing for the joint estimation of multiple joints simultaneously. Using the LOPES system, it has

been possible to correctly estimate the influence of added inertias to the lower legs and pelvis during regular walking gait [34].

Both the LOPES and the LOPER have been used in joint impedance estimation. The LOPES system has been used to estimate the joint impedance of the knee and hip during stance of elderly people [24]. Using the LOPER the joint impedance values for the knee and hip during the swing phase have been successfully estimated. It has thus far not been possible to estimate the joint impedance of both the hip, knee and ankle in tandem though. Due to the system only generating a minimal response from the ankle joint, the joint impedance estimations are inaccurate [1]. Using a new algorithm, Arami et al. have been able to increase the accuracy of the hip joint impedance estimation with the LOPER [35]. In this research, instead of using the total average of the unperturbed steps as is done most often, instead all the unperturbed steps are compared, and a number of different, slightly deviating gait patterns are identified, seperated and individually averaged. Each perturbed step is then compared to the average of each cluster of gait steps, and further analysis is done using the cluster which has the closest resemblance to the perturbed step. This method was chosen in order to more accurately estimate the joint impedance, even when larger gait variability was present during testing [35].

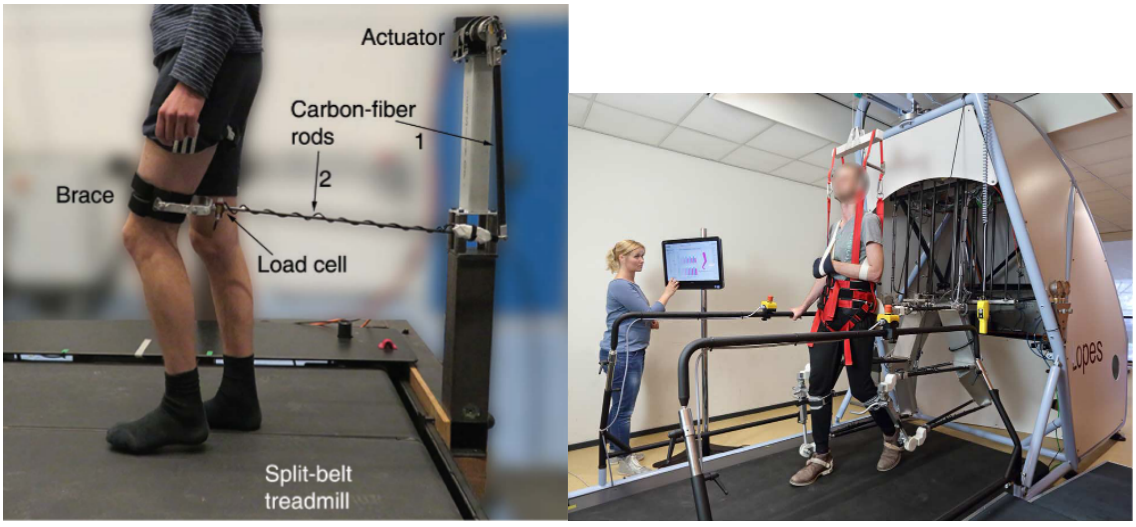

(a) The LOwer limb PERturbator (LOPER) system. This system is a simple single actuator system which can follow the leg movement allowing for minimal impedance, and apply linear forces to the thigh. Allowing for perturbing the leg at any time [1].

(b) the Lower Extremity Powered ExoSkeleton (LOPES) is created to be used as a gait trainer, allowing for more degrees of freedom and easier donning and doffing time than other gait trainers [33, 36].

Figure 3: The LOPER (a) and LOPES II (b) systems used by van Asseldonk and van der Kooij et al. Both function by using a robotic device behind the participant whose end effectors are attached to the leg of the participant. Both devices can track the human leg movement leading to minimal impedance felt by the participant, allowing for regular walking. Source: [1, 37]

1.4 Research question and goals

The research of this Master Thesis continues in the line of van der Kooij et al.'s research with the LOPER. In this research, a robotic pusher is added at the shank in addition to the previously used thigh pusher. The ultimate goal of this new setup will be that it is capable of directly perturbing all joints simultaneously. The hypothesis is that, with this added perturbator on the shank, it is possible to perturb all three joints of the leg sufficiently for the purposes of joint impedance estimation. In this report the following research question will be assessed: What is the feasibility of using a combined thigh and shank pushing system to perturb the leg in order to accurately estimate the leg joint impedance values during the swing phase of human walking?

In order to speak of a suitable setup for the purposes of the joint impedance estimation. Two distinct requirements have to be met. The system has to be sufficiently transparent, and the joint angle responses from the perturbations have to be large enough. To assess the transparency of the system, three criteria set by van der Kooij et al. can be used [1]. These criteria stat that the system is sufficiently transparent if the root mean square interaction forces between the human and the robot do not exceed 10 N, as well as if the peak interaction forces do not exceed 20 N. Moreover, the joint angle deviations with the LOPER attached should not be larger than the difference in joint angle deviations between different people.

The peak joint angle responses can be measured, and should give similar results to those found in previous research done in similar conditions. Therefore, the peak joint angle responses were measured for 4 different perturbation conditions. These were compared to a new criterion set in this research based on previous research, which stated that the peak joint angle response should be at least 0.07 rad. This way the suitability of the added shank perturbator was assessed, as well as what the ideal perturbation combinations are to use for further joint impedance estimation.

2 Methodology

The methods of this master assignment are based on the previous study done by van der Kooij et al. [1]. Using the expanded double pusher setup, participants were recruited and several experiments were done using different perturbation combinations. Each different combination was set as a different condition. The goal of these experiments was to assess the transparency and joint angle response with the setup. This chapter will first describe the physical setup used. Secondly, the protocols will be described. Thirdly the data collection processes will be explained, and finally the data processing and the outcome metrics will be specified and explained.

2.1 Experimental Setup

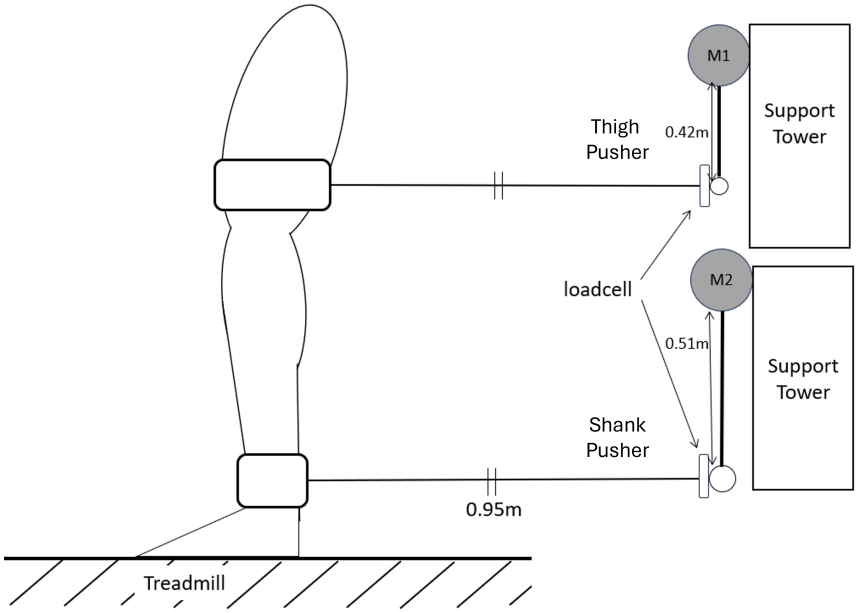

Figure 4: Schematic of the experimental setup as used in the experiments. The two pushers are attached to two support towers, which are rigidly attached to the ground to allow for better stability. The thigh pusher (M1) is attached just above the knee and the shank pusher (M2) is attached just above the ankle.

2.1.1 Physical pusher setup

The physical setup has been changed by adding a second perturbing robot which is attached to the shank (Fig. 4 and 5). The perturbators consist of two motors (SMH60, Parker, USA) that are attached to metal towers using sliders to allow for easy height adjustments for different participants. The towers are rigidly attached to the floor. Attached to each motor is a rigid carbon moment arm of 0.42 m and 0.51 m for the thigh and shank respectively. A longer carbon moment arm is chosen for the shank pusher to allow for a larger range of motion. Attached to the moment arms is a load cell (FUTEK FSH00086, USA) that records the interaction forces between the leg and motor. On the other side of the load cells is a carbon rod of 0.95 m. This rod is attached to the left leg using a brace consisting of a metal hinge joint and a leather strap which is fastened using Velcro. The motors are set to such a height that the the rods attached to the leg are horizontal during stance.

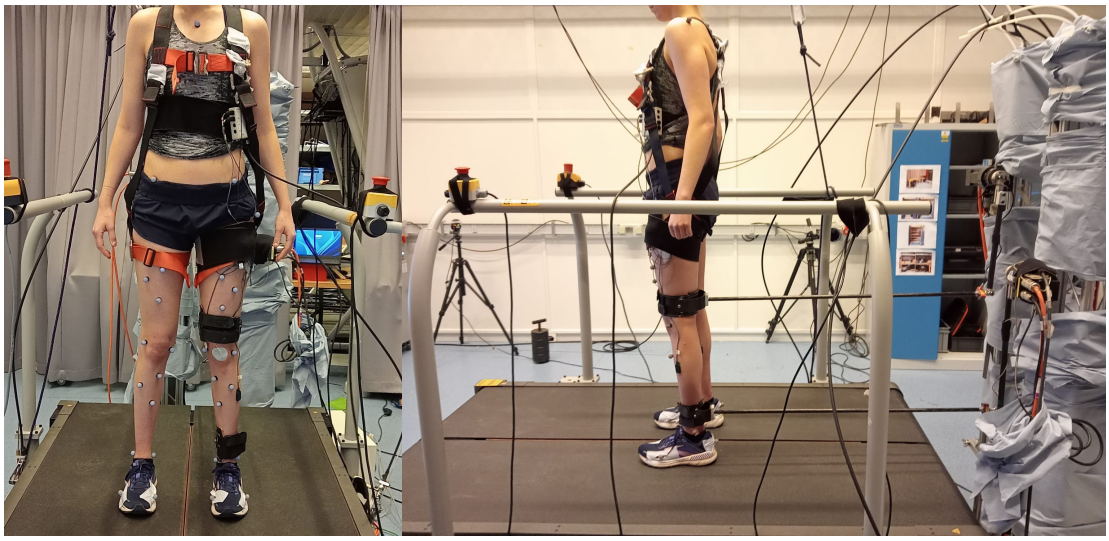

(a) (b)

Figure 5: Frontal (left) and sagittal (right) profile of the experimental setup. Both the pushers are set such that the carbon rods connected to the participant are horizontal during stance. The load cells are attached to the carbon rod close to the motors. The motors are attached to two rigid aluminium towers which are attached rigidly to the ground to minimise vibrations. The towers are covered to prevent reflections disturbing the motion capture signal.

2.1.2 Controller

The controller from [1] was implemented for both the thigh and the shank pusher (Fig. 6). It consists of a Low-pass filter (H_F) which lowers the virtual inertia of the perturbations. A filter was chosen instead of a feed-forward controller as the servo drive of the motors (H_A) does not allow feed-forward inputs. After the filter, the measured forces are subtracted to get the current interaction forces. At T, the forces are converted into the interaction torques at the motor. These torques are used as input for an admittance controller (H_C) that minimises the interaction torques. The admittance controller generates a desired angular velocity $\dot{\theta}_d$ which is used as an input for the servo drive of the motors (H_A). The servo drive outputs the actual angular velocities of the motors $\dot{\theta}_a$. The robotic and human dynamics are described in H_H. The output of H_H are the measured forces using the load cells. The parameters used in the controller H_C and H_F are: the stiffness $K_a = 0.017$ s, the inertia $I_v = 0.2$ kgm^2, and damping$B_v = 3$ Nm/rad, and finally a control gain to ensure stability during perturbations $c = 0.5$. These values are the same as the values used in [1]

During pilot testing of the experiments, the setup with the controller resulted in unstable behaviour. In order to ensure the system remains stable, an extra gain was added to the controller which is applied after H_C. This gain K_s had been set to 1.5 in the previous research and had been used to optimise the dynamics of the controller such that they led to the desired dynamics for the required bandwidth. In order to ensure stable walking behaviour, this gain was lowered such that it gives stable behaviour during walking gait and perturbations. The gains K_s are set to a value between 0.40 to 0.60 for the thigh and between 0.60 and 0.75 for the shank. The controller gains are tuned for each participant individually. Decreasing this gain comes at a cost of transparency during the experiments. Thus, a number of changes were made on the experimental setup during pilot testing. The goal was during these tests to identify the cause of the lowered stability and to improve the transparency and stability of the pushers. In Appendix B the tests done are reported, as well as their effects. It was not possible to identify the cause or implement changes which improved the stability using these changes.

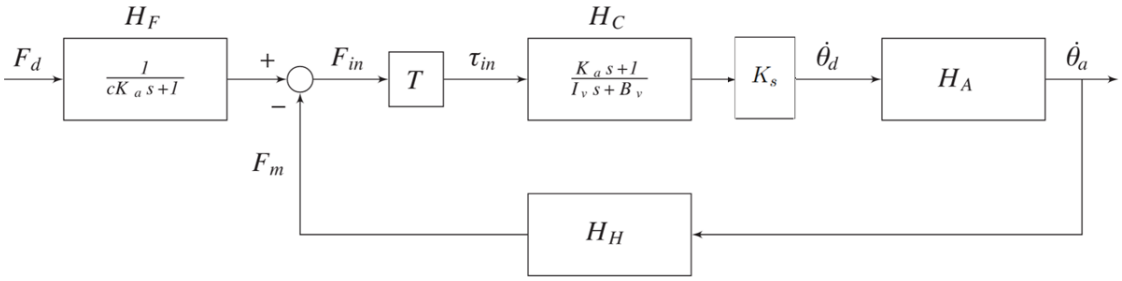

Figure 6: Block scheme of the control-loop of the filter H_F, the admittance controller H_C, the servo drive H_A, and the dynamics H_H. The desired forces are first filtered by H_F, afterwards the measured forces F_m are subtracted and the forces are converted to the input torques using the current moment arms in T. Next the controller calculates the new desired motor angular velocities $\dot{\theta}_d$ using the admittance controller H_C. The outputs of H_C are scaled using the K_s gain to ensure stability. The resultant $\dot{\theta}_d$ is used as inputs for the servodrive H_A, which finally calculates and outputs the actual angular velocity $\dot{\theta}_a$.

2.2 Protocol

The experimental setup has been approved by the ethics committee of University of Twente. All participants gave their informed written consent for the experiments. For this research only healthy, adult participants with no self-reported injuries in their legs were recruited. In the experiments, the participants walked on a treadmill at a speed of 0.5 m/s at a self-selected cadence. During each trial the participant was perturbed by the thigh pusher, shank pusher, or a combination of both the pushers using one of 5 conditions. All perturbations were applied 50 ms after toe off, and last for 100 ms. The perturbations were applied randomly every 5 to 10 steps. In total each trial consisted of 20 perturbations. During each trial, 1 of 5 distinct conditions were used (Fig. 7). Each condition was a variant in location, magnitude, and direction of the perturbations. In order to tune K_s, the participant walked at the target speed of 0.5 m/s. The K_s was tuned by increasing the gain in steps of 0.05 such that it was the maximum value for which no vibrations were felt by the participant. The K_s for the thigh was tuned first, after a satisfactory value was found, the K_s value was tuned for the shank. The K_s value was not changed between the different conditions. The specific K_s values used for each participant are given in Tab. 1.

2.2.1 Safety

In order to ensure the safety of the participant during the experiments, several different safety measures are in place. The controller is set with a position, velocity and acceleration (PVA) limiter, which prevents the controller to output a position, velocity or acceleration beyond a maximum value. These corresponded to a maximum velocity of 4.71 rad/s, an acceleration of 500 rad/s^2 and a maximum angle of 0.44 rad for the thigh pusher and 0.61 rad for the shank pusher. A larger maximum angle is chosen for the shank pusher to accomodate for the larger range of motion used by the lower leg. Moreover, the motors themselves have been given a maximum angle above which they will immediately shut off during testing, this angle is set to $\pm\frac{1}{4}\pi$ rad. Furthermore, the participant is hung into a safety harness which supports the participant if they were to fall. Finally, both the participant and the supervisor have two emergency buttons within reach at all times during testing: one to shut off the pusher and one to shut off the treadmill.

2.2.2 Conditions

All conditions were done in the same order for all participants. The order of the conditions is the same order as they are described in the report below, as well as how they are shown in Fig. 7. All trials were done directly after one another without pauses.

Before the pushing trials, a single 1 minute baseline trial is done in which the participant walks at 0.5 m/s without the pushers attached. This trial is used as a comparison between unperturbed walking gait with and

without pusher.

For condition 1, a singular thigh push of 40 N is applied. This condition is identical to one of the conditions of the previous research to assess whether it is possible to replicate the results of the previous research with the current setup.

Condition 2 is a pull with the shank perturbator with a force of 40 N. This condition assesses the feasibility of the shank perturbator to effectively perturb the ankle joint, and to see how the shank perturbator perturbs the other joints.

Two different types of combined pushes are used to assess their effectiveness and to find which perturbation combination may allow for better perturbing of all joints simultaneously. For condition 3, a combined push is chosen in which the thigh pusher gives a push of 40 N and the shank pusher gives a push of 70 N. The increased amplitude for the shank is chosen as a result of the larger lower leg velocities during swing phase.

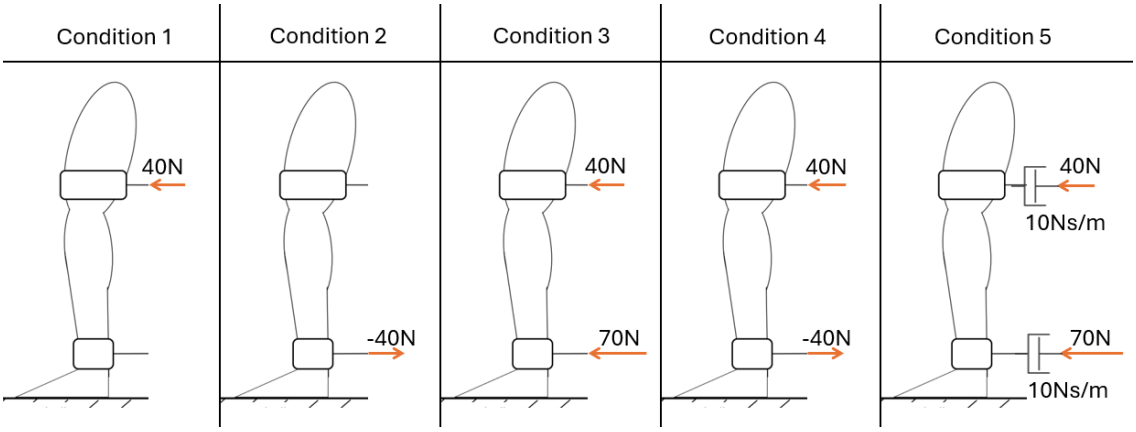

Figure 7: The 5 different conditions used in the experiments. Condition 5 is the same as condition 3 with added damping on the controller. All trials are done using 20 pushes and with the participant walking at 0.5 m/s at a self-selected cadence.

Condition 4 is a thigh push of 40 N and a shank pull of 40 N. This perturbation combination is chosen for two distinct reasons. Firstly, it was found in pilot testing that a singular shank push of 70 N does not meaningfully perturb any of the joints in the leg, but a shank pull of 40 N does perturb the ankle. Secondly, it is believed that the combined push of both the shank and the thigh pusher might cause the knee joint response of the thigh pusher to be counteracted by the shank pusher, causing no perceptible knee joint angle deviation. Therefore it is hypothesised that a combined push-pull may give better joint angle responses.

Condition 5 uses the same combined push of 40N for the thigh and 70N for the shank as in condition 3. In this condition however, the damping constant of the controller, B_v, was increased with 10 Ns/m during walking. This is done to see if the model would be able to correctly estimate the joint impedance during changed walking circumstances. Due to results of the transparency analysis of objective 1, the joint impedance estimations were not completed. Therefore the results of this conditions are not discussed in this work any further. The Experimental results from these experiments are provided in Appendix C for further reference.

2.3 Data collection

The participant walks on a split belt treadmill (Bertec, Columbus, OH) which also measures the Ground Reaction Forces (GRF) of the participant during walking. All force data from the treadmill and load cells, and the motor encoder values are connected to a Master PC which runs an EtherCAT real-time protocol built as a simulink Model (Matlab 2018b, Mathworks US). This system collects and saves all data. It controls

the LOPER pushers using the load cell data as input. All data processing and collection is done at 1000 Hz. In addition to the force and motor data collected, the system also collects motion capture (Qualysis AB, Sweden) and Electromyography data (EMG) (Delsys NA, US). The motion capture is collected with 8 Oqus 600+ cameras. The human motion is collected using a 35 Marker setup on the body. The markers were put on bony landmarks on the participants according to the gait2392 model from OpenSim. The motion capture and the EMG data are collected in Qualysis Track Manager (QTM) at 100 Hz and 2000 Hz respectively. The GRFs are also collected in QTM. Finally a synchronisation signal is sent to both EtherCAT and QTM at 2000 Hz using an analog to digital converter. The EMG sensors are placed on six different muscles: the tibialis anterior, the soleus, the gastrocnemius medialis and lateralis, the rectus femoris, and the biceps femoris. Before starting with testing, Maximum Voluntary Contractions (MVC) are taken from all muscles to normalise the muscle activity for all trials.

2.4 Data Analysis

The data collected from the experiments has been analysed, filtered and parsed. This data required additional processing for comparison of the outcome metrics. First the general data processing will be described. Then the specific methods of gaining the outcome metrics are described.

2.4.1 Data processing

The motion capture, load cell, and GRF data is filtered through a 0-phase 4th order lowpass butterworth filter with a cutoff frequency of 40 Hz. Strides are parsed using the GRFs from left heelstrike to left heelstrike. Using the pusher input data the perturbed steps are collected separately and removed from the other steps. All unperturbed steps are normalised to make them equal in length.

The motion capture data is processed in OpenSim using the gait2392 model. The model is first scaled using a static trial. Afterwards the joint angles, segment angles, and centre of mass position of the pelvis are estimated using the inverse kinematics and analysis tools from OpenSim.

In order to ensure that the data is consistent, outlying gaitcycles are removed from the data as follows. For the unperturbed steps, the average and standard deviation of the joint angles are taken. For each point in a gaitcycle, a point is considered an outlier if the difference between that point and the average is more than 1.5 the interquartile range. If a given step has more than 20 % outliers in it, the entire step is considered an outlier and removed from the data set.

2.4.2 Outcome metrics

2.4.2.1 Transparency

The LOPER should not influence the walking gait of the participant when no perturbation is applied. For any interaction may influence the walking gait of the participant, and therefore change it compared to regular walking gait in daily life. This means that the LOPER needs to be sufficiently transparent during unperturbed walking gait. In the previous research, three criteria have been set that test the transparency of the pusher setup. It is believed that the system is sufficiently transparent if these criteria are met [1].

The first criteria states that the average difference between the joint angles of the unperturbed steps of a given participant should be lower than twice the standard deviation of the walking gait without the pusher of all participants. This metric is called the average Intra-participant variability (ISV). This means that if the root mean square (rms) difference between walking with and without the pusher for a single participant is smaller than twice the average intra-participant variability, it is assumed that walking with the pusher is considered regular [34].

The second and third criterion both consider the interaction forces of the pushers during unperturbed walking gait. For the second criterion it is stated that the total rms of the forces during both stance and swing phase should be lower than 10 N. The third criterion is that the average peak interaction forces during unperturbed walking gait should not exceed 20 N. If these two criteria are also met, it can be assumed that the pushers

do not meaningfully change the unperturbed walking gait [1, 34].

Finally, in addition to these criteria, the average cadence and normalised toe off point during the unperturbed gait are also calculated for the trials with and without the pushers attached. These are used to see the further effects of the pusher on the walking pattern. These metrics also help visualise if the walking gait may change in any other ways which may not become apparent when only considering the interaction forces.

2.4.2.2 Joint angle response

In order to be able to use the LOPER setup for joint impedance estimations, it is also necessary that the joint angles are sufficiently perturbed due to the pushes. There is no set criterion yet given for how strong a perturbation has to be to allow accurate joint impedance estimations. Therefore, a new criterion has been set in this report based on the previous research done by van der Kooij et al. and Lee et al. Based on the average peak joint angle response reported by Lee et al. and van der Kooij et al. It is expected that the joint angle responses need to at least deviate 0.07 radians compared to unperturbed walking in order for them to be used effectively for joint impedance estimation [1, 28]. Using this new set criterion, the joint angle responses will be assessed as follows to see if the perturbations in this research are sufficient.

For the perturbed joint angles, the joint angles are collected from left toe off until 0.5 s after toe off. Both the unperturbed and perturbed joint angles are averaged and the rms difference between the unperturbed and perturbed steps is taken for each participant. The maximum of this difference is taken for each participant and for each condition. As no maximum joint angle deviations have been given as angles, only the plots of the joint angle deviations of this research have been compared to the average plots of the previous research.

In addition to the joint angle responses, the force tracking during and directly after the perturbations are assessed in order to better compare the actual joint angle output with the perturbation input. The load cell data is parsed into segments of 0.5 s starting from left toe off. All the unperturbed steps are collected and averaged, and outliers are removed similarly to the joint angles in the transparency analysis using the interquartile range. The average of the unperturbed steps is then used to normalise all the perturbed steps. These steps are then plotted against the input of the pushers to visualise the perturbation responses during walking gait. The rise time and the overshoot cannot be calculated as no steady state is achieved during these perturbations.

3 Results

The experiments have successfully been completed on 10 different participants (4 male 6 female) (23.0±2.3 years 1.73±0.124 m, 68.2±12.1 kg). The sex, age, length and mass of each participant can be found in Tab. 1. One participant (participant 5) had to be disqualified as they did not meet the inclusion criteria due to a prior knee injury. All subjects are perturbed 19 times during all testing, as the last perturbation was not applied correctly because of a software bug that became apparent during post-processing.

Table 1: All participant info from the experiments. Due to a knee injury, participant 5 has been excluded from this research, and has not been assessed in any of the results.

Participant	1	2	3	4	5	6	7	8	9	10
Age	23	26	18	23	21	19	25	23	24	22
Sex	m	f	m	f	f	f	m	m	f	f
Height	1.71m	1.64m	1.80m	1.64m	1.65m	1.62m	1.92kg	1.93m	1.60m	1.69m
Mass	71kg	65kg	68kg	64kg	58kg	62kg	88kg	87kg	55kg	57kg
K_s thigh	0.50	0.65	0.50	0.50	0.60	0.60	0.55	0.40	0.55	0.60
K_s shank	0.65	0.75	0.60	0.70	0.65	0.70	0.60	0.60	0.70	0.75

3.1 Transparency

3.1.1 Unperturbed joint angles

In order to assess the transparency of the system, both the joint angles and the interaction forces during the unperturbed steps have to be assessed. For the ankle joint, the joint angle deviation is larger during the swing phase than during the stance phase (Fig. 8, lowest plot). This corresponds to the interaction forces of the shank pusher (Fig. 8, top plot, purple line). At the start of the stance phase, there is consistent oscillatory behaviour in the shank and thigh pusher. These oscillations cause minor oscillations in the ankle joint at the start of the stance phase. The thigh pusher has the largest interaction forces at the end of the stance phase. The hip joint angle deviation is highest at the same time at the end of the stance phase (Fig. 8 1st and 2nd plot).

In order for the walking of the participants to be considered unaltered by the LOPER, the first criterion stated in [1] should be met. This criterion stated that the average joint angle deviations should not be larger than the $\bar{\text{ISV}}$. the $\bar{\text{ISV}}$ is 0.044 ± 0.009 rad, 0.076 ± 0.021 rad, and 0.043 ± 0.009 rad for the hip, knee and ankle joint respectively. The average of all joint angle deviations with the LOPER attached are 0.054 ± 0.015 rad for the hip, 0.089 ± 0.014 rad for the knee, and 0.072 ± 0.010 rad for the ankle during stance phase. During swing phase these joint angle deviations increase to 0.073 ± 0.018 rad, 0.209 ± 0.037 rad, and 0.089 ± 0.009 rad. The criterion set is therefore not met for any of the joints during unperturbed walking. This means that the walking gait with the LOPER attached cannot be considered regular. In Fig. 9a the average joint angle deviations can be seen for all participants as well as for the total average. During both stance and swing phase, several subjects have one or two joints beneath the $\bar{\text{ISV}}$. However, none of the subjects have an average joint angle error that is lower than the $\bar{\text{ISV}}$ for all joint angles at the same time in the stance or swing phase.

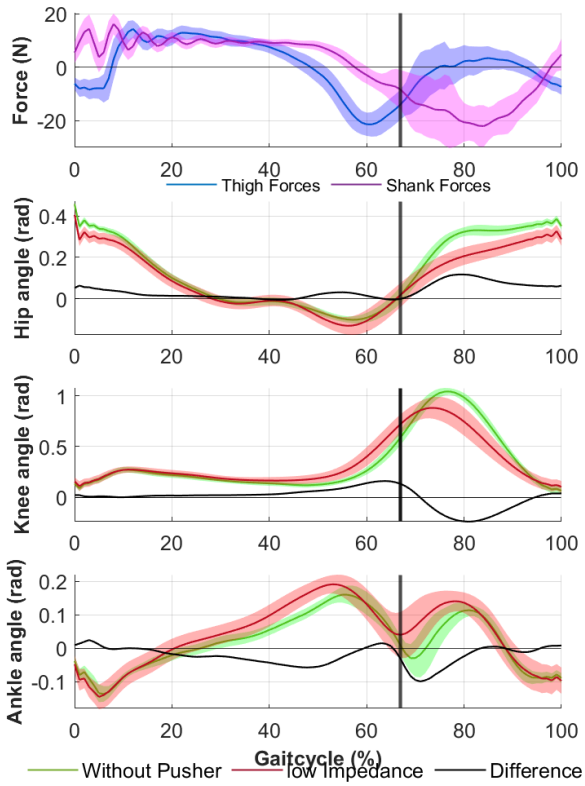

Figure 8: The top plot shows the average (line) and standard deviations (shaded area) of the thigh (blue) and shank (purple) forces during a gait cycle. The bottom three plots show the average and standard deviations of the joint angles during unperturbed steps with (red) and without (green) the pusher attached to the leg, as well as the difference (black). The vertical black line corresponds to the average normalised toe off point during the gait cycle. Oscillations during the beginning of the stance phase are a results of the controller responding to heel strike. The forces are highest just before and after toe off. The largest joint angle deviations also happen just after or before toe off.

3.1.2 Interaction forces

In order to assess whether the double pusher setup does not meaningfully influence the walking of the participants, the results are compared to the two criteria set by van der Kooij et al. The first criterion states that the rms force should be < 10 N at all times. The second criterion states that the maximum force during walking gait should be < 20 N at all times [1]. The root mean square forces are 10.0 ± 1.20 N and 8.14 ± 0.86 N for the thigh and shank respectively during stance phase, and they are 4.80 ± 0.98 N for the thigh and 13.7 ± 1.49 N for the shank during swing phase. The maximum forces found during unperturbed walking gait are: 20.63 ± 3.71 N and 15.20 ± 4.02 N for the thigh and shank respectively. From here it can be seen that the thigh does not meet the first criterion during the stance phase, and the shank pusher does not meet the first criterion during swing phase. The thigh pusher also does not meet the second criterion. When comparing the current experimental results to the set criteria it becomes clear that the setup is not sufficiently transparent for joint impedance estimation.

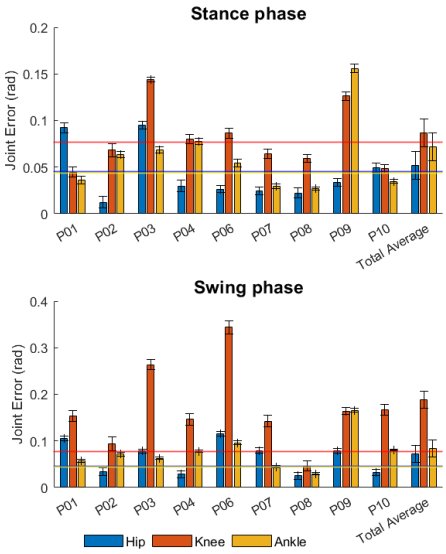

(a) The rms joint angle error during unperturbed steps when compared to walking without a pusher attached. Top figure is during stance phase and the bottom is the swing phase. The horizontal lines are the ISV_{av}, with the colour corresponding to the specific joint. the average does not satisfy the condition of being smaller than the interpersonal difference during either swing or stance phase. None of the participants satisfy the criterions with all joints during either swing or stance phase.

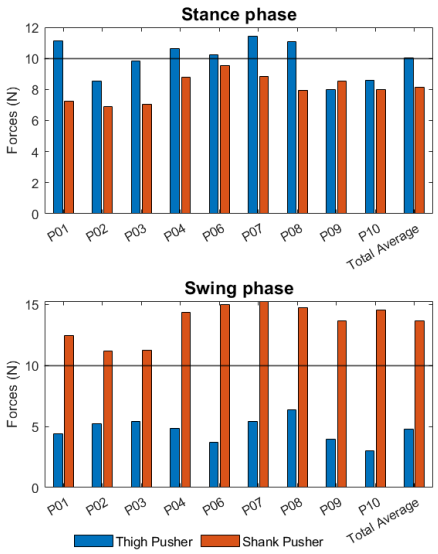

(b) The rms thigh and shank forces during unperturbed gait of the different subjects and the total average. Top figure is during stance phase and the bottom is the swing phase. The horizontal black line is the 10 N mark which corresponds to the transparency criterion set.

Figure 9: The mean joint angle deviations and forces during unperturbed steps compared to walking without the pusher device attached.

3.1.3 General gait analysis

The average and standard deviation of the forces and joint angles during walking with and without the pusher attached can be seen in Fig. 8. The biggest errors are created just before and after toe off. This corresponds to the peak interaction forces for both the thigh and shank pusher. The toe off point changes from 62 % to 59 % of the gait cycle when the pusher is attached. The average cadence does not change when comparing walking with and without the pusher. However, specific subjects seem to either increase or decrease their cadence. The latter suggests different possible adaptation strategies. In appendix 2 the table can be found with the participant specific cadences and the different toe off points.

Table 2: Different gait parameters For specific participants and the total average. When looking at the different cadences with and without the pushers, it can be seen that specific participants either tend increase or decrease their cadence.

		1	2	3	4	5	7	8	9	10	Total Average
Cadence (Strides/minute)	Without LOPER	33.2	36.9	35.9	41.5	53.1	37.1	35.4	34.0	39.0	38.5
	With LOPER	32.0	37.8	31.9	41.5	50.3	38.2	35.0	36.7	41.3	38.3
	With LOPER and Damping	31.6	35.5	30.6	39.7	52.0	35.3	36.1	33.3	38.4	36.9
Toe Off point normalised (%)	Without LOPER	69.4	70.9	69.6	69.2	70.4	71.5	69.2	69.3	62.2	69.1
	With LOPER	66.8	65.4	65.7	64.8	66.9	66.8	65.1	67.2	58.8	65.3
	With LOPER and Damping	63.3	61.9	59.7	62.1	63.5	66.1	59.1	64.0	55.5	61.7

3.2 Joint Angle Response

Each perturbation condition has a unique effect on each of the joints. Fig. 13 shows the average joint angle responses of one participant during the the perturbations of condition 3 (combined thigh and shank push). For a complete overview, appendix D.2 shows the complete overview of all the joint angle responses of all participants for each condition.

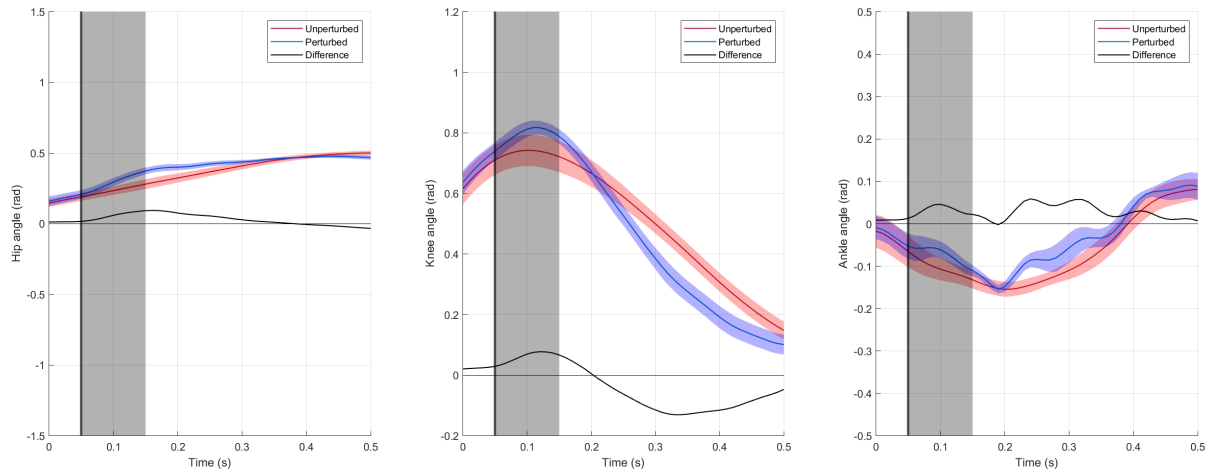

(a) (b) (c)

Figure 10: The joint angle responses of participant 8 for the condition 3 perturbation (combined push). This participant was chosen to show the ideal joint angle responses. The blue line is the perturbed joint angles and the red the unperturbed joint angles. The black line shows the difference between the perturbed and unperturbed joint angles. The shaded area indicates the time window in which the perturbation is applied.

The criterion set in section 2.4.2 stated that a peak joint angle deviation of at least 0.070 rad is necessary for sufficient deviation for the purposes of joint impedance estimation. Fig. 11 and tab. 3 show the average joint angle responses of the different conditions, as well as the participant specific responses. On average, all perturbations led to a sufficient knee flexion for it to satisfy the criterion (0.077-0.178 rad). The ankle joint sufficiently deviated whenever the shank pusher (conditions 2-5) perturbed the leg (0.071-0.091 rad), but showed a weak response during only thigh perturbations (condition 1) (0.038 rad) as is expected from the previous results from H. vd Kooij. This confirms the hypothesis that the shank pusher is capable of effectively perturbing the ankle joint. The hip joint showed minimal response to the perturbations (conditions 1, 2, 4, 5) (0.029-0.051 rad), only satisfying the condition during the combined push (condition 3) (0.074 rad). Comparing the results to the joint angle response criterion. Only condition 3 satisfies the criterion.

Condition 1 only meaningfully perturbs the knee joint angle, leading to a weak response from the hip and a minimal response from the ankle angle. When comparing the joint angle deviations from this research with the previous results, the perturbations have elicited a similar response from all joint angles. The condition 2 perturbations only leads to a response from the ankle angle. Showing no real response from either the knee or the hip. Both combined perturbation conditions (3 and 4) elicited a larger joint angle response compared to the single perturbations (1 and 2). The hip joint seems to be have a bigger reaction however to condition 3 than 4. However, the knee seems to have a stronger perturbation reaction to the condition 4 perturbation. The ankle does not meaningfully change in perturbation response when comparing the condition 3 or condition 4 perturbation.

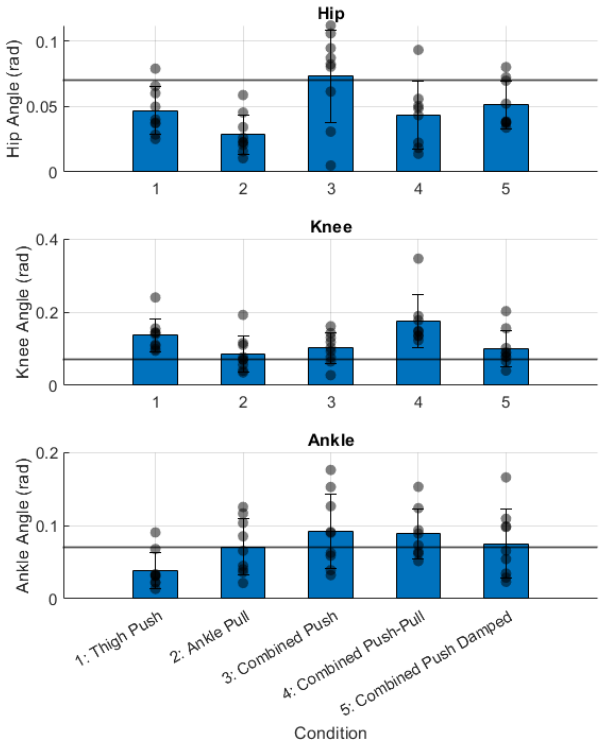

Figure 11: The average peak joint angle responses as a result of the perturbations. The blue bars are the total average for each condition. Each black dot corresponds to the average joint angle response of a single participant. The black bar denotes the minimum joint angle response needed as was set in the criterion discussed in Sections 2.4.2.2

Table 3: The average peak joint angle response per condition for each joint. The responses are given in radians. Only condition 3 shows sufficient joint angle responses to fulfil the criterion set in this research.

	1: Thigh Push	1: Shank Pull	3: Combined Push	4: Combined Push-Pull	5: Combined Push with Damping
Hip	0.047	0.029	0.074	0.043	0.051
Knee	0.137	0.085	0.102	0.175	0.100
Ankle	0.038	0.071	0.092	0.089	0.075

4 Discussion

The goal of this research is to assess the feasibility of a double pusher setup for the purposes of joint impedance identification of the hip, knee, and ankle joints. This feasibility analysis has been done by comparing the results from this research to the transparency criteria set in the previous research by van der Kooij et al. in [1], and a new criterion set in this research based on previous joint impedance identification from van der Kooij et al, and Lee et al. [1, 19]. None of the transparency criteria have been met with the current setup, the joint angle response criterion has been met by all joints only during condition 3.

4.1 Transparency

When compared to the previous research, the average unperturbed joint angle deviations of the double pusher setup have substantially worsened. The joint angle deviations have more than doubled in both the swing and stance phase. This is a result of the substantially lowered transparency of the pusher setup in this research. The rms thigh pusher interaction forces have increased 5-fold during stance phase, and have doubled during swing phase. The maximum interaction forces have also increased over 5-fold. Though no direct comparison can be made for the shank pusher compared to the previous research. It exceeds rms interaction force criterion during the swing phase. Due to the lowered transparency, the participants need to put in more active effort to move their leg which influences their walking gait. For this reason, the unperturbed walking gait during this research cannot be considered "regular".

The mathematical model is built upon the assumption that unperturbed walking gait uses only 'feed-forward' control for walking. This means that in general, the body would not need to correct the walking gait in real time [1]. As the current setup most certainly forces feed-back control from the human due to the high interaction forces, this assumption becomes false. This means that the joint impedance estimations will not be able to correctly model the real world phenomenon, which will lead to inaccuracies as it would not be able to correctly model the human feed-forward and feed-back control separately. Moreover, the joint stiffness and damping will be higher at the start of the perturbation than it would be in "regular" pure feed-forward walking. This is because of the increased muscle activity needed to accommodate the higher impedance required when walking with the resistance of the pusher attached. This, in turn, creates a different response and subsequent impedance value estimations. Therefore, in order for this setup to be used effectively with the purposes of joint impedance estimation, a more transparent robotic controller will have to be used in order to lower the interaction forces and create a more "regular" walking gait during unperturbed steps. For these purposes it would be good to assess the previous steps taken in appendix B and use the recommendations set in this section, those state that it is believed that the best course of action would be to create a new controller which better satisfies the requirements of this setup.

4.2 Joint Angle Response

For the joint angle responses, only condition 3 has reached the criterion stated in this research. The criterion set in this research is set to be specific enough to guarantee sufficiently large joint angle responses for joint impedance estimation. However, due to minimal reporting of the actual joint angle responses of the joints in the leg during joint impedance estimations, it is hard to create a correct idea of the exactly needed joint angle responses needed. This means that the currently used condition is not very sensitive, and smaller joint angles responses may suffice as well, particularly for the hip joint. The combined push-pull perturbation used in condition 4 may for example be of particular interest to be used in the future despite not satisfying the condition for the hip joint. This is because, although the hip joint does not satisfy the condition set in this research, the joint angle response of the hip is very similar to the joint angle response found in condition 1 of this research. Since condition 1 is known to be capable of correctly, and accurately estimating the joint impedance of the hip. Condition 4 may therefore also be capable of correctly estimating the joint impedance of all three joints of the leg during walking. Comparing the estimations of the joints may also help in setting a more accurate standard to be used in future joint impedance estimation research.

Next to the results discussed in the previous paragraph, some interesting observations have been found. First and foremost, Fig. 13 shows that the ankle joint oscillates during the swing phase even after the pertur-

bation. Using Fig. 12, this phenomenon may be explained by the strong oscillations of the shank pusher after the perturbation, most likely due to minimal stability of the system. The knee joint has a tendency to overcompensate after perturbations. If such a response is for example a specific active response to correct incorrect leg positions, then it is of interest to evaluate the mechanisms which cause this response.

4.2.1 Perturbation Force Tracking

To properly understand the nature of the joint angle responses, it is of interest to compare this to the actual perturbations given to the leg. Therefore, a quantitative analysis of the pusher responses was attempted. This analysis did not prove to be useful. As seen in Fig. 12, the pushers are unable to reach a steady state during the perturbations before the perturbation was over. This makes more in depth quantitative analysis on the pushers during walking gait difficult, as no overshoot or rise-time compared to a steady state can be calculated. This may in part be due to the weak transparency of the system, it takes the pusher ∼50 ms to reach the maximum value (fig 12), compared to 20 ms of the previous research [1].

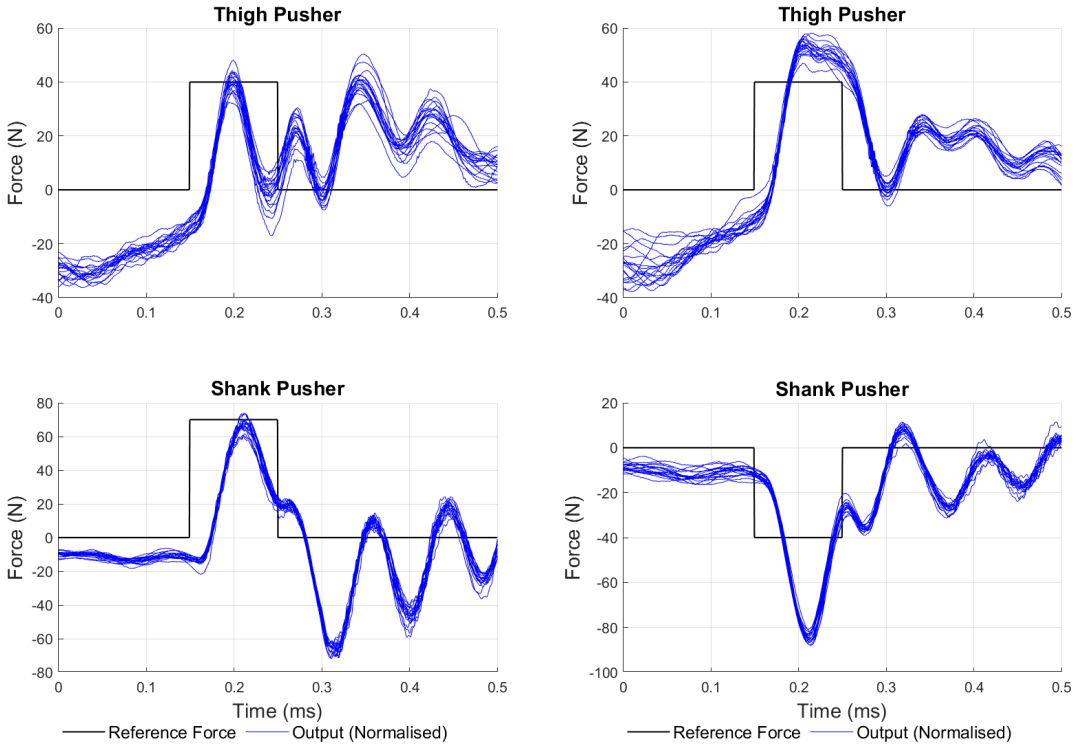

(a) The pusher responses during the combined push trial without added damping (condition 3)

(b) The pusher responses during the combined push-pull trial without added damping (condition 4)

Figure 12: Pusher Response of participant P09 during the condition 3 combined push (a) perturbation and the condition 4 combined push-pull (b) perturbation. The thigh pusher shows a different response between the two perturbation types, most likely due to different segment velocities as a result of the shank pusher.

The lack of steady state and long rise time may be ascribed to the dynamic circumstances during the pushes. The previous research only tested the perturbation response during static conditions with a free hanging leg [1]. The fact that the perturbations did not reach a steady for example, could also be described due to the fact that the participant's leg was continuously adapting to the perturbations. It may still be of interest to compare the perturbations given by the pushers during these dynamic conditions however, as the conditions are then similar to those in which the perturbations will be given during the actual joint impedance estimation.

4.3 Limitations

In this research, it has become clear that as of current, the expanded LOPER setup is not yet capable of being used for experiments with the purpose of joint impedance estimation. This is mainly due to the poor transparency and stability of the system. Therefore, it is imperative to tune or rebuild the controller before continuing with joint impedance estimation using this setup.

Furthermore, the model and setup are still limited to only the swing phase of walking. If stance phase impedance values are to be evaluated, an expansion of the mathematical model is needed. This would allow for joint impedance estimation of all joints during the entire gait cycle using only one setup.

Currently the perturbations are relatively slow due to the force tracking of the system. As it has been shown that perturbation speed does influence the joint impedance [22]. This would require position or velocity perturbations to allow for joint impedance estimations under more conditions.

The setup is only able to estimate the impedance values in the Anterior-posterior direction. This would mean that any sideways perturbations, and the resultant joint impedance values in these directions cannot be compared as of now.

Another major limitation in this research has been that certain gait parameters have shown to be very subject specific, at times even showing two different responses between groups participants, as can be seen in Appendix 2 and E. This means that averages may not show a good representation of reality, and general remarks about phenomena found are not possible on the scale used for this research. For this reason, using larger subject populations would the different responses to be clustered together, and as such get a better understanding of different control mechanisms used by the human body.

4.4 Feasibility of experimental setup and future recommendations

For now the setup is not yet ready to be used. First and foremost, a new controller will have to be designed for the system in order to have a system which is transparent enough to allow for reasonably "regular" gait during unperturbed steps. If this controller is built, at least one condition (condition 3) will be capable of giving perturbations which result in a sufficiently large joint angle response for the purposes of joint impedance estimation.

When designing and testing this new controller, a reevaluation and further testing of the currently set criteria for both the transparency and joint angle responses can be valuable. All criteria are currently based on previous literature which was not focused on setting these standards. Creating better and more accurate criteria for setups such as these creates a standard. Such a standard would allow for the easier design and improvement of this and similar setups that focus on joint impedance estimation. This can help in particular for future joint impedance estimations under a wider range of conditions such as faster walking speeds, impaired walking, or other other types of perturbations.

When redesigning the controller, an expansion of the controller, allowing for position or velocity perturbations is also of added value. These perturbations would be faster and allow for comparing the passive impedance with the active neurological response during walking gait [22].

When a new and improved transparent system is created, the setup does show promise to correctly estimate the joint impedance values of all the leg joints during regular walking. For future tests delayed combined perturbations could be an interesting direction to experiment. These perturbations would work by letting one pusher deliver their perturbation with a slight delay compared to the other perturbation. This may influence the impedance values during walking due to differing muscle activities in the upper and lower leg for example. Moreover, if the joint impedance values of the leg in later stages of the swing phase are to be researched, a new system will be needed to allow for swing phase progression estimation regardless of the

current walking gait cadence. This is particularly necessary as people with neural impairments have a larger walking gait have a larger variability in their walking gait [38]. One such a system could be using real time pusher or motion capture marker position data as a basis for when to perturb the leg.

5 Conclusion

The goal of this research is to assess the feasibility of the expanded double pusher setup in order to do perturbation experiments which could be used to accurately estimate the joint impedance values of the the ankle, hip and knee joints of the leg during the swing phase of regular walking gait. This was tested by assessing the transparency of the double pusher setup during unperturbed steps, and the joint angle deviation during perturbations using three criteria set up in the previous research and a new criterion set up in this research based on literature.

During unperturbed steps, the double pushers had an rms interaction force of 13.7 ± 1.49 N and 15.2 ± 4.02 N for the thigh and shank respectively during the swing phase. The maximum forces for the thigh and shank were: 20.63±3.71 N and 15.20±4.02 N. The error between the joint angles with and without pusher were larger than the ISV_{av}. Using the three criteria set by Van der Kooij et al. As of now, the double pusher setup is not yet sufficiently transparent to allow for proper joint impedance estimation as the expanded LOPER setup does not satisfy any of the conditions [1]. The combined pushes show promise in successfully perturbing all three joints during the swing phase to allow for joint impedance estimations when compared to perturbations by a singular pusher. The doube push perturbation of condition 3 was able to satisfy the criterion set up in this research of generating a joint angle response greater than 0.07 rad for all three joints simultaneously. Therefore this particular perturbation will be capable of delivering sufficiently strong enough perturbations. Due to the limited data used to set the criterion for the joint angle response perturbations however, other perturbation combinations should not be disregarded for future testing as these could also elicit a sufficiently large response.

According to the criteria set by this and the previous research, the current setup is not yet ready to be used to estimate the joint impedance values due to the poor transparency of the system. However, if a new controller would be implemented this would increase the transparency. This should decrease the interaction forces and therefore also lead to a more "regular" walking gait which would satisfy the transparency criteria set in [1]. The combined pushes give promising results, suggesting that these are useful for the purposes of joint impedance estimation, if the transparency criteria are met.

A References

[1] Herman van der Kooij et al. "Identification of Hip and Knee Joint Impedance During the Swing Phase of Walking". In: *IEEE Transactions on Neural Systems and Rehabilitation Engineering* 30 (2022), pp. 1203–1212. DOI: 10.1109/TNSRE.2022.3172497.

[2] M Patrice Lindsay et al. "World Stroke Organization (WSO): Global Stroke Fact Sheet 2019". In: (). DOI: 10.1177/1747493019881353. URL: http://ghdx.healthdata.org/gbd-results-tool.

[3] W Ding et al. "Spinal cord injury: the global incidence, prevalence, and disability from the global burden of disease study 2019". In: *journals.lww.com* (). URL: https://journals.lww.com/spinejournal/fulltext/2022/11010/Spinal_Cord_Injury__The_Global_Incidence,.8.aspx.

[4] Amanda L. Shorter and Elliott J. Rouse. "Mechanical Impedance of the Ankle during the Terminal Stance Phase of Walking". In: *IEEE Transactions on Neural Systems and Rehabilitation Engineering* 26.1 (Jan. 2018), pp. 135–143. ISSN: 15344320. DOI: 10.1109/TNSRE.2017.2758325.

[5] *Spinal cord injury.* URL: https://www.who.int/news-room/fact-sheets/detail/spinal-cord-injury.

[6] Juan-Manuel Belda-Lois et al. "Rehabilitation of gait after stroke: a review towards a top-down approach". In: *Journal of NeuroEngineering and Rehabilitation* 8 (2011), p. 66. DOI: 10.1186/1743-0003-8-66. URL: http://www.jneuroengrehab.com/content/8/1/66.

[7] Stefano Masiero et al. "The value of robotic systems in stroke rehabilitation". In: *Expert Review of Medical Devices* 11.2 (2014), pp. 187–198. ISSN: 1745-2422. DOI: 10.1586/17434440.2014.882766. URL: https://www.tandfonline.com/action/journalInformation?journalCode=ierd20.

[8] Daniel M. Wolpert, Jörn Diedrichsen, and J. Randall Flanagan. "Principles of sensorimotor learning". In: *Nature Reviews Neuroscience 2011 12:12* 12.12 (Oct. 2011), pp. 739–751. ISSN: 1471-0048. DOI: 10.1038/nrn3112. URL: https://www.nature.com/articles/nrn3112.

[9] Giovanni Morone et al. "Robot-assisted gait training for stroke patients: current state of the art and perspectives of robotics Neuropsychiatric Disease and Treatment Dovepress Robot-assisted gait training for stroke patients: current state of the art and perspectives of robotics". In: (2017). DOI: 10.2147/NDT.S114102. URL: https://www.tandfonline.com/action/journalInformation?journalCode=dndt20.

[10] Alberto Esquenazi, Mukul Talaty, and Arun Jayaraman. "Narrative Review Powered Exoskeletons for Walking Assistance in Persons with Central Nervous System Injuries: A Narrative Review". In: (). DOI: 10.1016/j.pmrj.2016.07.534. URL: https://onlinelibrary.wiley.com/doi/10.1016/j.pmrj.2016.07.534.

[11] Alberto Esquenazi et al. "A Comparison of Locomotor Therapy Interventions: Partial-Body Weight-Supported Treadmill, Lokomat, and G-EO Training in People With Traumatic Brain Injury". In: *PM&R* 9.9 (Sept. 2017), pp. 839–846. ISSN: 1934-1563. DOI: 10.1016/J.PMRJ.2016.12.010. URL: https://onlinelibrary.wiley.com/doi/full/10.1016/j.pmrj.2016.12.010%20https://onlinelibrary.wiley.com/doi/abs/10.1016/j.pmrj.2016.12.010%20https://onlinelibrary.wiley.com/doi/10.1016/j.pmrj.2016.12.010.

[12] R. E. Kearney and I. W. Hunter. "Dynamics of human ankle stiffness: Variation with displacement amplitude". In: *Journal of Biomechanics* 15.10 (Jan. 1982), pp. 753–756. ISSN: 0021-9290. DOI: 10.1016/0021-9290(82)90090-2.

[13] Daniel Ludvig et al. "Estimation of Joint Impedance Using Short Data Segments". In: (). DOI: 10.1109/IEMBS.2011.6091023.

[14] Serena Maggioni et al. "Robot-aided assessment of lower extremity functions: a review". In: *Journal of NeuroEngineering and Rehabilitation 2016 13:1* 13.1 (Aug. 2016), pp. 1–25. ISSN: 1743-0003. DOI: 10.1186/S12984-016-0180-3. URL: https://link.springer.com/articles/10.1186/s12984-016-0180-3%20https://link.springer.com/article/10.1186/s12984-016-0180-3.

[15] Elliott J. Rouse et al. "Estimation of human ankle impedance during the stance phase of walking". In: *IEEE Transactions on Neural Systems and Rehabilitation Engineering* 22.4 (2014), pp. 870–878. ISSN: 15344320. DOI: 10.1109/TNSRE.2014.2307256.

[16] David T Westwick and Eric J Perreault. "Estimates of Acausal Joint Impedance Models". In: (). DOI: 10.1109/TBME.2012.2213339.

[17] P. L. Weiss, R. E. Kearney, and I. W. Hunter. "Position dependence of ankle joint dynamics—II. Active mechanics". In: *Journal of Biomechanics* 19.9 (Jan. 1986), pp. 737–751. ISSN: 0021-9290. DOI: 10.1016/0021-9290(86)90197-1.

[18] I. W. Hunter and R. E. Kearney. "Dynamics of human ankle stiffness: Variation with mean ankle torque". In: *Journal of Biomechanics* 15.10 (Jan. 1982), pp. 747–752. ISSN: 0021-9290. DOI: 10.1016/0021-9290(82)90089-6.

[19] Hyunglae Lee and Neville Hogan. "Time-varying ankle mechanical impedance during human locomotion". In: *IEEE Transactions on Neural Systems and Rehabilitation Engineering* 23.5 (Sept. 2015), pp. 755–764. ISSN: 15344320. DOI: 10.1109/TNSRE.2014.2346927.

[20] Yves Nazon. *Estimation of Knee Joint Impedance During Walking and Its Implications for Robotic Control and Beyond*. Tech. rep. Michigan: University of Michigan, 2024. URL: https://deepblue.lib.umich.edu/handle/2027.42/193279.

[21] Piet Lammertse. *Admittance control and impedance control - a dual*. Tech. rep. 2004.

[22] Erwin de Vlugt et al. "Short range stiffness elastic limit depends on joint velocity". In: *Journal of Biomechanics* 44.11 (July 2011), pp. 2106–2112. ISSN: 0021-9290. DOI: 10.1016/J.JBIOMECH.2011.05.022.

[23] HY Huang et al. "The influence of posture, applied force and perturbation direction on hip joint viscoelasticity". In: *ieeexplore.ieee.orgHY Huang, A Arami, I Farkhatdinov, D Formica, E BurdetIEEE Transactions on Neural Systems and Rehabilitation Engineering, 2020•ieeexplore.ieee.org* (). URL: https://ieeexplore.ieee.org/abstract/document/9047926/.

[24] Bram Koopman, Edwin H.F. Van Asseldonk, and Herman Van Der Kooij. "Estimation of Human Hip and Knee Multi-Joint Dynamics Using the LOPES Gait Trainer". In: *IEEE Transactions on Robotics* 32.4 (Aug. 2016), pp. 920–932. ISSN: 15523098. DOI: 10.1109/TRO.2016.2572695.

[25] Robert E. Kearney, Richard B. Stein, and Luckshman Parameswaran. "Identification of intrinsic and reflex contributions to human ankle stiffness dynamics". In: *IEEE Transactions on Biomedical Engineering* 44.6 (June 1997), pp. 493–504. ISSN: 00189294. DOI: 10.1109/10.581944.

[26] Li Qun Zhang et al. "In vivo human knee joint dynamic properties as functions of muscle contraction and joint position". In: *Journal of Biomechanics* 31.1 (Nov. 1997), pp. 71–76. ISSN: 0021-9290. DOI: 10.1016/S0021-9290(97)00106-1.

[27] Daniel Ludvig et al. "Mechanisms contributing to reduced knee stiffness during movement". In: *Experimental Brain Research* 235.10 (Oct. 2017), pp. 2959–2970. ISSN: 14321106. DOI: 10.1007/S00221-017-5032-2/FIGURES/8. URL: https://link.springer.com/article/10.1007/s00221-017-5032-2.

[28] Hyunglae Lee, Elliott J. Rouse, and Hermano Igo Krebs. "Summary of Human Ankle Mechanical Impedance during Walking". In: *IEEE Journal of Translational Engineering in Health and Medicine* 4 (2016). ISSN: 21682372. DOI: 10.1109/JTEHM.2016.2601613. URL: https://ieeexplore.ieee.org/document/7547952.

[29] Amanda L. Shorter et al. "Characterization and clinical implications of ankle impedance during walking in chronic stroke". In: *Scientific Reports 2021 11:1* 11.1 (Aug. 2021), pp. 1–13. ISSN: 2045-2322. DOI: 10.1038/s41598-021-95737-6. URL: https://www.nature.com/articles/s41598-021-95737-6.

[30] Michael R. Tucker et al. "Design and Characterization of an Exoskeleton for Perturbing the Knee during Gait". In: *IEEE Transactions on Biomedical Engineering* 64.10 (Oct. 2017), pp. 2331–2343. ISSN: 15582531. DOI: 10.1109/TBME.2017.2656130.

[31] Michael R. Tucker. "Development of a Tool and a Method for Estimating Knee Impedance during Gait". In: (2016). DOI: 10.3929/ETHZ-A-010739715.

[32] Christopher Nesler et al. "Enhancing Voluntary Motion with Modular, Backdrivable, Powered Hip and Knee Orthoses". In: (2022).

[33] Jos Meuleman et al. "LOPES II-Design and Evaluation of an Admittance Controlled Gait Training Robot With Shadow-Leg Approach". In: *IEEE TRANSACTIONS ON NEURAL SYSTEMS AND REHABILITATION ENGINEERING* 24.3 (2016). DOI: 10.1109/TNSRE.2015.2511448. URL: http://www.ieee.org/publications_standards/publications/rights/index.html.

[34] Jos H Meuleman, Edwin Hf Van Asseldonk, and Herman Van Der Kooij. "The effect of directional inertias added to pelvis and ankle on gait". In: (2013). URL: http://www.jneuroengrehab.com/content/10/1/40.

[35] Arash Arami et al. "A Clustering-Based Approach to Identify Joint Impedance during Walking". In: *IEEE Transactions on Neural Systems and Rehabilitation Engineering* 28.8 (Aug. 2020), pp. 1808–1816. ISSN: 15580210. DOI: 10.1109/TNSRE.2020.3005389.

[36] Jan F Veneman et al. "Design and Evaluation of the LOPES Exoskeleton Robot for Interactive Gait Rehabilitation". In: *IEEE TRANSACTIONS ON NEURAL SYSTEMS AND REHABILITATION ENGINEERING* 15.3 (2007). DOI: 10.1109/TNSRE.2007.903919.

[37] J Meuleman, E Van Asseldonk - IEEE transactions on ..., and undefined 2015. "LOPES II—design and evaluation of an admittance controlled gait training robot with shadow-leg approach". In: *ieeexplore.ieee.org* (). URL: https://ieeexplore.ieee.org/abstract/document/7369983/.

[38] Melvyn Roerdink et al. "Rhythm Perturbations in Acoustically Paced Treadmill Walking After Stroke". In: *Neurorehabilitation and Neural Repair* 23 (2009), pp. 668–678. DOI: 10.1177/1545968309332879. URL: http://nnr.sagepub.com.

B Changes in setup for Transparency Improvement

The main challenge during this master assignment has been the decreased stability of the setup. This is particularly of note as it is not entirely clear what caused the instability, and therefore why it was needed to lower the transparency in order to make the system stable. Due to the fact that the setup had changed in some hardware ways, but the controller was exactly the same, the choice had been made to focus on changing the physical setup, as it was expected that this was the cause of the lowered stability.

First and foremost the support structure of the LOPER was changed. However, it should be noted that this change had not made any meaningful changes to the performance of the physical setup. The new support towers were more stable, and as they were affixed to the ground instead of to the treadmill, actually resonated and vibrated less with the system, this makes it unlikely that the new dynamics from these support towers would cause the instability. Moreover, pilot testing with the old support structure had been done, and the interaction forces had not changed in any meaningful way compared to the new support towers in these trials.

Secondly, the load cells were attached to the other side of the carbon fibre rods, between the rod and the brace in order to move as much of the dynamics of the physical setup behind the sensors. Additionally, a thicker carbon rod was used between the moment arms and the leg, as the rod had a tendency to buckle when the 70N pushes were applied to the lower leg. The moving of the sensor did not meaningfully change the dynamics of the setup. The thicker, and therefore stiffer carbon rod did allow for a reduction in internal vibrations and was incorporated into the physical setup. The thicker rod also prevented any buckling during testing.

The moment arms of the pushers were also increased in order to allow the motors to require less motion for the system to follow the leg. The moment arm of the shank perturbator was increased up to 0.78m and the thigh arm was increased to 0.53m. However this resulted in less stable behaviour as the increased length of the (shank) perturbator arm changed the internal dynamics of the robot creating stronger, low frequency oscillations in the setup which lowered the stability of the system.

The unstable behaviour may have also been a result of high frequency noise from the load cells. This noise may have led to internal resonance with the moment arms or carbon rods. In order to possibly combat this issue a 4th order low-pass filter was applied over the load cell signal in realtime with a cutoff frequency of 50Hz. This however, did not seem to have any effect on the stability of the system, lowering the cutoff frequency decreased the stability of the setup. Next to this, the moment arms themselves were also reinforced in order to try and increase the stiffness of the system, in order to prevent any resonance with other parts of the system. This did not influence the stability of the experimental setup.

Finally, a parameter sweep was tried on the controller, to see if it was possible to generate a new controller which would have improved stability and transparency. In order to do this K_a was varied between 0.015 and 0.02 in steps of 0.001 and B_v varied between 1.0 and 3.0 in steps of 0.5. During each configuration the c value was tuned to find better results. Using this parameter sweep it was not possible to find a stable and more transparent controller for the current setup. Despite these results, it is still best to try and tune the controller values in the future in order to increase the stability and therefore allowing for a more transparent setup. The reason why this parameter sweep was not sufficient is most likely due to time constraints and not due to a larger problem.

In the end, the cause of the increased instability of the system was not identified or fixed due to time constraints. Before future research is done on this system, it is expected that a new or modified controller will be needed which better is able to remain stable for the required frequency bandwidth of the setup. In order to set up this controller it is suggested to do a more thorough analysis using the frequency bandwith as set up in the previous research [1]. Another possible solution which has not been tried would be to change the input of the controller to be the internal load cells of the motors themselves instead of the load cells used for measuring the interactions between the participant and the robot. Using the data collected in this research, it may even be possible to set up a simple parametric model which could describe the internal dynamics of the pusher system by comparing the internal load cells of the motors and the load cells attached to the moment

arms. This would allow for a more thorough and mathematical controller design and optimisation. This can also allow for more thorough identification of the problem, as then the internal dynamics of the robot and the human can be separated. Due to time constraints it was not possible to do apply these methods in this research however.

C Experimental findings for combined push with added damping

Comparing the unperturbed walking with the regular controller to the unperturbed walking with the added damping, shows that the cadence lowers to 37 strides per minute from the original 39 strider per minute. The relative moment of toe off changes to 61% from 65% with the LOPER without pusher. Together, this means that the swing phase becomes longer, both compared to the stance as in general. The joint angles seem to mainly influence the knee and ankle joint. the interaction forces have more than doubled due to the added damping in the system (Fig.13). The oscillations at the start of the stance phase are lowered substantially as a direct result of the damping.

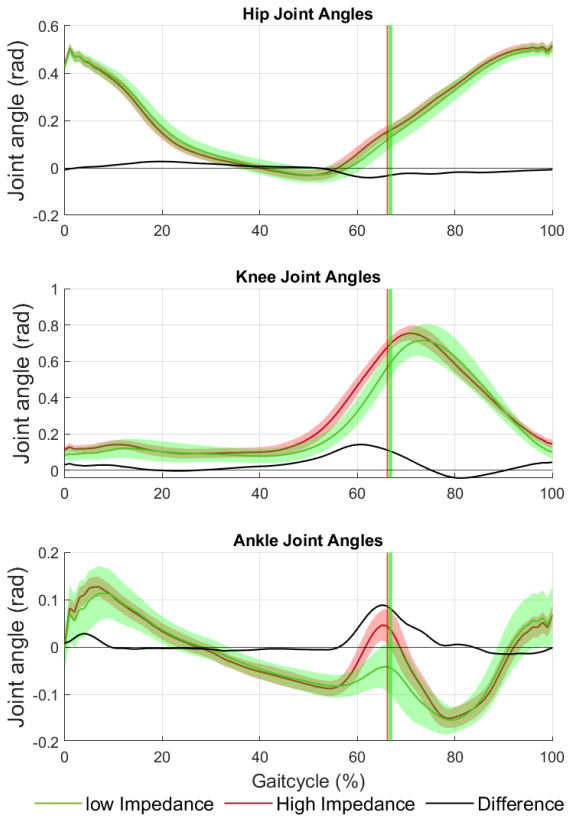

(a) the joint angles during unperturbed gait cycles with and without damping applied on the subject.

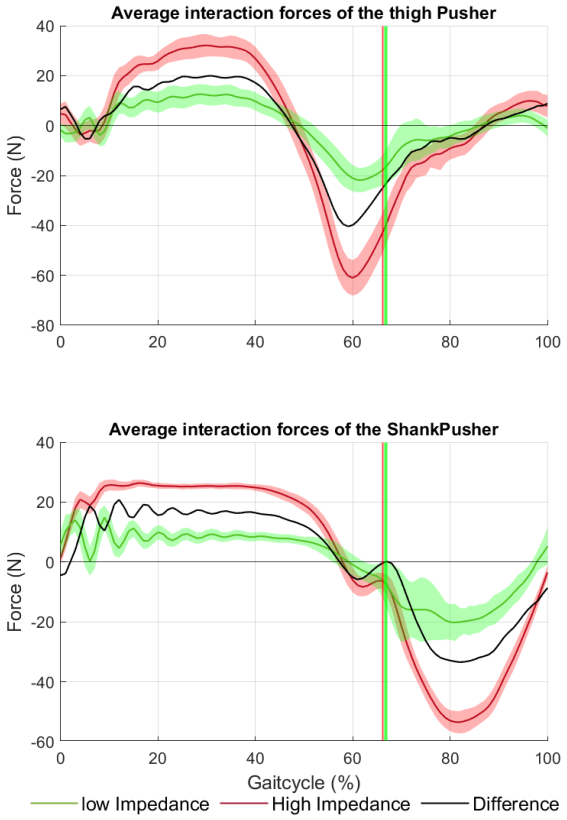

(b) Forces of the pusher with and without the added damping of 10Ns/m. The red and green line show when Toe Off happens exactly with and without damping respectively.

Figure 13

Fig. 11 shows that the responses of the joint angles are greatly reduce in amplitude. However the joint angle responses do take longer to recover compared to the regular joint angles (Appendix E). Therefore, these perturbations may still be capable of allowing for joint impedance estimation.

D Figures

D.1 Transparency Figures all Participants

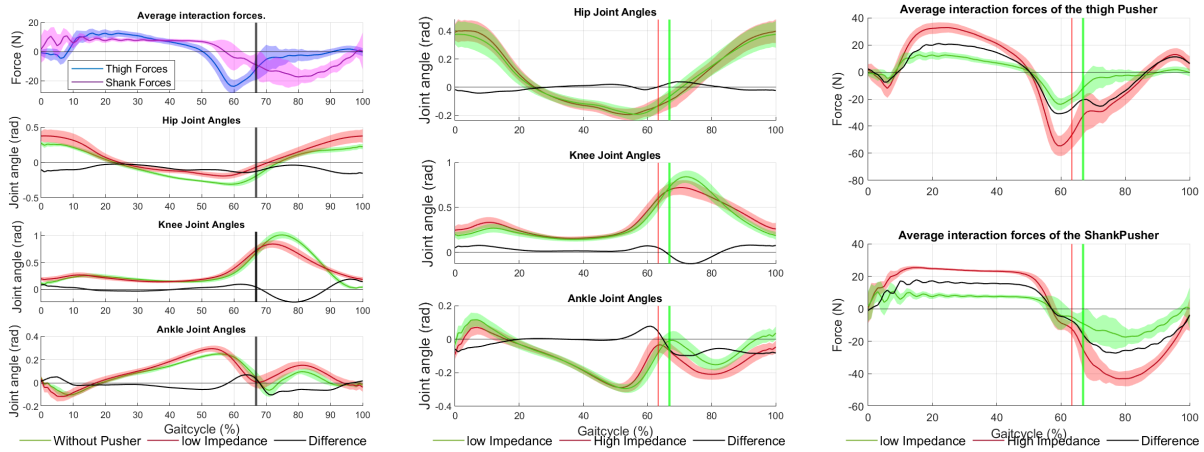

(a) (b) (c)

Figure 14: The average joint angles and forces during unperturbed gait cycles of subject P02

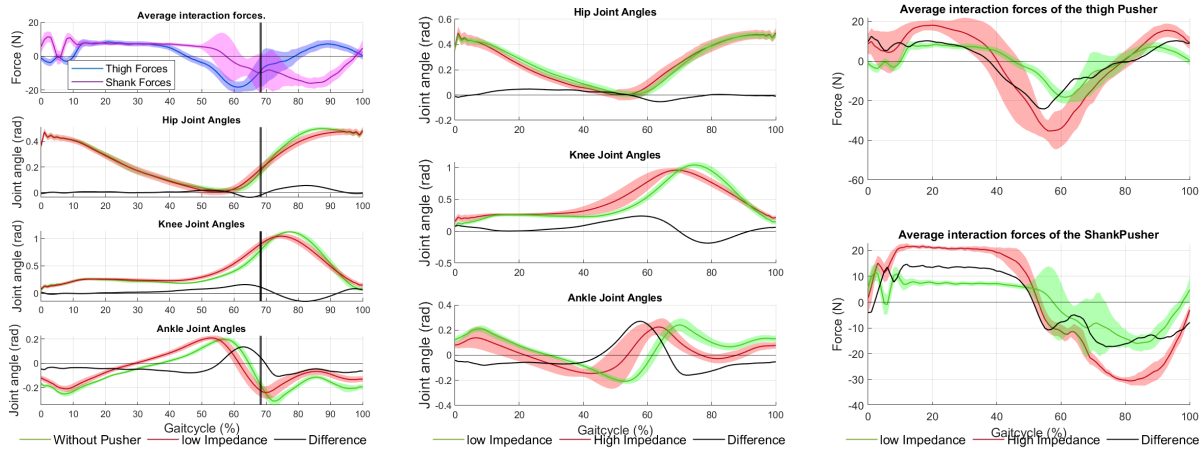

(a) (b) (c)

Figure 15: The average joint angles and forces during unperturbed gait cycles of subject P03

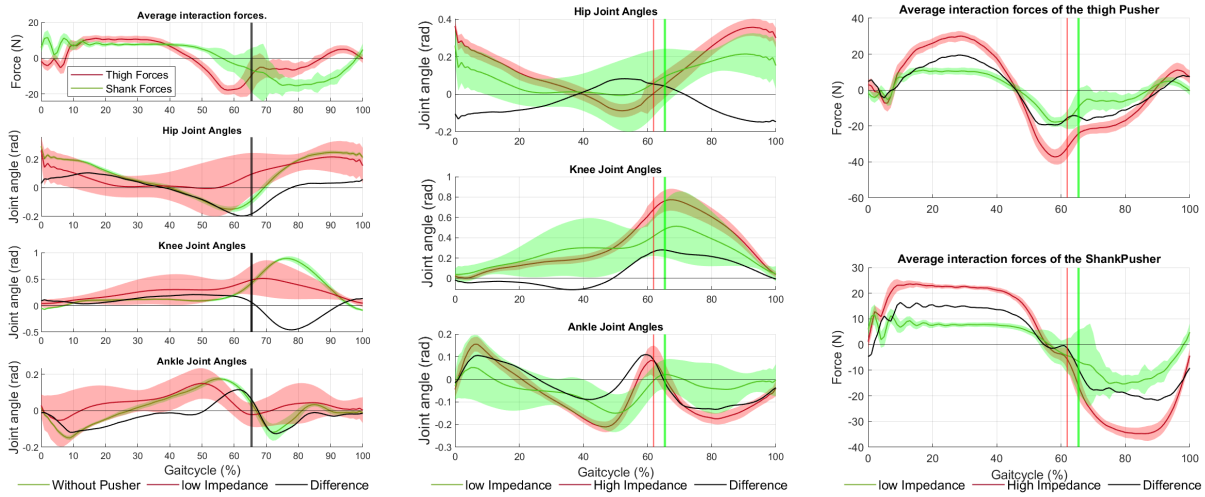

(a) (b) (c)

Figure 16: The average joint angles and forces during unperturbed gait cycles of subject P04

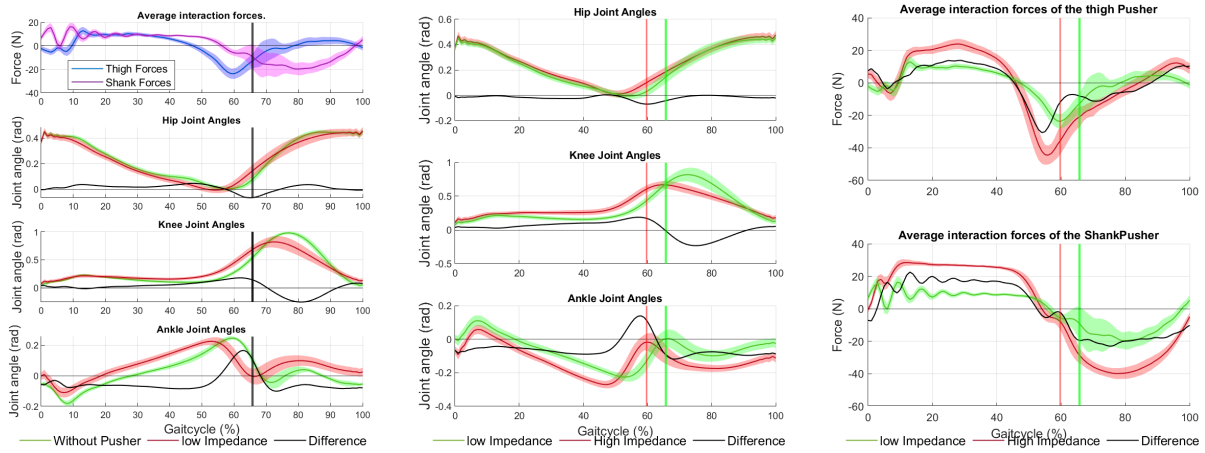

(a) (b) (c)

Figure 17: The average joint angles and forces during unperturbed gait cycles of subject P05

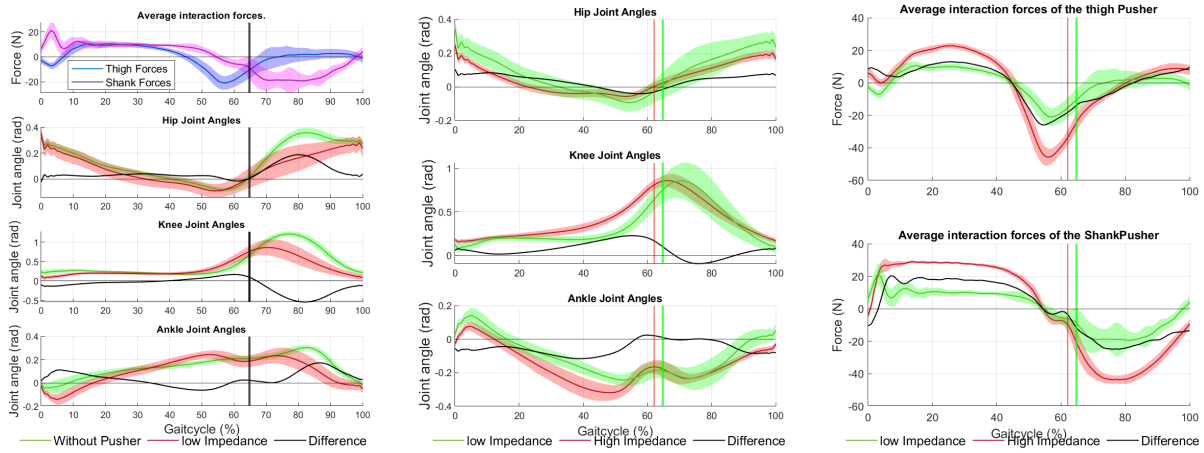

(a) (b) (c)

Figure 18: The average joint angles and forces during unperturbed gait cycles of subject P07

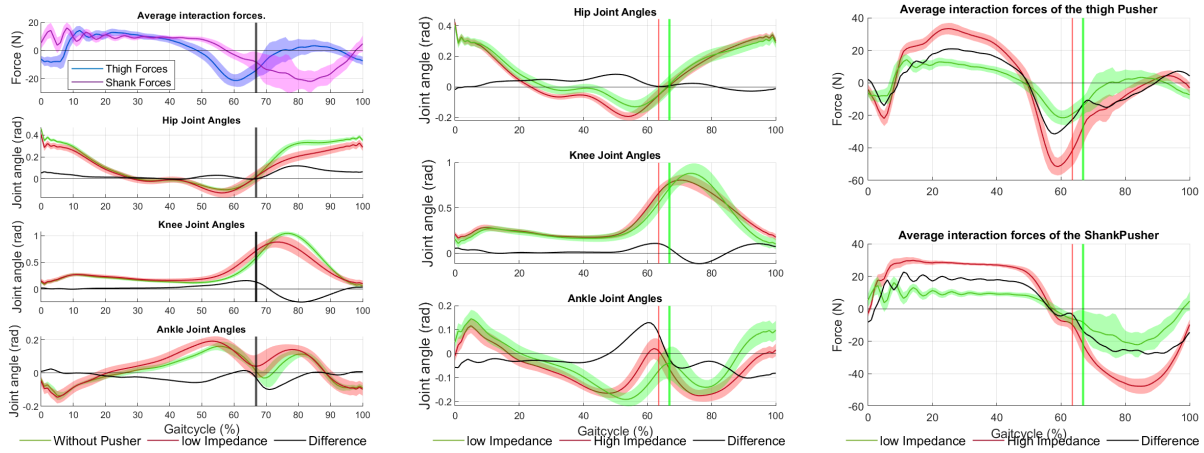

(a) (b) (c)

Figure 19: The average joint angles and forces during unperturbed gait cycles of subject P08

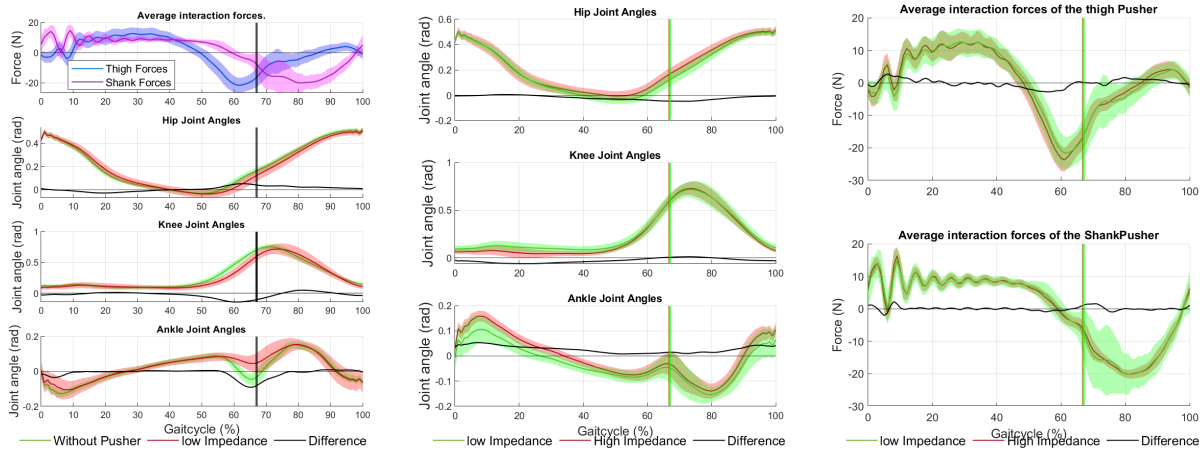

(a) (b) (c)

Figure 20: The average joint angles and forces during unperturbed gait cycles of subject P09

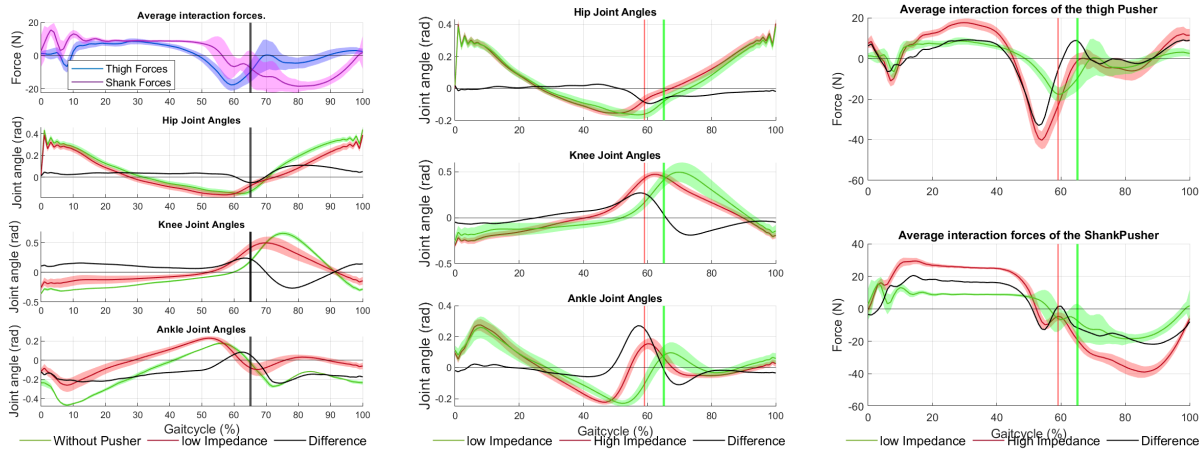

(a) (b) (c)

Figure 21: The average joint angles and forces during unperturbed gait cycles of subject P10

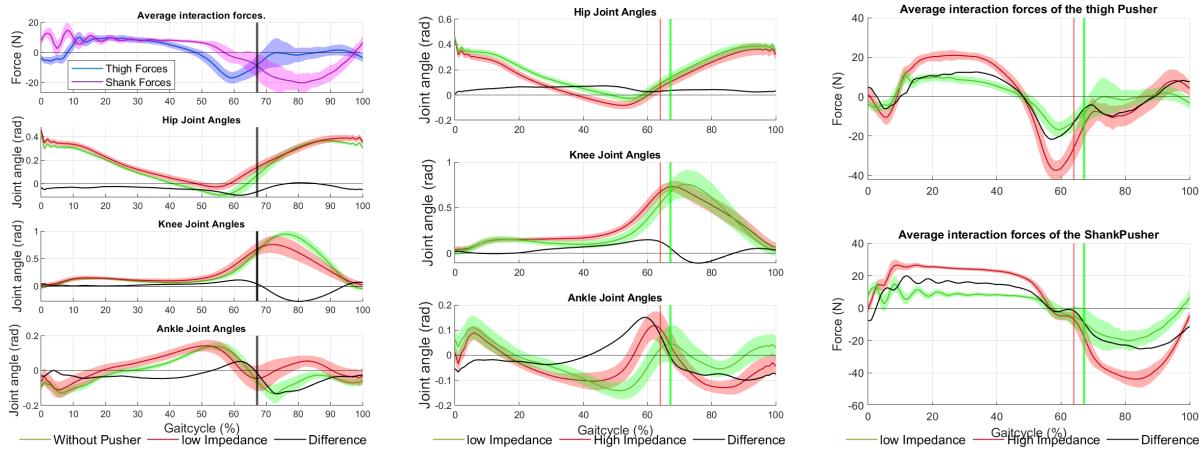

(a) (b) (c)

Figure 22: The average joint angles and forces during unperturbed gait cycles of subject P11

D.2 Pusher Response figures all subjects

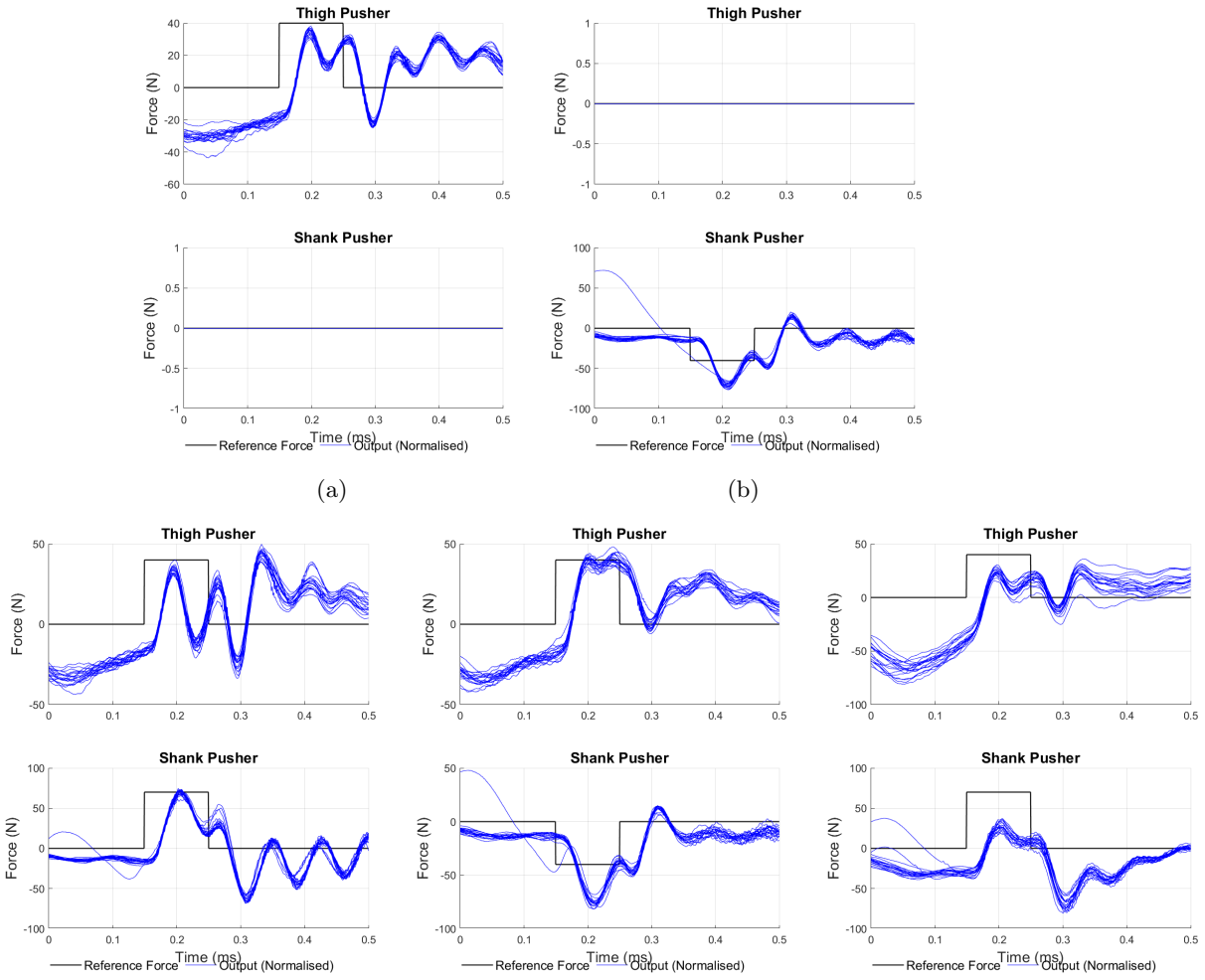

(a) (b)

(c) (d) (e)

Figure 23

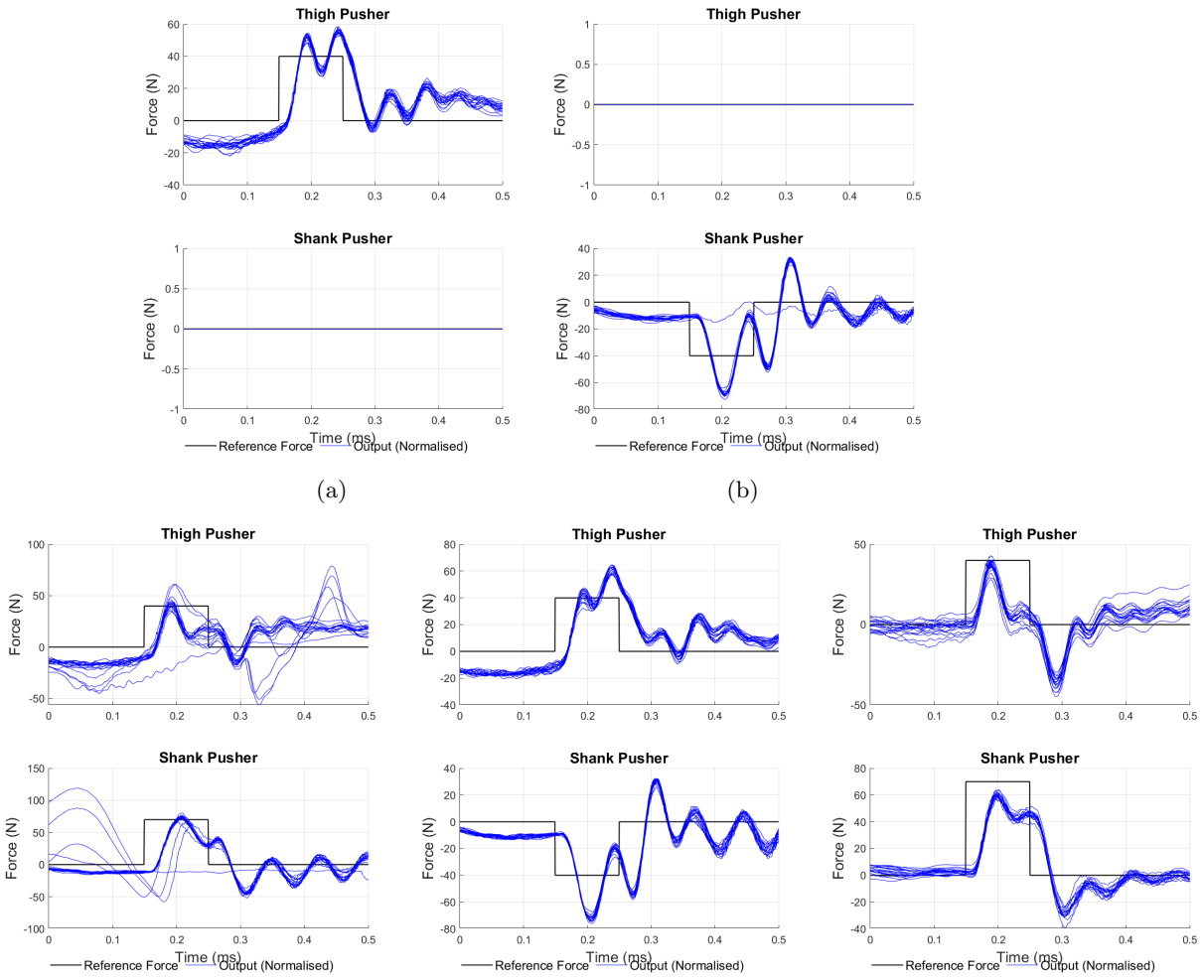

(a) (b)

(c) (d) (e)

Figure 24

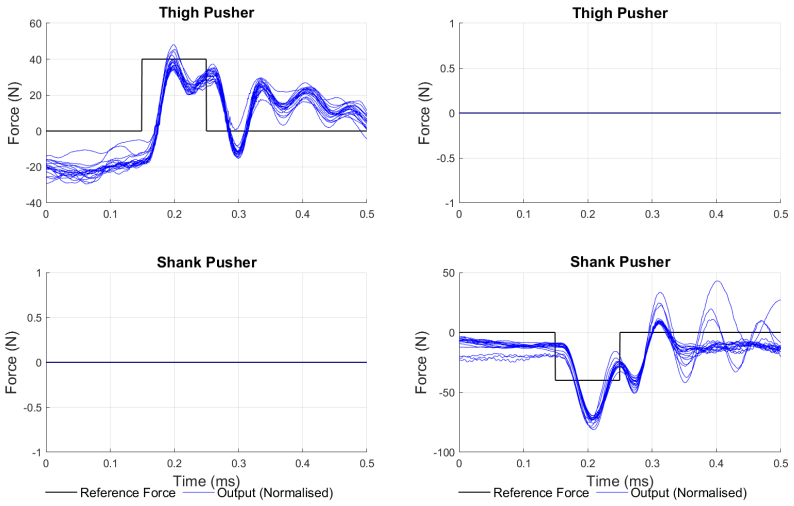

(a)

(b)

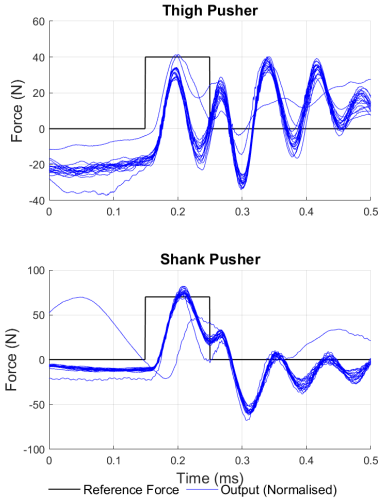

(c)

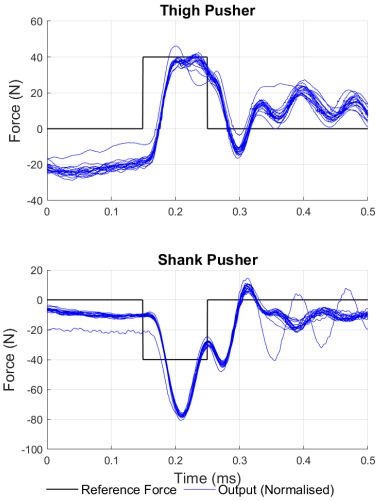

(d)

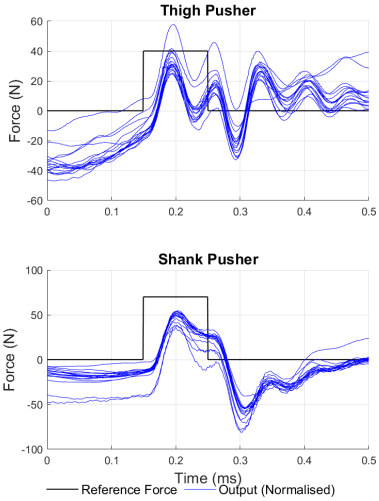

(e)

Figure 25

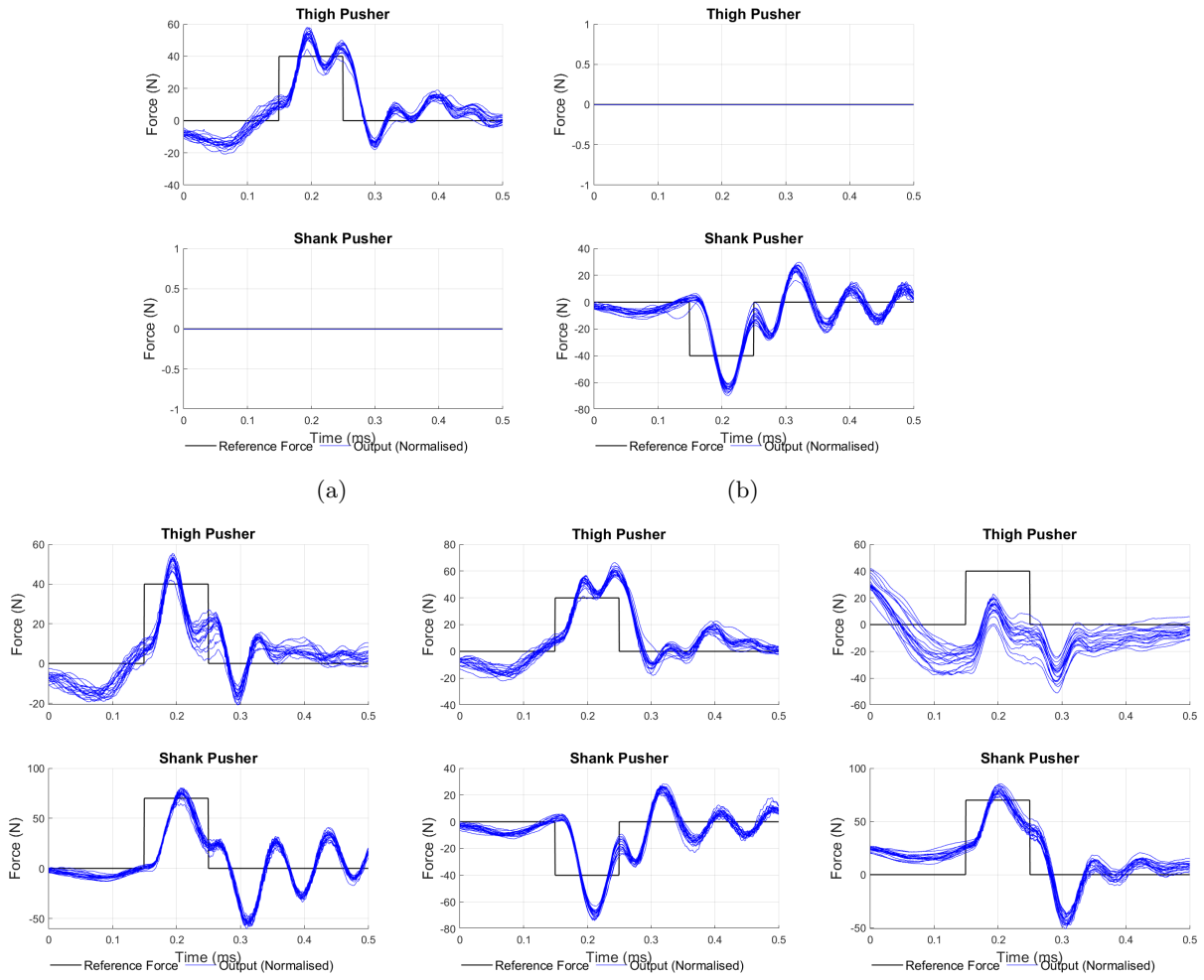

(a) (b)

(c) (d) (e)

Figure 26

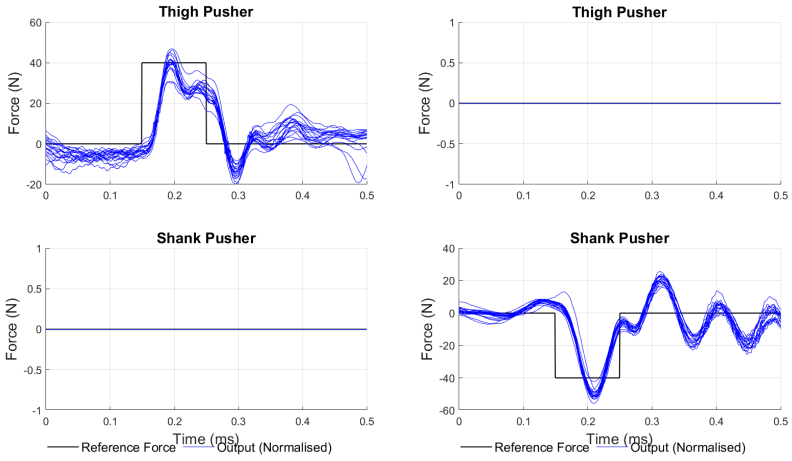

(a)

(b)

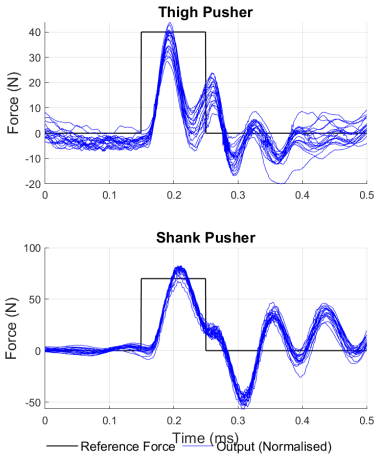

(c)

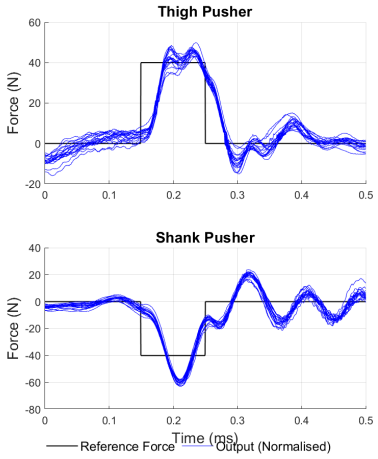

(d)

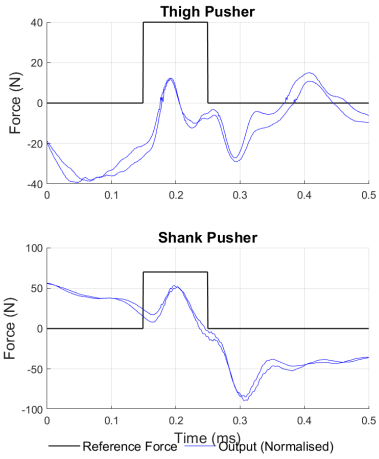

(e)

Figure 27

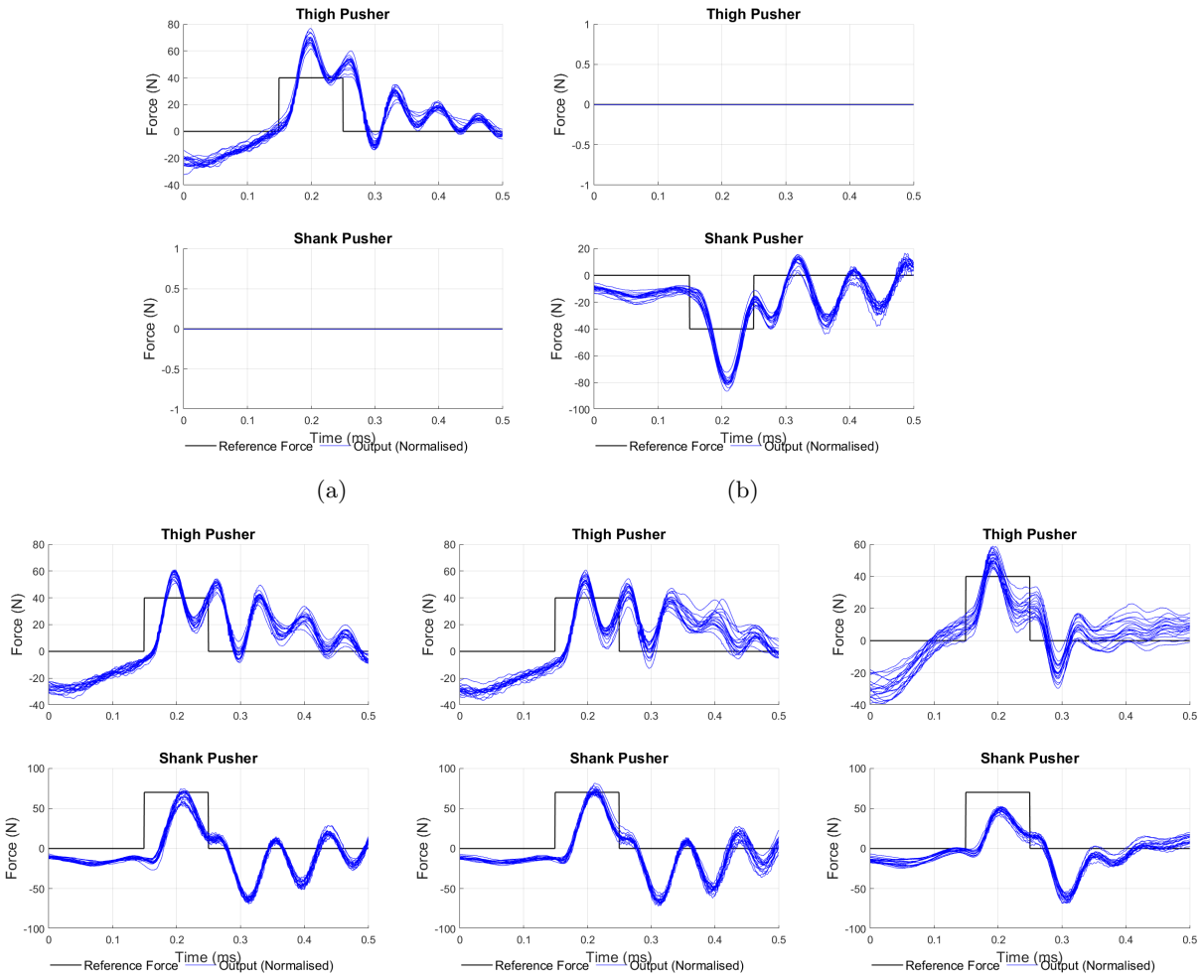

(a) (b)

(c) (d) (e)

Figure 28

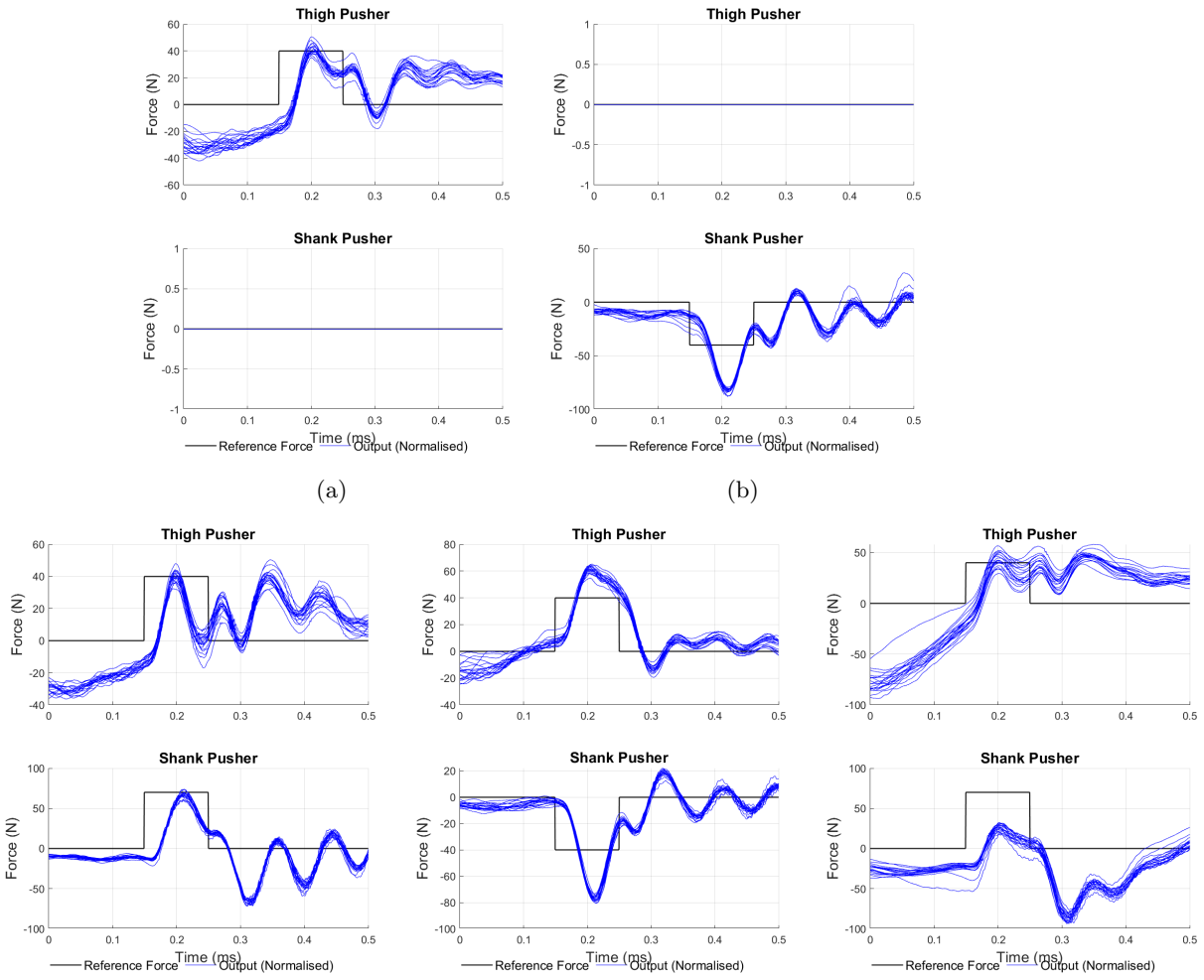

(a) (b)

(c) (d) (e)

Figure 29

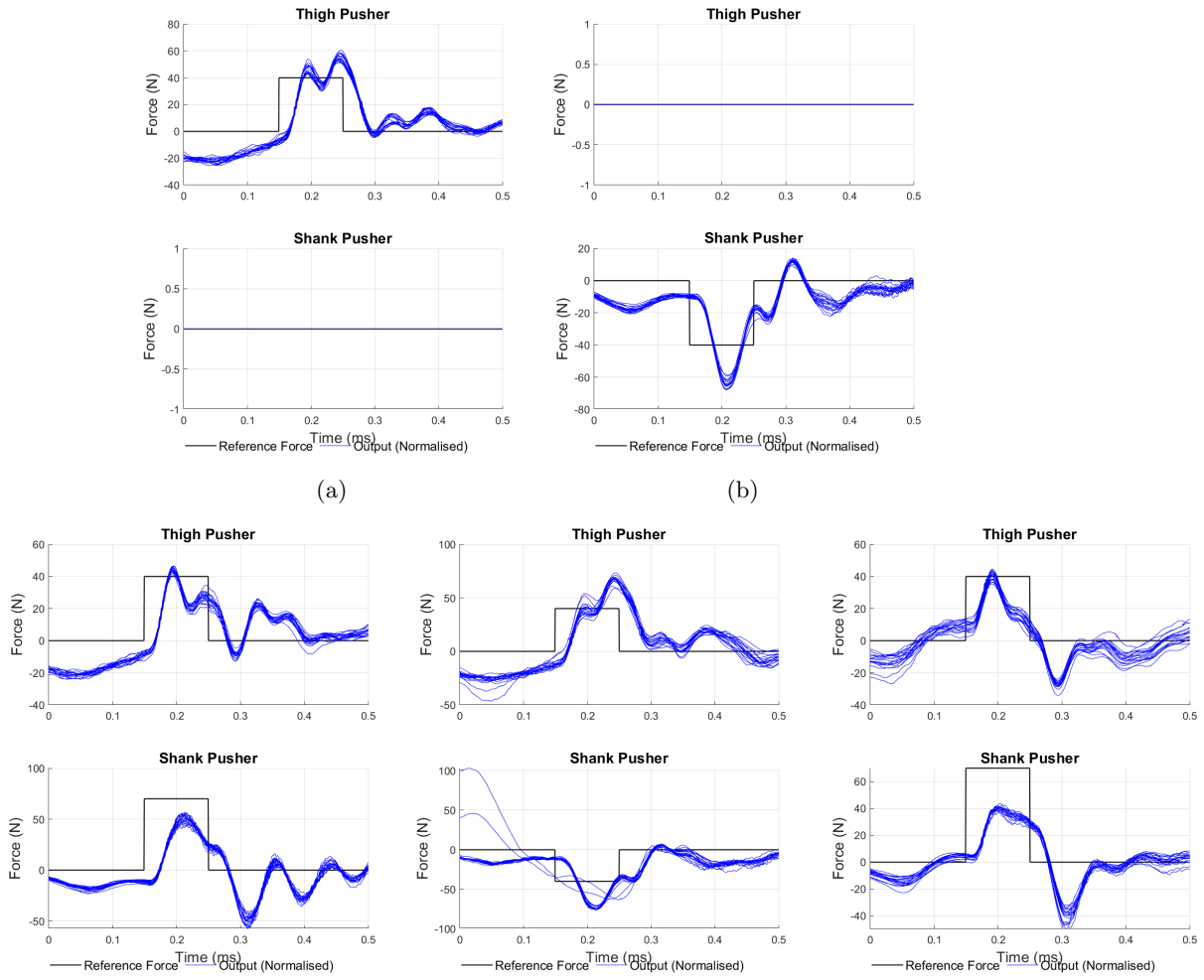
Thigh Pusher
Force (N)
Shank Pusher
Force (N)
Time (ms)
Reference Force
Output (Normalised)
(a)
Thigh Pusher
Force (N)
Shank Pusher
Force (N)
Time (ms)
Reference Force
Output (Normalised)
(b)
Thigh Pusher
Force (N)
Shank Pusher
Force (N)
Time (ms)
Reference Force
Output (Normalised)
(c)
Thigh Pusher
Force (N)
Shank Pusher
Force (N)
Time (ms)
Reference Force
Output (Normalised)
(d)
Thigh Pusher
Force (N)
Shank Pusher
Force (N)
Time (ms)
Reference Force
Output (Normalised)
(e)

Figure 30

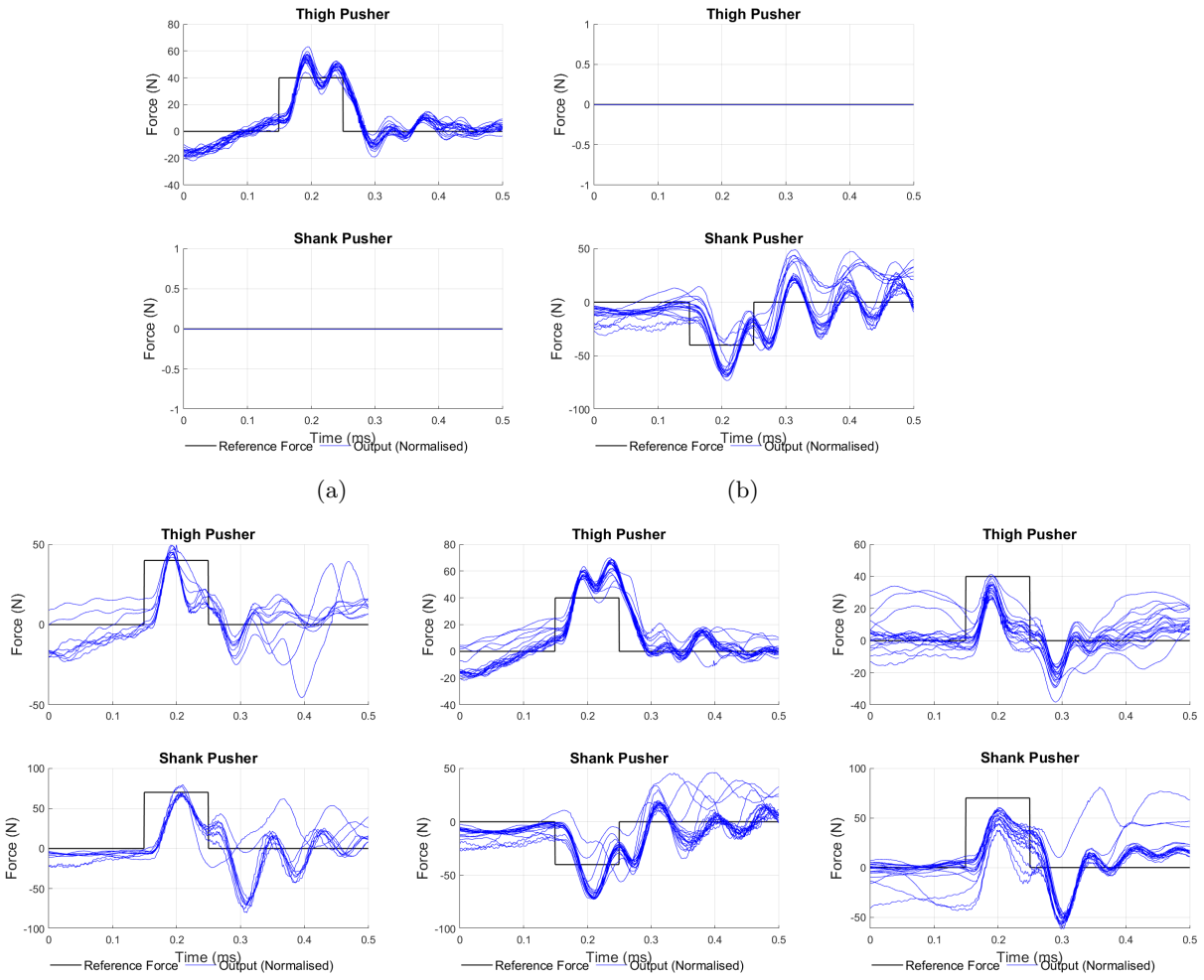

(a) (b)

(c) (d) (e)

Figure 31

E Joint angle responses of all participants

E.1 Participant 1

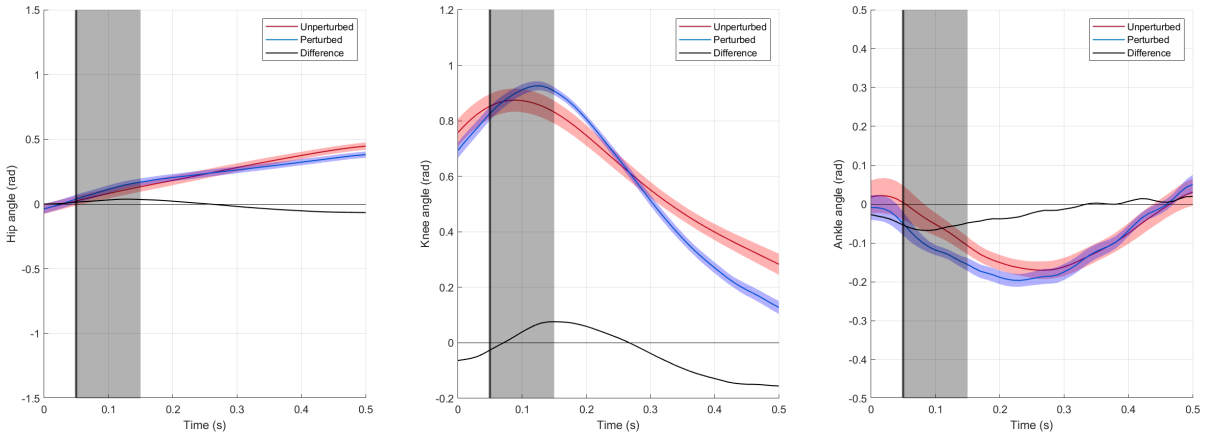

(a) Hip response of Participant 1 for the thigh push (b) Knee response of Participant 1 for the thigh push (c) Ankle response of Participant 1 for the thigh push

Figure 32: Joint angle responses of the thigh push for participant 1 in radians. the grey box is the perturbation time.

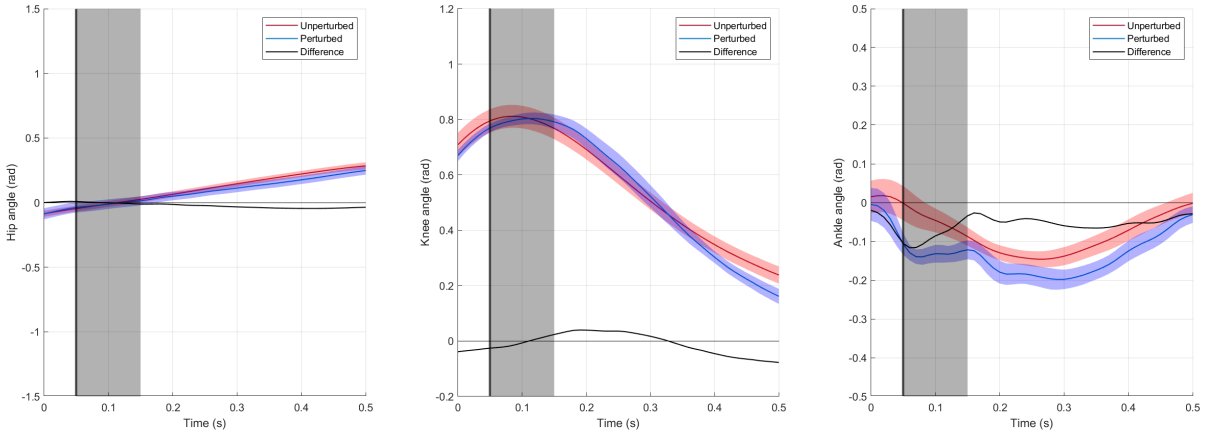

(a) Hip response of Participant 1 for the shank pull (b) Knee response of Participant 1 for the shank pull (c) Ankle response of Participant 1 for the shank pull

Figure 33: Joint angle responses of the shank pull for participant 1 in radians. the grey box is the perturbation time.

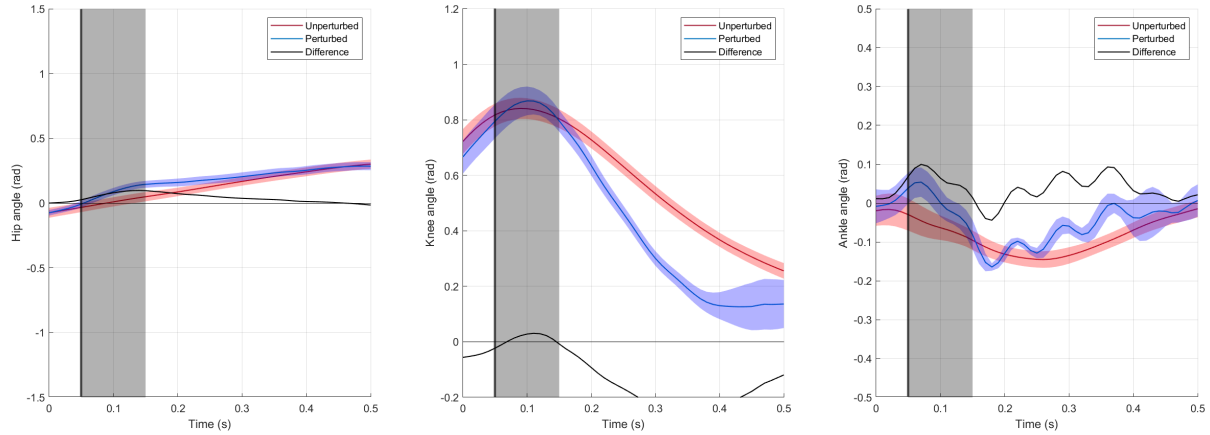

(a) Hip response of Participant 1 for the combined push

(b) Knee response of Participant 1 for the combined push

(c) Ankle response of Participant 1 for the combined push

Figure 34: Joint angle responses of the combined push for participant 1 in radians. the grey box is the perturbation time.

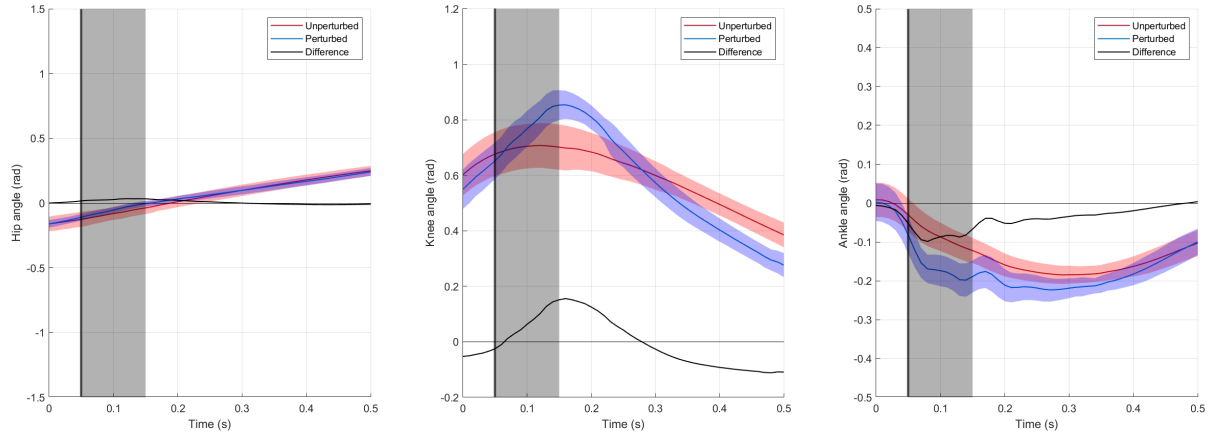

(a) Hip response of Participant 1 for the combined pushwith added damping.

(b) Knee response of Participant 1 for the combined pushwith added damping.

(c) Ankle response of Participant 1 for the combined pushwith added damping.

Figure 35: Joint angle responses of the combined push with added damping for participant 1 in radians. the grey box is the perturbation time.

E.2 Participant 2

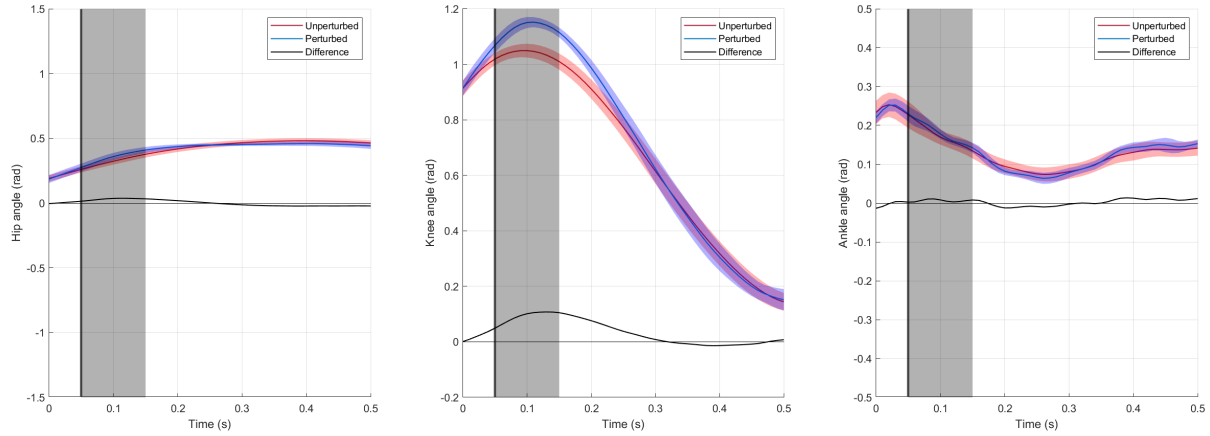

(a) Hip response of Participant 2 for the thigh push (b) Knee response of Participant 2 for the thigh push (c) Ankle response of Participant 2 for the thigh push

Figure 36: Joint angle responses of the thigh push for participant 2 in radians. the grey box is the perturbation time.

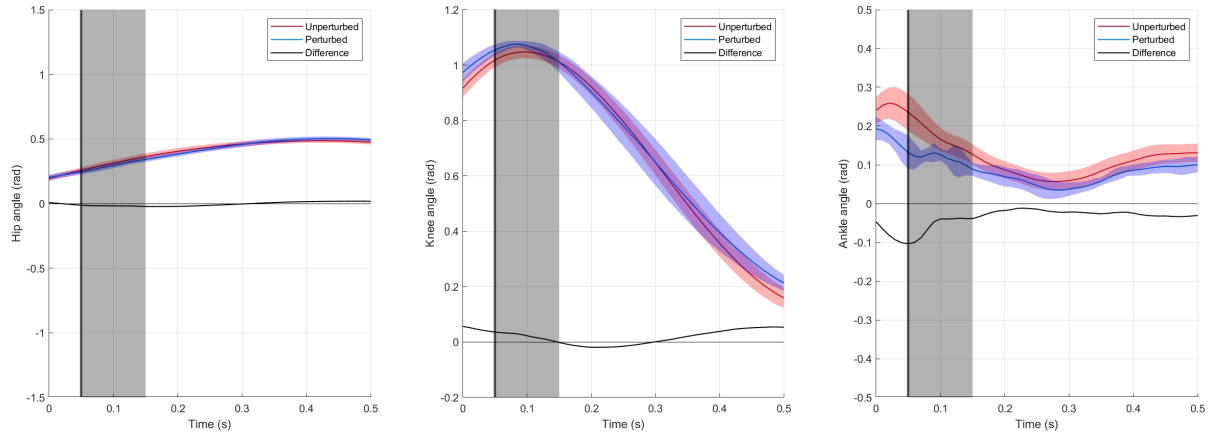

(a) Hip response of Participant 2 for the shank pull (b) Knee response of Participant 1 for the shank pull (c) Ankle response of Participant 1 for the shank pull

Figure 37: Joint angle responses of the shank pull for participant 2 in radians. the grey box is the perturbation time.

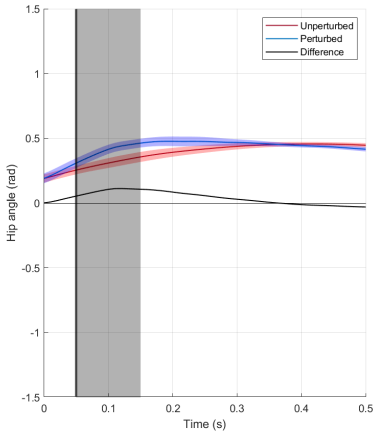

(a) Hip response of Participant 2 for the combined push

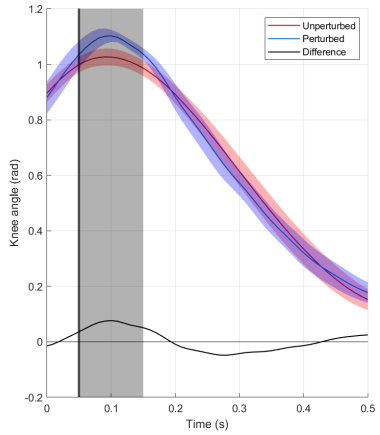

(b) Knee response of Participant 2 for the combined push

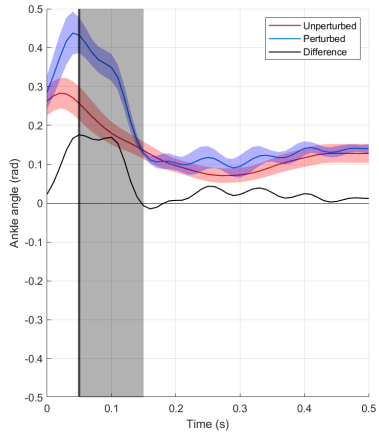

(c) Ankle response of Participant 2 for the combined push

Figure 38: Joint angle responses of the combined push for participant 2 in radians. the grey box is the perturbation time.

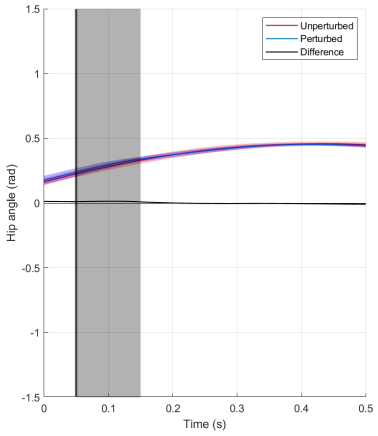

(a) Hip response of Participant 2 for the combined push-pull.

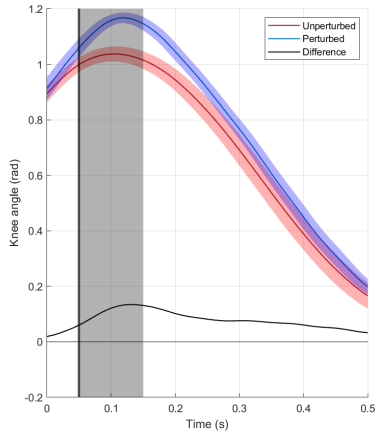

(b) Knee response of Participant 2 for the combined push-pull.

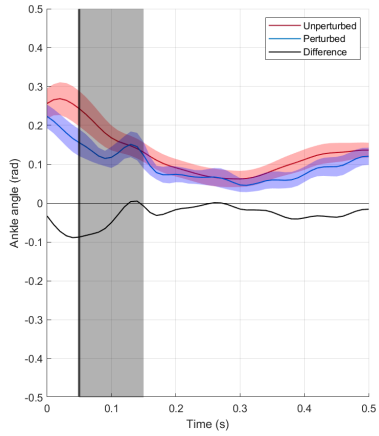

(c) Ankle response of Participant 2 for the combined push-pull.

Figure 39: Joint angle responses of the combined push-pull for participant 2 in radians. the grey box is the perturbation time.

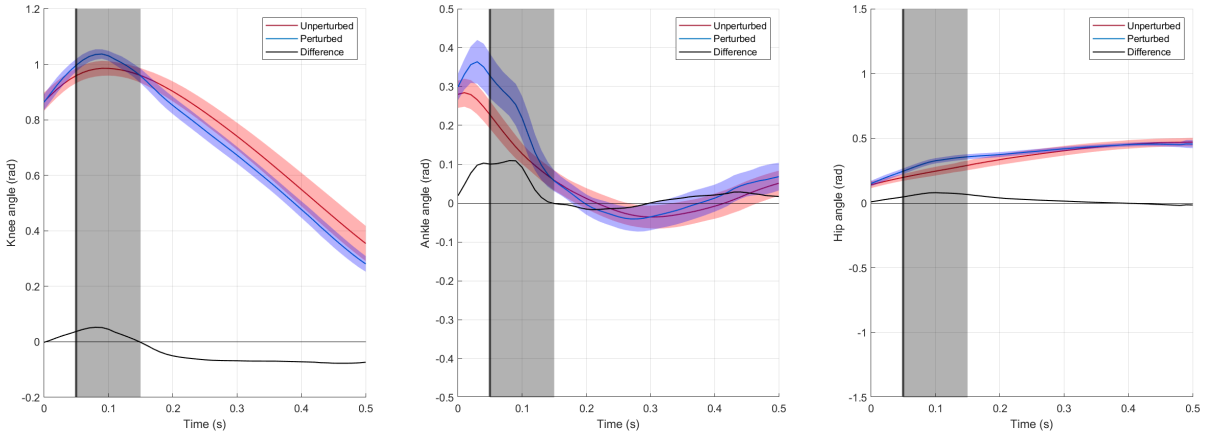

(a) Hip response of Participant 2 for the combined pushwith added damping.

(b) Knee response of Participant 2 for the combined pushwith added damping.

(c) Ankle response of Participant 2 for the combined pushwith added damping.

Figure 40: Joint angle responses of the combined push with added damping for participant 2 in radians. the grey box is the perturbation time.

E.3 Participant 3

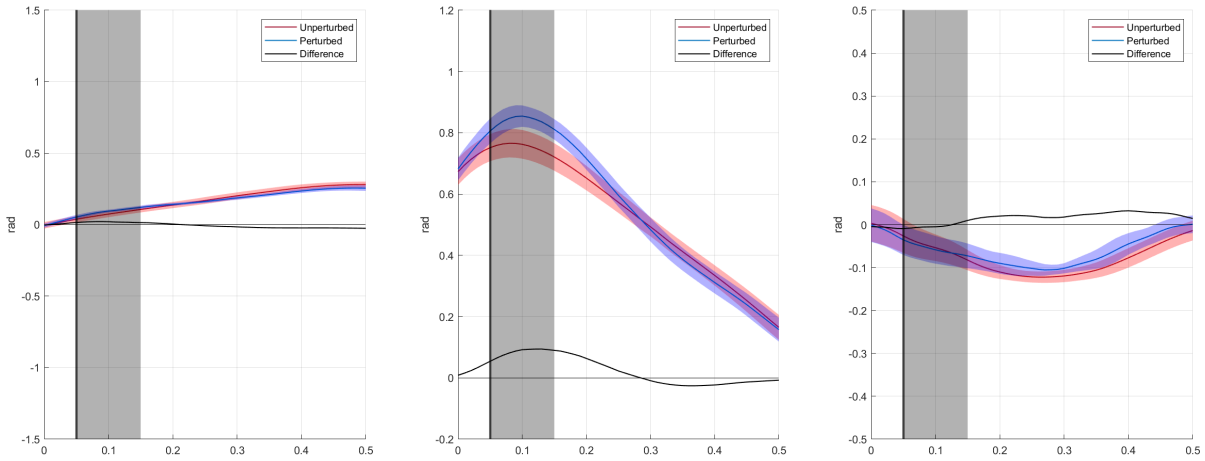

(a) Hip response of Participant 3 for the thigh push

(b) Knee response of Participant 3 for the thigh push

(c) Ankle response of Participant 3 for the thigh push

Figure 41: Joint angle responses of the thigh push for participant 3 in radians. the grey box is the perturbation time.

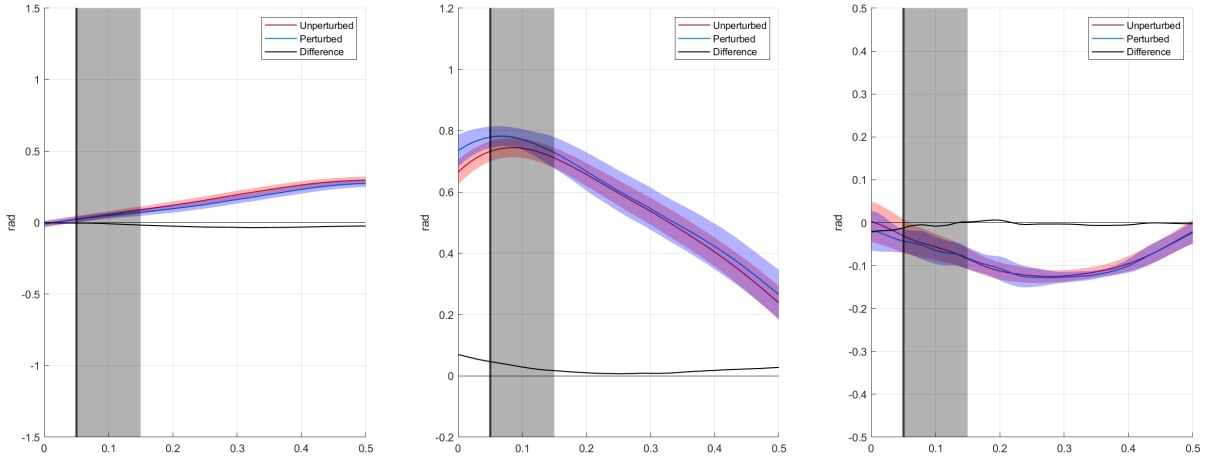

(a) Hip response of Participant 3 for the shank pull (b) Knee response of Participant 3 for the shank pull (c) Ankle response of Participant 3 for the shank pull

Figure 42: Joint angle responses of the shank pull for participant 3 in radians. the grey box is the perturbation time.

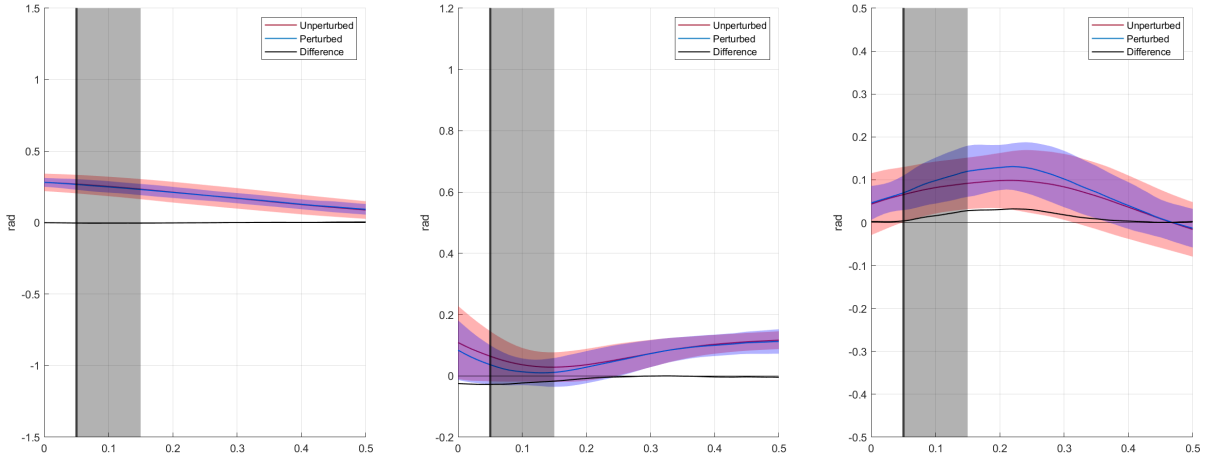

(a) Hip response of Participant 3 for the combined push (b) Knee response of Participant 3 for the combined push (c) Ankle response of Participant 3 for the combined push

Figure 43: Joint angle responses of the combined push for participant 3 in radians. the grey box is the perturbation time.

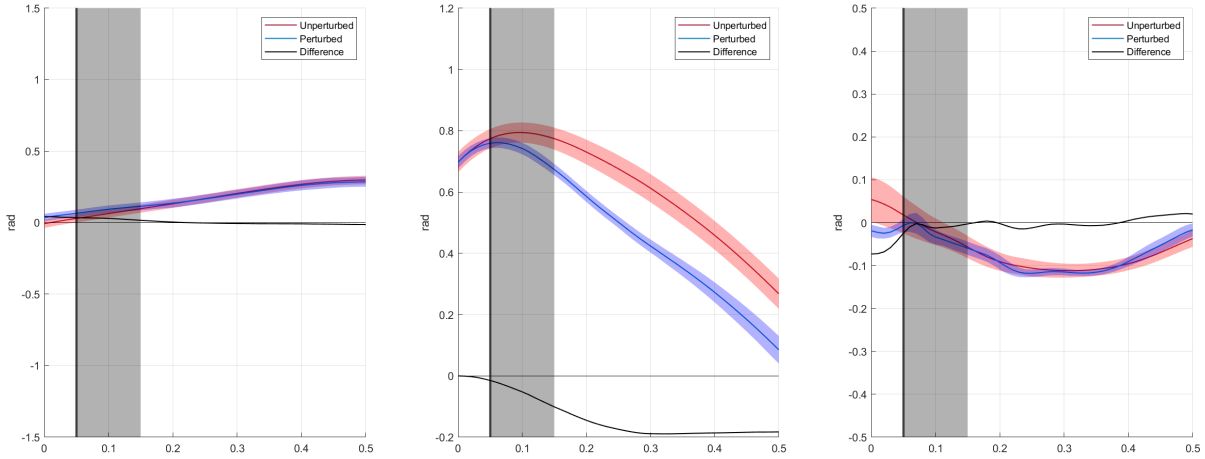

(a) Hip response of Participant 3 for the combined push-pull.

(b) Knee response of Participant 3 for the combined push-pull.

(c) Ankle response of Participant 3 for the combined push-pull.

Figure 44: Joint angle responses of the combined push-pull for participant 3 in radians. the grey box is the perturbation time.

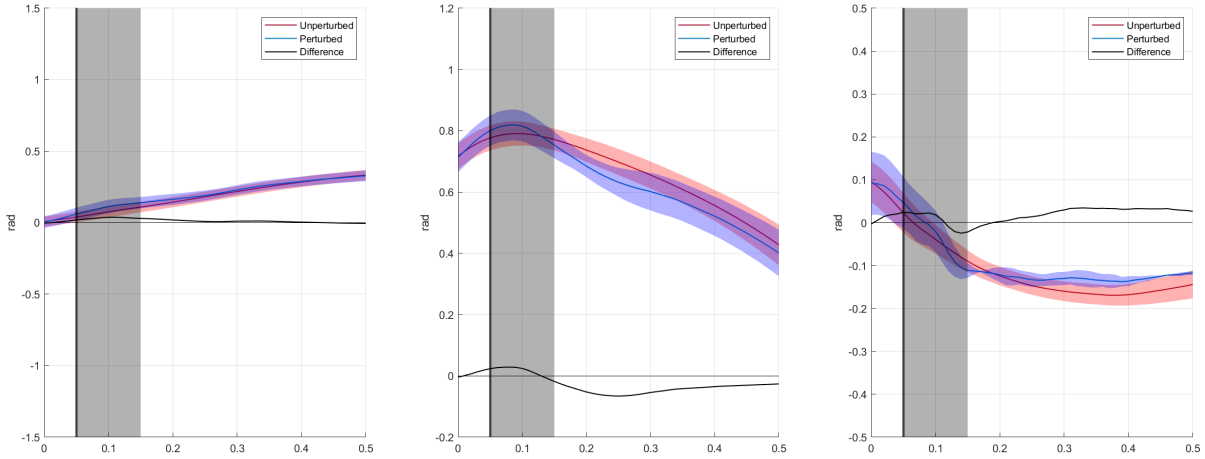

(a) Hip response of Participant 3 for the combined pushwith added damping.

(b) Knee response of Participant 3 for the combined pushwith added damping.

(c) Ankle response of Participant 3 for the combined pushwith added damping.

Figure 45: Joint angle responses of the combined push with added damping for participant 3 in radians. the grey box is the perturbation time.

E.4 Participant 4

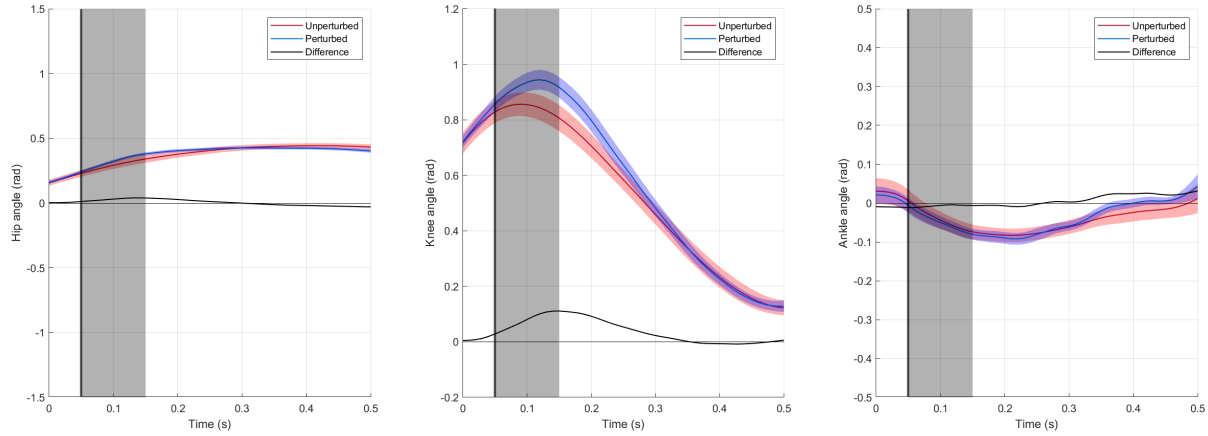

(a) Hip response of Participant 4 for the thigh push (b) Knee response of Participant 4 for the thigh push (c) Ankle response of Participant 4 for the thigh push

Figure 46: Joint angle responses of the thigh push for participant 4 in radians. the grey box is the perturbation time.

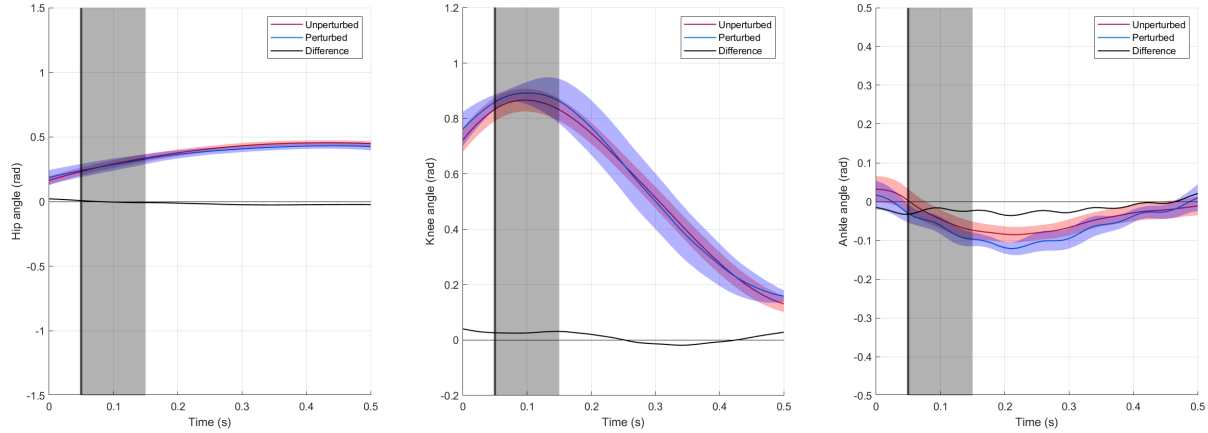

(a) Hip response of Participant 4 for the shank pull (b) Knee response of Participant 4 for the shank pull (c) Ankle response of Participant 4 for the shank pull

Figure 47: Joint angle responses of the shank pull for participant 4 in radians. the grey box is the perturbation time.

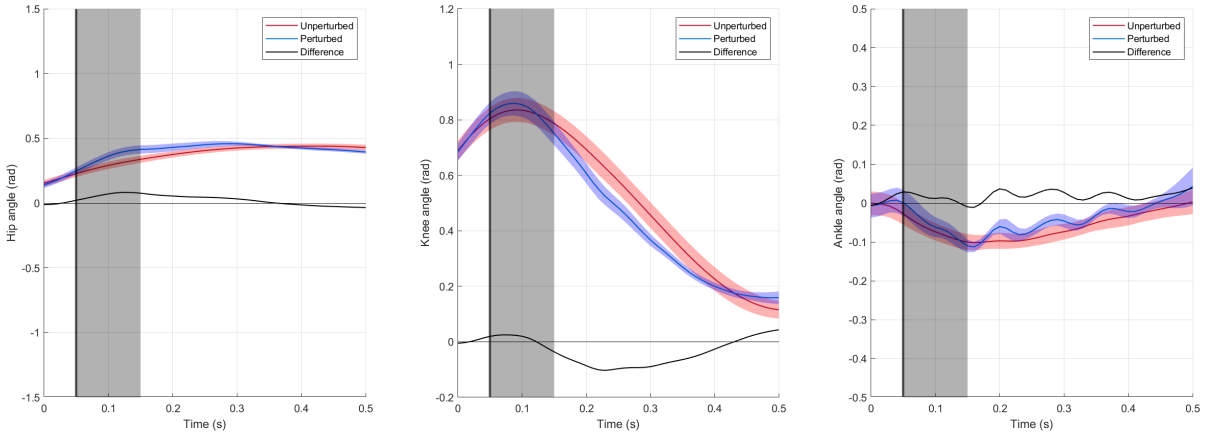

(a) Hip response of Participant 4 for the combined push

(b) Knee response of Participant 4 for the combined push

(c) Ankle response of Participant 4 for the combined push

Figure 48: Joint angle responses of the combined push for participant 4 in radians. the grey box is the perturbation time.

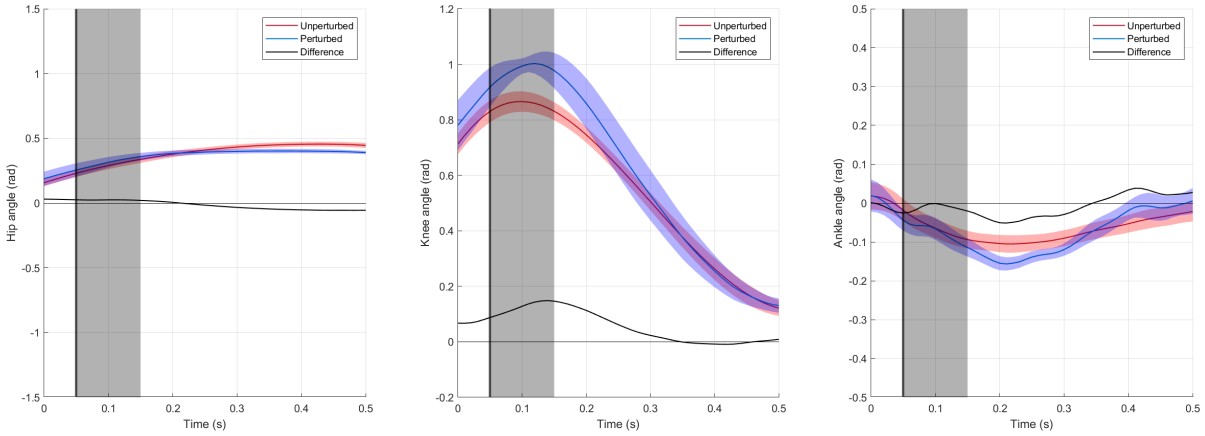

(a) Hip response of Participant 4 for the combined push-pull.

(b) Knee response of Participant 4 for the combined push-pull.

(c) Ankle response of Participant 4 for the combined push-pull.

Figure 49: Joint angle responses of the combined push-pull for participant 4 in radians. the grey box is the perturbation time.

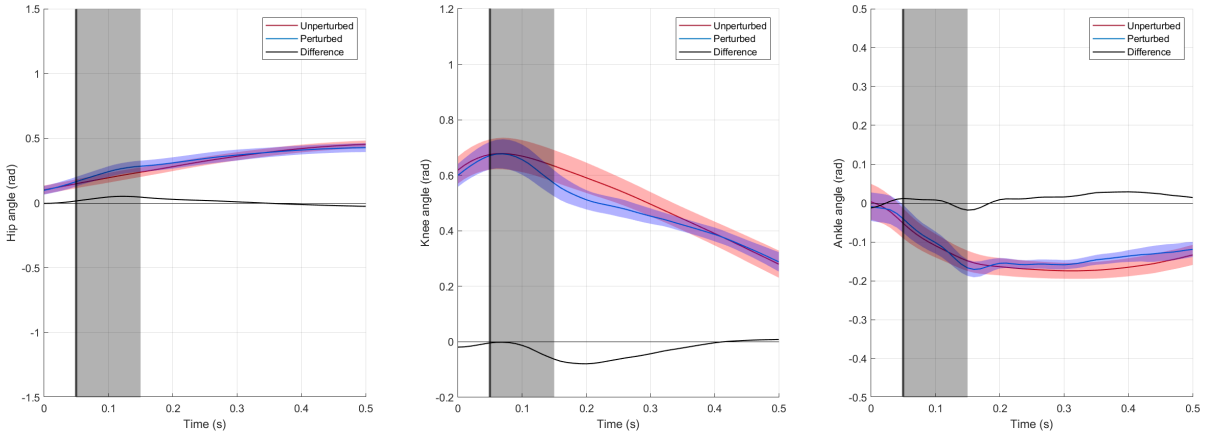

(a) Hip response of Participant 4 for the combined pushwith added damping.

(b) Knee response of Participant 4 for the combined pushwith added damping.

(c) Ankle response of Participant 4 for the combined pushwith added damping.

Figure 50: Joint angle responses of the combined push with added damping for participant 4 in radians. the grey box is the perturbation time.

E.5 Participant 6

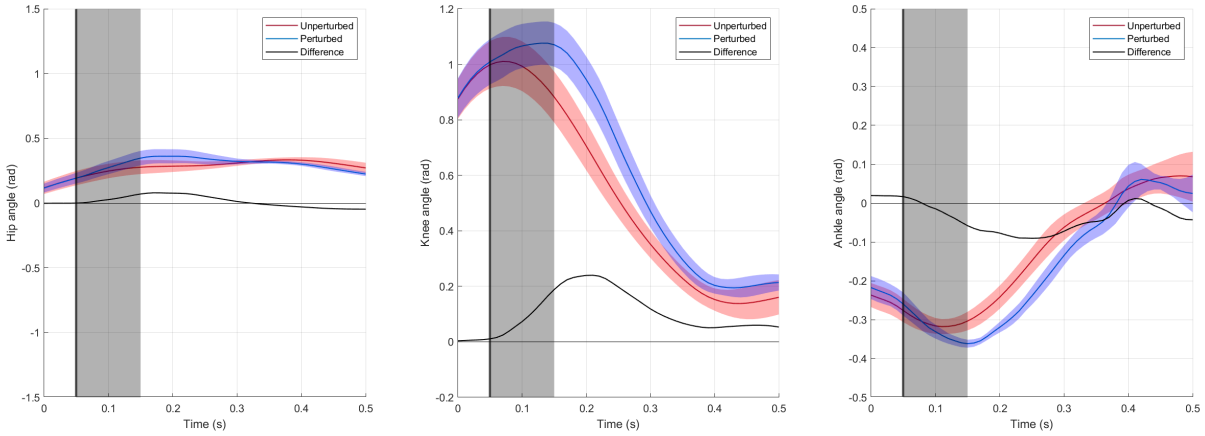

(a) Hip response of Participant 6 for the thigh push

(b) Knee response of Participant 6 for the thigh push

(c) Ankle response of Participant 6 for the thigh push

Figure 51: Joint angle responses of the thigh push for participant 6 in radians. the grey box is the perturbation time.

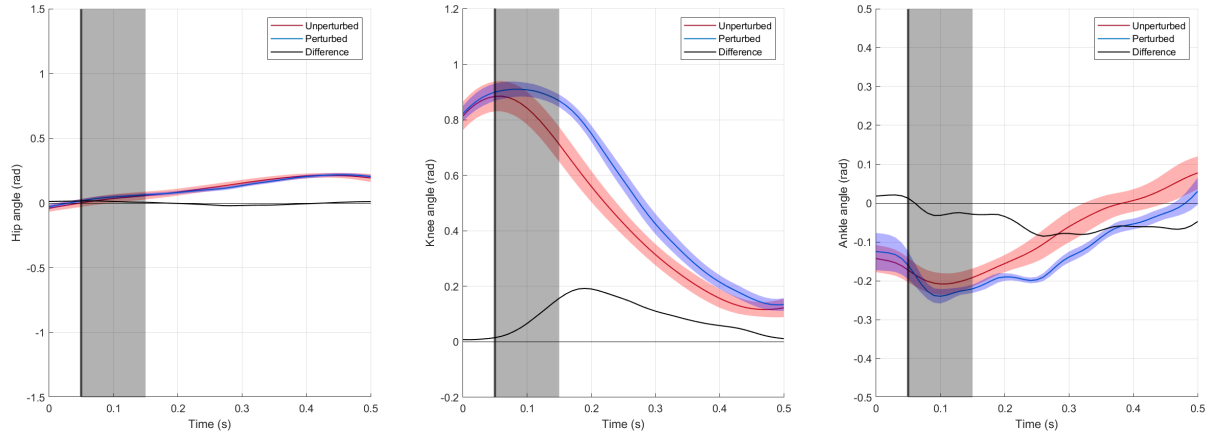

(a) Hip response of Participant 6 for the shank pull (b) Knee response of Participant 6 for the shank pull (c) Ankle response of Participant 6 for the shank pull

Figure 52: Joint angle responses of the shank pull for participant 6 in radians. the grey box is the perturbation time.

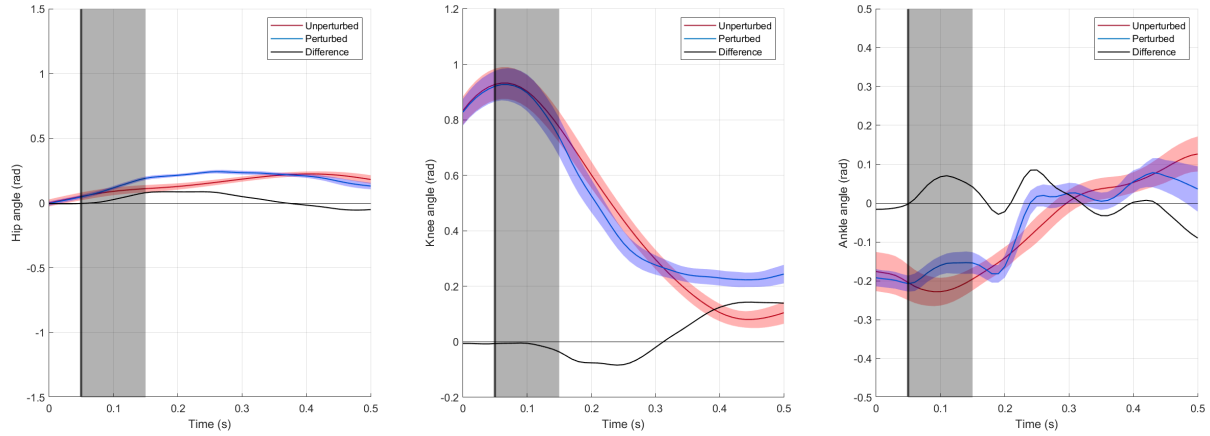

(a) Hip response of Participant 6 for the combined push (b) Knee response of Participant 6 for the combined push (c) Ankle response of Participant 6 for the combined push

Figure 53: Joint angle responses of the combined push for participant 6 in radians. the grey box is the perturbation time.

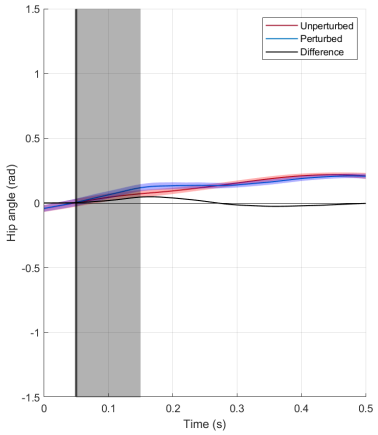

(a) Hip response of Participant 6 for the combined push-pull.

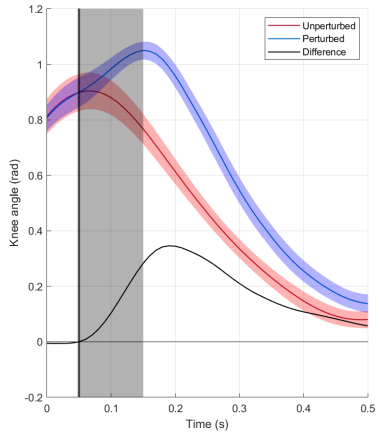

(b) Knee response of Participant 6 for the combined push-pull.

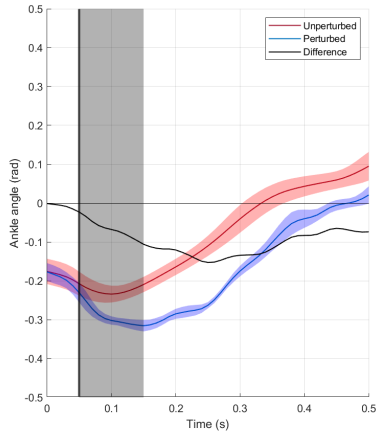

(c) Ankle response of Participant 6 for the combined push-pull.

Figure 54: Joint angle responses of the combined push-pull for participant 6 in radians. the grey box is the perturbation time.

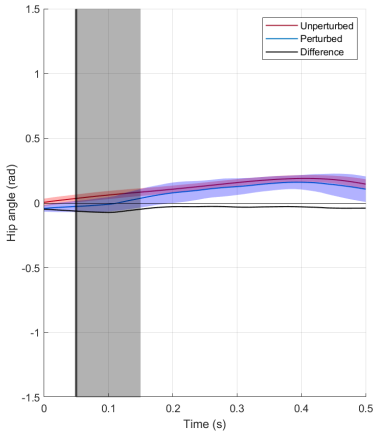

(a) Hip response of Participant 6 for the combined pushwith added damping.

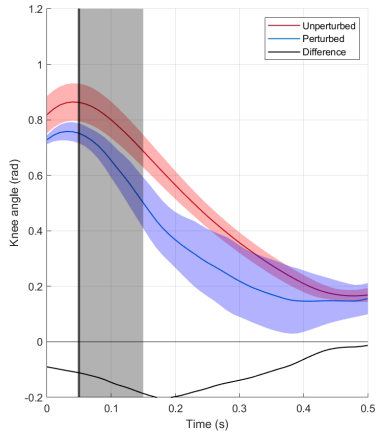

(b) Knee response of Participant 6 for the combined pushwith added damping.

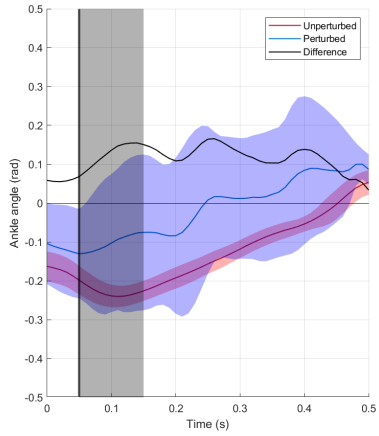

(c) Ankle response of Participant 6 for the combined pushwith added damping.

Figure 55: Joint angle responses of the combined push with added damping for participant 6 in radians. the grey box is the perturbation time.

E.6 Participant 7

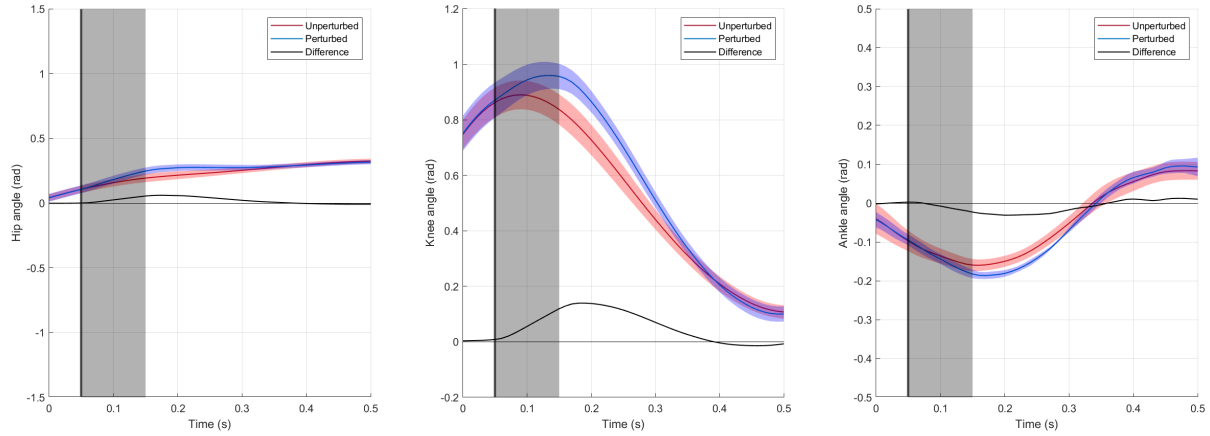

(a) Hip response of Participant 7 for the thigh push (b) Knee response of Participant 7 for the thigh push (c) Ankle response of Participant 7 for the thigh push

Figure 56: Joint angle responses of the thigh push for participant 7 in radians. the grey box is the perturbation time.

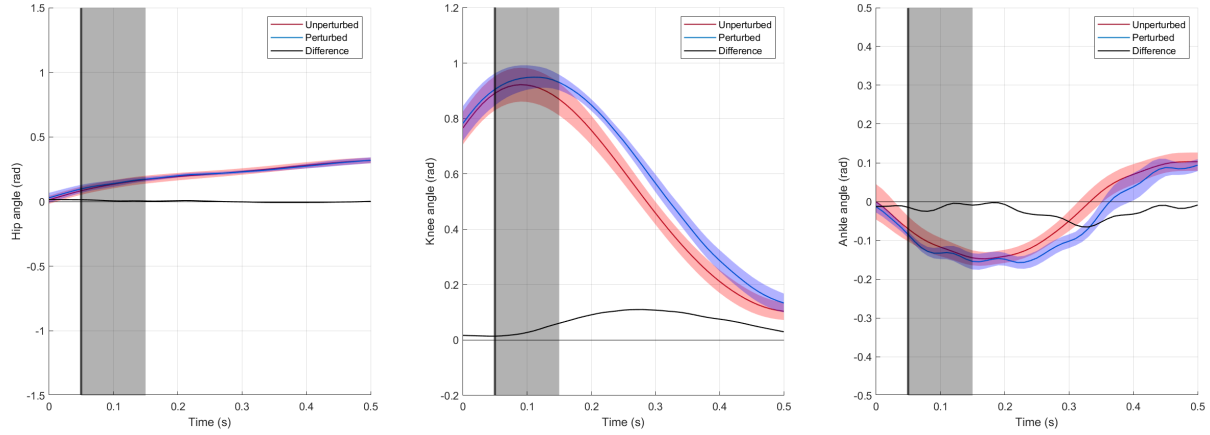

(a) Hip response of Participant 7 for the shank pull (b) Knee response of Participant 7 for the shank pull (c) Ankle response of Participant 7 for the shank pull

Figure 57: Joint angle responses of the shank pull for participant 7 in radians. the grey box is the perturbation time.

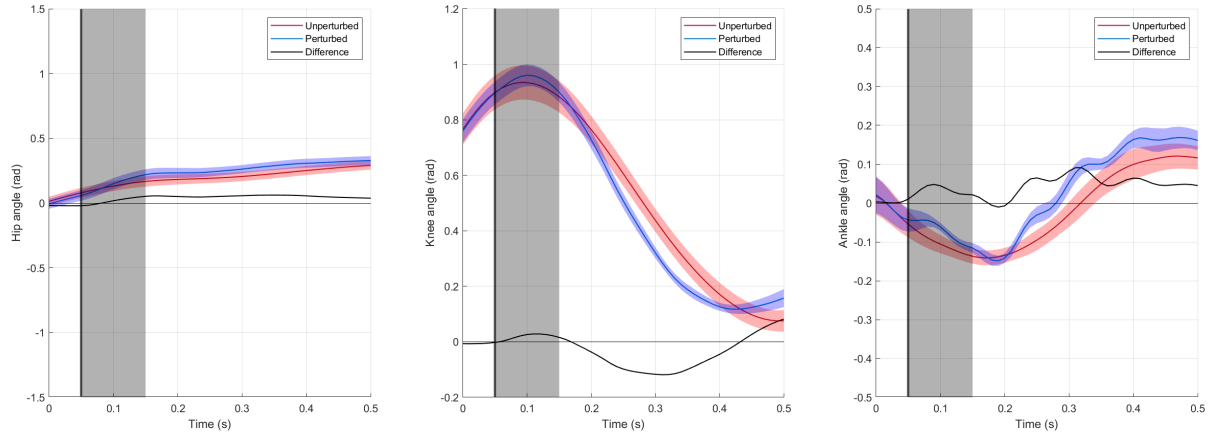

(a) Hip response of Participant 7 for the combined push

(b) Knee response of Participant 7 for the combined push

(c) Ankle response of Participant 7 for the combined push

Figure 58: Joint angle responses of the combined push for participant 7 in radians. the grey box is the perturbation time.

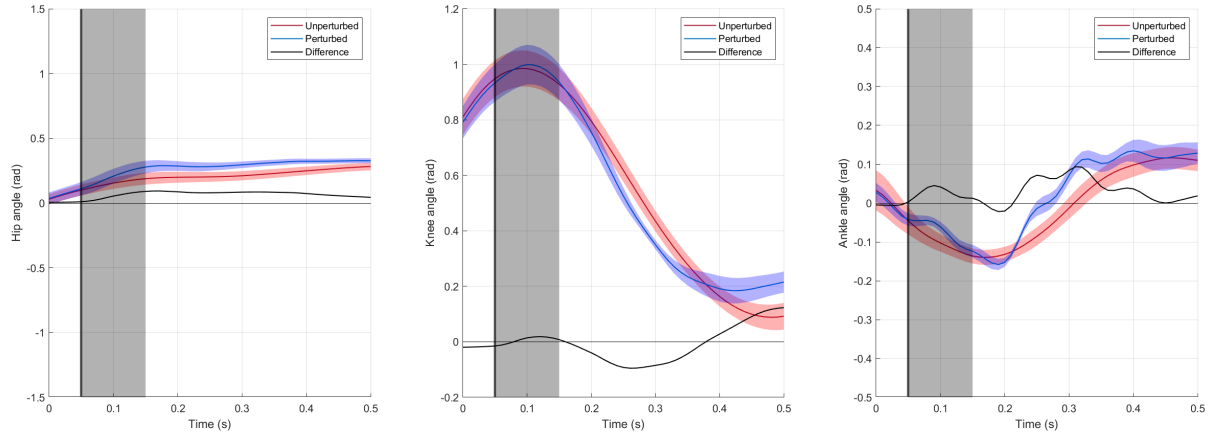

(a) Hip response of Participant 7 for the combined push-pull.

(b) Knee response of Participant 7 for the combined push-pull.

(c) Ankle response of Participant 7 for the combined push-pull.

Figure 59: Joint angle responses of the combined push-pull for participant 7 in radians. the grey box is the perturbation time.

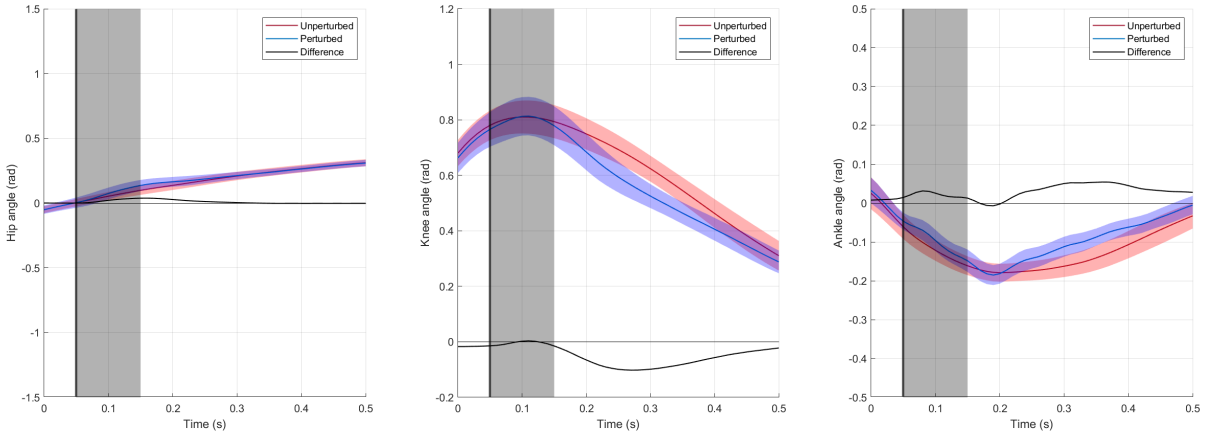

(a) Hip response of Participant 7 for the combined pushwith added damping.

(b) Knee response of Participant 7 for the combined pushwith added damping.

(c) Ankle response of Participant 7 for the combined pushwith added damping.

Figure 60: Joint angle responses of the combined push with added damping for participant 7 in radians. the grey box is the perturbation time.

E.7 Participant 8

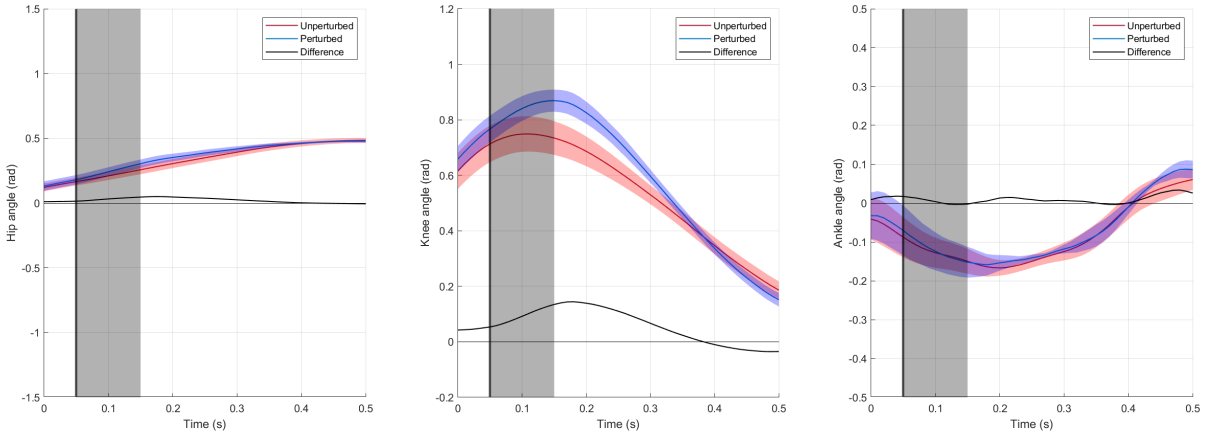

(a) Hip response of Participant 8 for the thigh push

(b) Knee response of Participant 8 for the thigh push

(c) Ankle response of Participant 8 for the thigh push

Figure 61: Joint angle responses of the thigh push for participant 8 in radians. the grey box is the perturbation time.

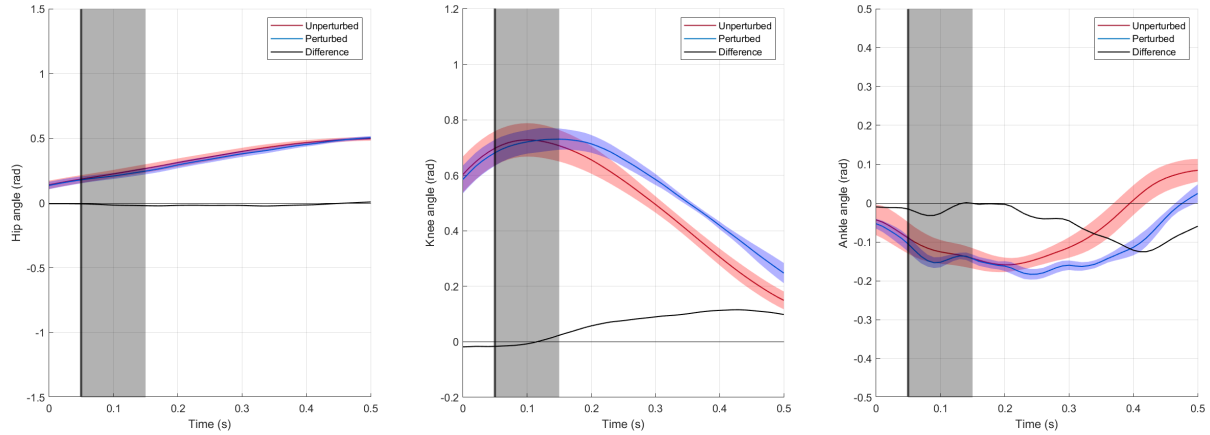

(a) Hip response of Participant 8 for the shank pull (b) Knee response of Participant 8 for the shank pull (c) Ankle response of Participant 8 for the shank pull

Figure 62: Joint angle responses of the shank pull for participant 8 in radians. the grey box is the perturbation time.

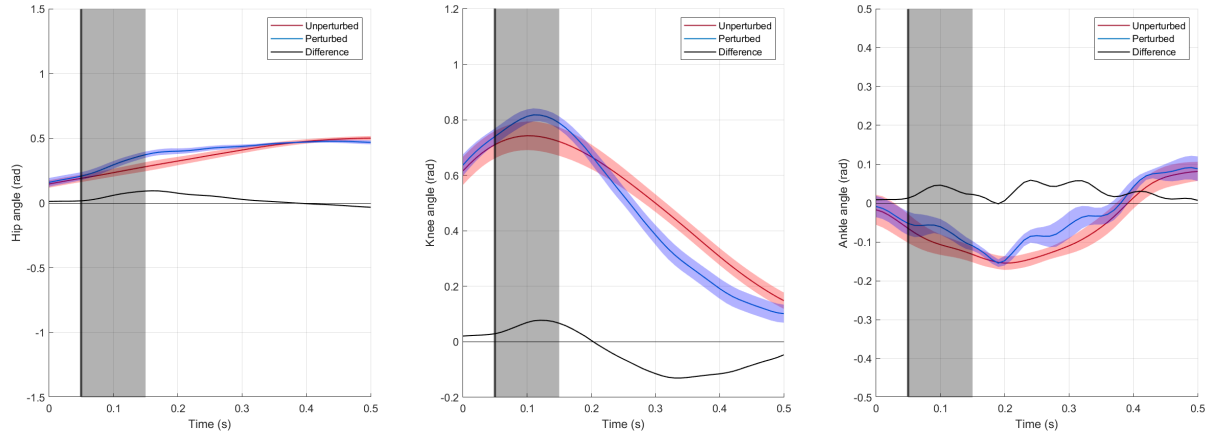

(a) Hip response of Participant 8 for the combined push (b) Knee response of Participant 8 for the combined push (c) Ankle response of Participant 8 for the combined push

Figure 63: Joint angle responses of the combined push for participant 8 in radians. the grey box is the perturbation time.

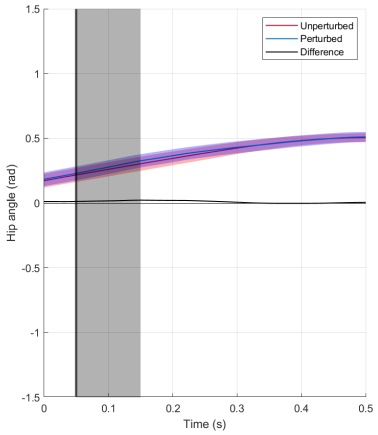

(a) Hip response of Participant 8 for the combined push-pull.

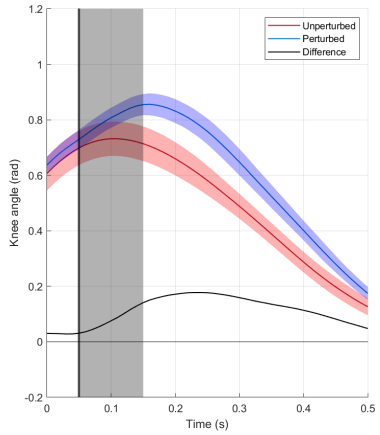

(b) Knee response of Participant 8 for the combined push-pull.

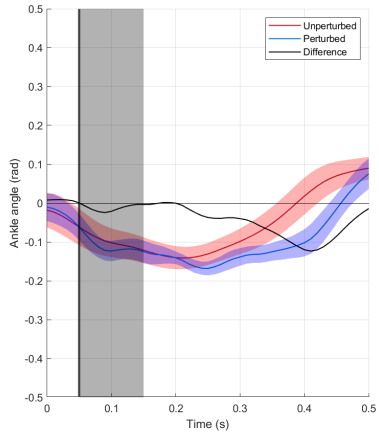

(c) Ankle response of Participant 8 for the combined push-pull.

Figure 64: Joint angle responses of the combined push-pull for participant 8 in radians. the grey box is the perturbation time.

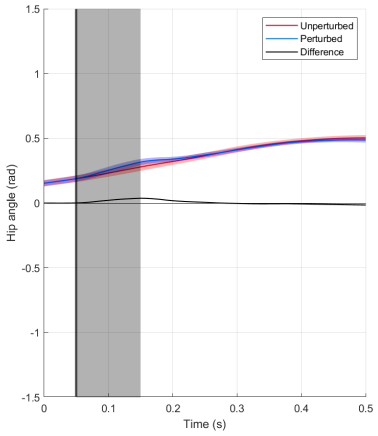

(a) Hip response of Participant 8 for the combined pushwith added damping.

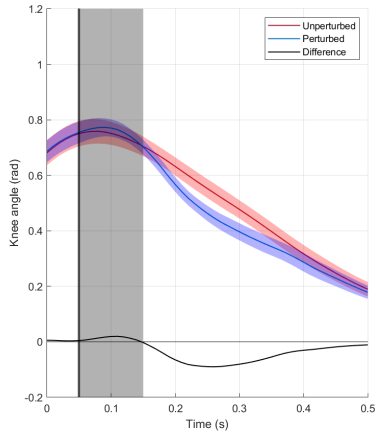

(b) Knee response of Participant 8 for the combined pushwith added damping.

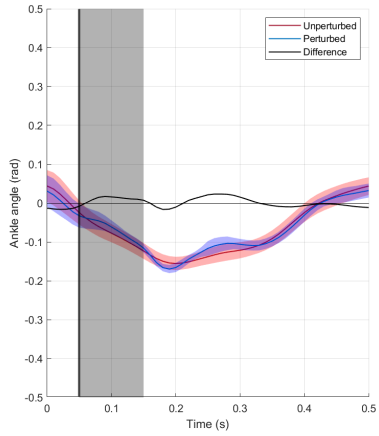

(c) Ankle response of Participant 8 for the combined pushwith added damping.

Figure 65: Joint angle responses of the combined push with added damping for participant 8 in radians. the grey box is the perturbation time.

E.8 Participant 9

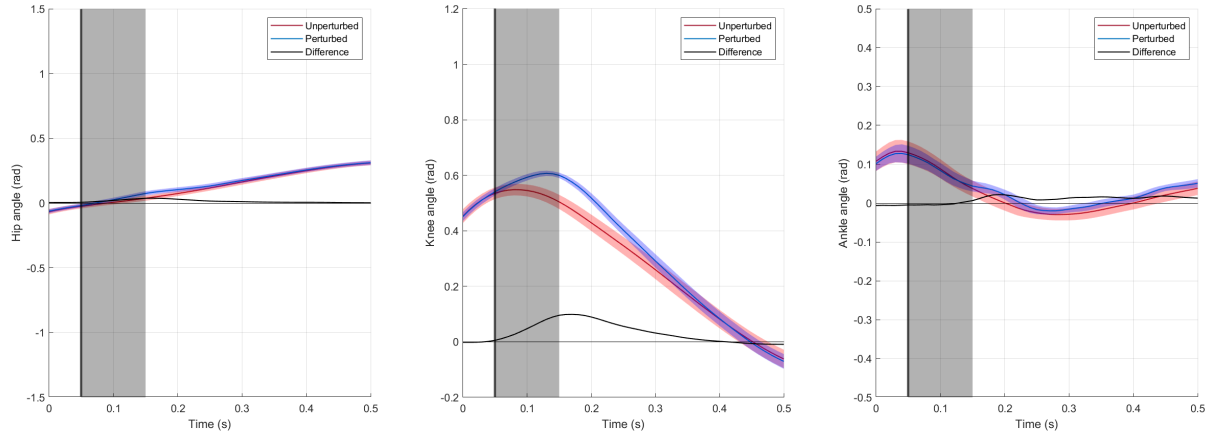

(a) Hip response of Participant 9 for the thigh push (b) Knee response of Participant 9 for the thigh push (c) Ankle response of Participant 9 for the thigh push

Figure 66: Joint angle responses of the thigh push for participant 9 in radians. the grey box is the perturbation time.

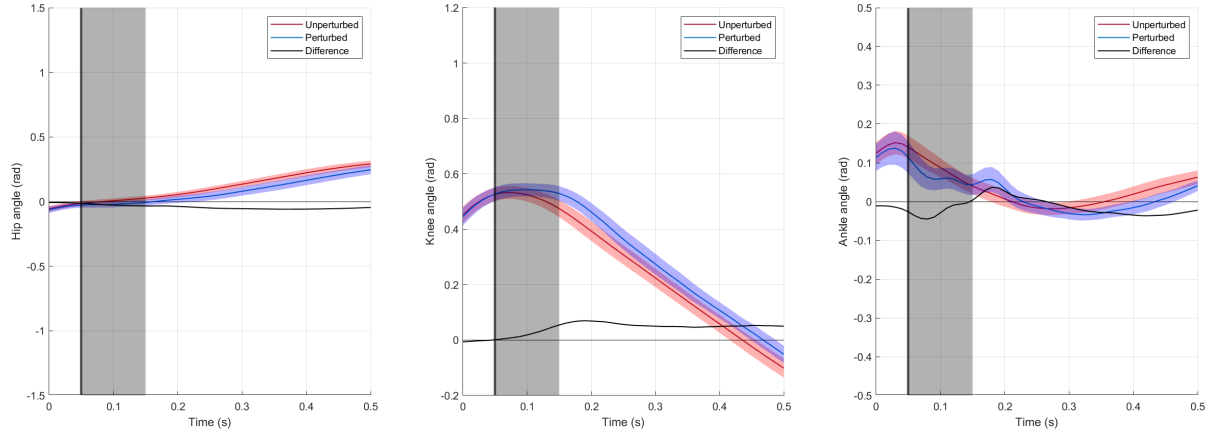

(a) Hip response of Participant 9 for the shank pull (b) Knee response of Participant 9 for the shank pull (c) Ankle response of Participant 9 for the shank pull

Figure 67: Joint angle responses of the shank pull for participant 9 in radians. the grey box is the perturbation time.

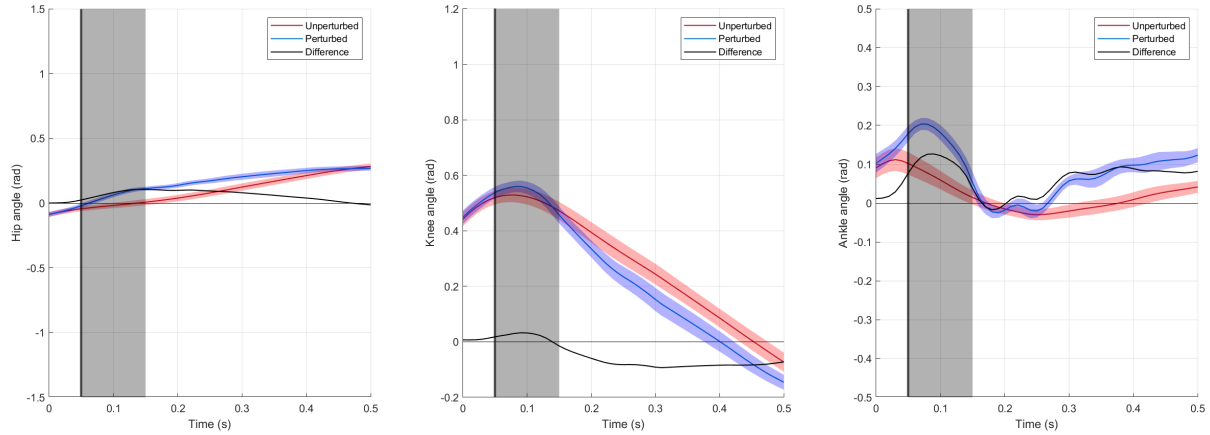

(a) Hip response of Participant 9 for the combined push

(b) Knee response of Participant 9 for the combined push

(c) Ankle response of Participant 9 for the combined push

Figure 68: Joint angle responses of the combined push for participant 9 in radians. the grey box is the perturbation time.

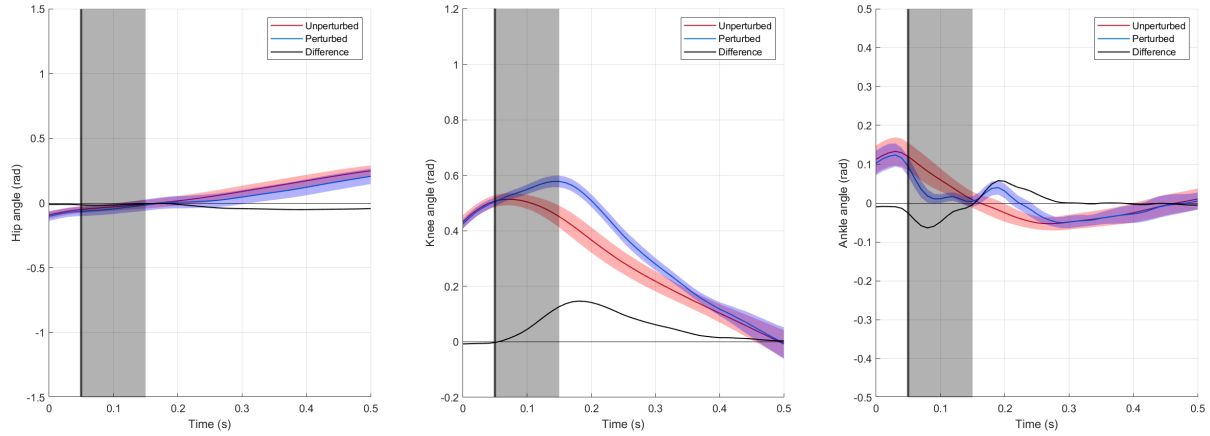

(a) Hip response of Participant 9 for the combined push-pull.

(b) Knee response of Participant 9 for the combined push-pull.

(c) Ankle response of Participant 9 for the combined push-pull.

Figure 69: Joint angle responses of the combined push-pull for participant 9 in radians. the grey box is the perturbation time.

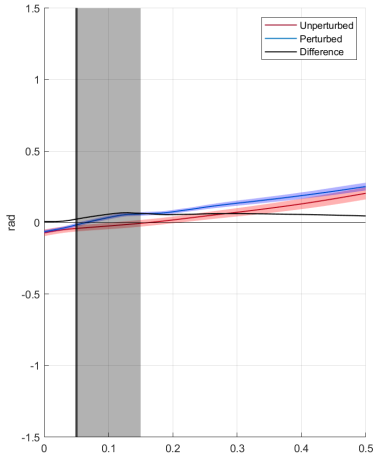

(a) Hip response of Participant 9 for the combined pushwith added damping.

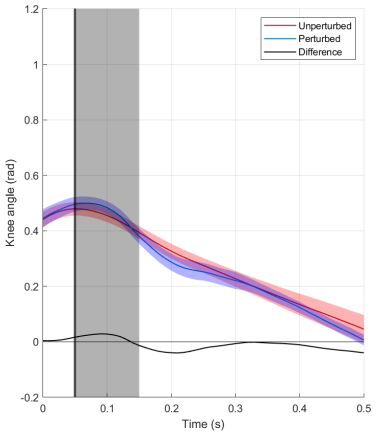

(b) Knee response of Participant 9 for the combined pushwith added damping.

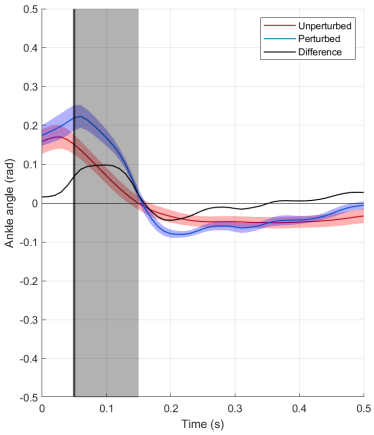

(c) Ankle response of Participant 9 for the combined pushwith added damping.

Figure 70: Joint angle responses of the combined push with added damping for participant 9 in radians. the grey box is the perturbation time.

E.9 Participant 10

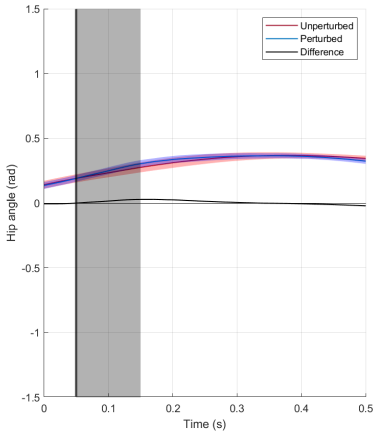

(a) Hip response of Participant 10 for the thigh push

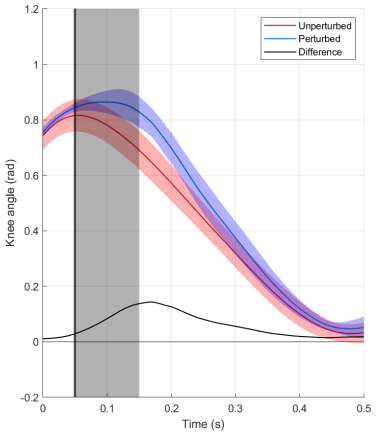

(b) Knee response of Participant 10 for the thigh push

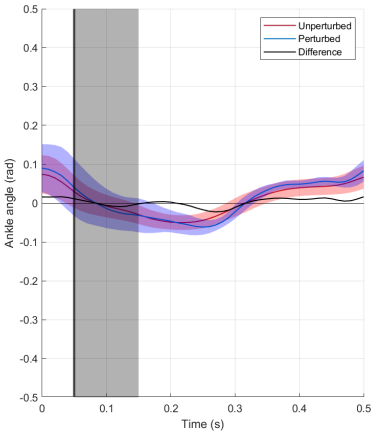

(c) Ankle response of Participant 10 for the thigh push

Figure 71: Joint angle responses of the thigh push for participant 10 in radians. the grey box is the perturbation time.

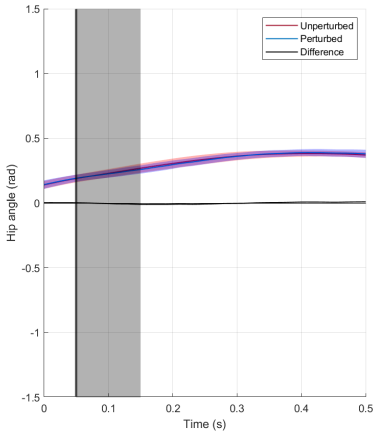

(a) Hip response of Participant 10 for the shank pull

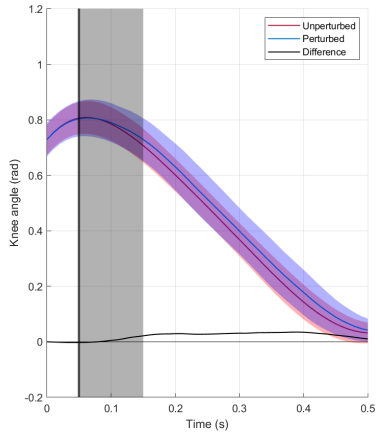

(b) Knee response of Participant 10 for the shank pull

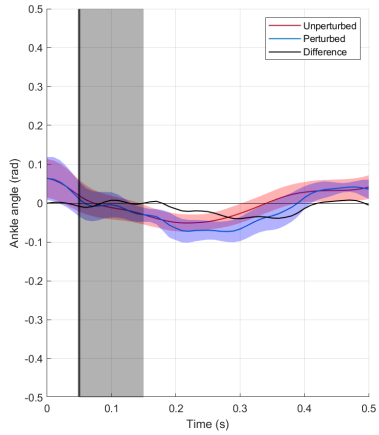

(c) Ankle response of Participant 10 for the shank pull

Figure 72: Joint angle responses of the shank pull for participant 10 in radians. the grey box is the perturbation time.

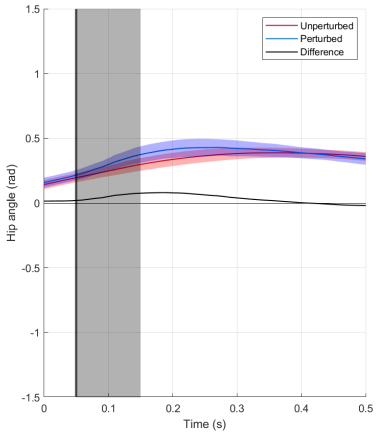

(a) Hip response of Participant 10 for the combined push

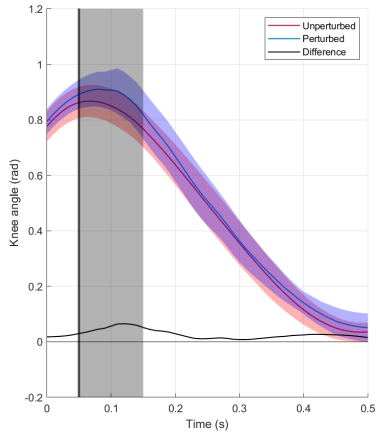

(b) Knee response of Participant 10 for the combined push

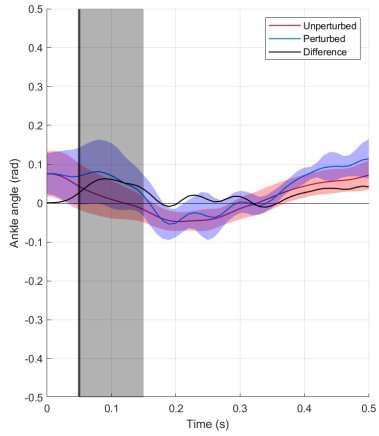

(c) Ankle response of Participant 10 for the combined push

Figure 73: Joint angle responses of the combined push for participant 10 in radians. the grey box is the perturbation time.

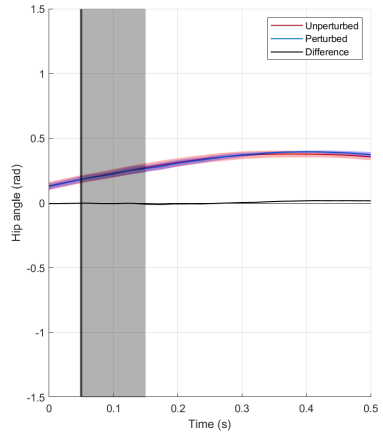

(a) Hip response of Participant 10 for the combined push-pull.

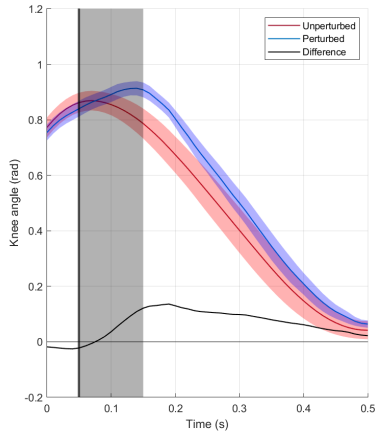

(b) Knee response of Participant 10 for the combined push-pull.

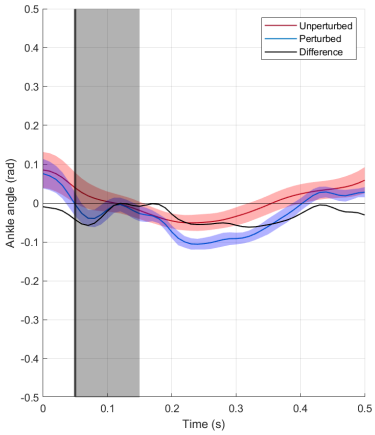

(c) Ankle response of Participant 10 for the combined push-pull.

Figure 74: Joint angle responses of the combined push-pull for participant 10 in radians. the grey box is the perturbation time.

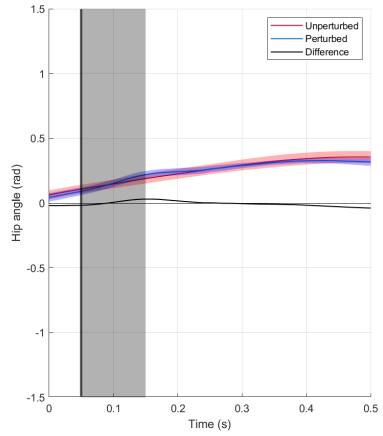

(a) Hip response of Participant 10 for the combined pushwith added damping.

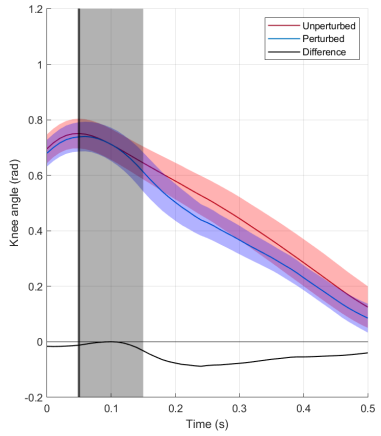

(b) Knee response of Participant 10 for the combined pushwith added damping.

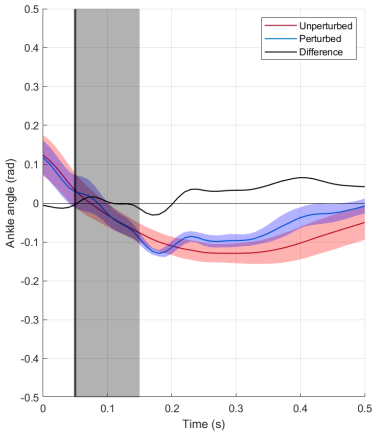

(c) Ankle response of Participant 10 for the combined pushwith added damping.

Figure 75: Joint angle responses of the combined push with added damping for participant 10 in radians. the grey box is the perturbation time.